

Copyright
by
Pius D. Wong
2012

**Methodology for Creating Human-Centered Robots:
Design and System Integration of a Compliant Mobile Base**

by

Pius D. Wong, B.S.

THESIS

Presented to the Faculty of the Graduate School of

The University of Texas at Austin

in Partial Fulfillment

of the Requirements

for the Degree of

MASTER OF SCIENCE

THE UNIVERSITY OF TEXAS AT AUSTIN

May 2012

**Methodology for Creating Human-Centered Robots:
Design and System Integration of a Compliant Mobile Base**

APPROVED BY

SUPERVISING COMMITTEE:

Luis Sentis, Supervisor

Ashish Deshpande

Dedicated to my brothers and my parents –

I would never have made it this far without you.

Acknowledgments

I wish to thank numerous people who have made this work possible, including my main adviser Dr. Luis Sentis for overseeing the entire project, and former colleague Somudro Gupta ('11) for his large work on this project from 2010 to 2011, especially for Trikey Versions 1 and 3. I must further thank Frank Lima, Matt Gonzalez, Josh Petersen, Nick Paine, Sehoon Oh, Vansi Vallabhaneni, Emily Chen, Alan Kwok, and Kwan Suk Kim for aiding in various technical parts of the overall “Dreamer” project. I also received helpful feedback and relevant knowledge from Dr. Ashish Desphande, the second reviewer of my thesis, and also from courses taught by Dr. Kristin Wood, Dr. Rick Neptune, and Dr. Glenn Masada. I thank the students and Lonny Stern at the Skillpoint Alliance in Austin, Texas, for initiating this project idea and Meka Robotics in San Francisco, California, for assistance in its implementation. I thank my sources of funding for graduate study that have greatly helped me with my education: the National Defense Science & Engineering Graduate Fellowship and the University of Texas Cockrell School of Engineering Thrust 2000 Charles W. Merritt Endowed Graduate Fellowship in Engineering. Finally, I want to thank my past colleagues in Chicago, Memphis, and Leuven, who had helped me tremendously on my path to Texas, including Abraham Salehi, Stanley Tsai, Mary Anthony, Luc Labey, Bernardo Innocenti, Prof. Kaat Desloovere, Dr. Scott Banks, and so many others of whom there are far too many to name here.

Thanks, guys.

**Methodology for Creating Human-Centered Robots:
Design and System Integration of a Compliant Mobile Base**

Pius D. Wong, M.S.

The University of Texas at Austin, 2012

Supervisor: Luis Sentis

Robots have growing potential to enter the daily lives of people at home, at work, and in cities, for a variety of service, care, and entertainment tasks. However, several challenges currently prevent widespread production and use of such human-centered robots. The goal of this thesis was first to help overcome one of these broad challenges: the lack of basic safety in human-robot physical interactions. Whole-body compliant control algorithms had been previously simulated that could allow safer movement of complex robots, such as humanoids, but no such robots had yet been documented to actually implement these algorithms. Therefore a wheeled humanoid robot “Dreamer” was developed to implement the algorithms and explore additional concepts in human-safe robotics. The lower mobile base part of Dreamer, dubbed “Trikey,” is the focus of this work. Trikey was iteratively developed, undergoing cycles of concept generation, design, modeling, fabrication, integration, testing, and refinement. Test results showed that Trikey and Dreamer safely performed movements under whole-body compliant control, which is a novel

achievement. Dreamer will be a platform for future research and education in new human-friendly traits and behaviors. Finally, this thesis attempts to address a second broad challenge to advancing the field: the lack of standard design methodology for human-centered robots. Based on the experience of building Trikey and Dreamer, a set of consistent design guidelines and metrics for the field are suggested. They account for the complex nature of such systems, which must address safety, performance, user-friendliness, and the capability for intelligent behavior.

Table of Contents

Acknowledgments	v
Abstract	vi
List of Tables	xii
List of Figures	xiii
Chapter 1. Introduction	1
1.1 Structure and Goals of This Work	2
1.2 Human-Centered Robotics	6
1.3 Omnidirectional Wheeled Robots	9
1.4 Next Steps in Human-Centered Robotics	14
1.5 Project Tasks & Timeline	17
Chapter 2. Design History	20
2.1 <i>Trikey</i> Version 1	20
2.2 <i>Trikey</i> Version 2	22
2.3 <i>Trikey</i> Version 3	26
2.4 <i>Trikey</i> Version 4	27
2.4.1 Electronics Module Version 1	30
2.4.2 Electronics Module Version 2	31
2.4.3 Electronics Module Version 3	34
Chapter 3. Implemented Design: <i>Trikey</i> Version 5	36
3.1 Functions	36
3.2 Modules	44
3.3 Bill of Materials	46
3.4 Exploded Views	55

3.5	Component Selection	58
3.6	Fabrication	63
3.7	Assembly & Disassembly	65
3.7.1	General Assembly Steps for Trikey/Dreamer	65
3.7.2	Assembly Steps for Motor-Wheel Modules	67
3.7.3	Assembly Steps for Electronics Module	69
Chapter 4.	Design Analysis	72
4.1	Kinematics Models	72
4.1.1	Level Flat Terrain Kinematics	72
4.1.2	Inclined Flat Terrain Kinematics	74
4.2	Dynamics Models	76
4.2.1	Level Flat Terrain Dynamics, Zero Wheel Inertia	76
4.2.2	Level Flat Terrain Dynamics, Nonzero Wheel Inertia	78
4.2.3	Inclined Flat Terrain Dynamics, Zero Wheel Inertia	84
4.2.4	Transmission Losses	88
4.3	Worst-Case Analysis of Safe Kinematic Operating Limits on Flat Ground	89
4.3.1	Extreme Configuration	90
4.3.2	Worst-Case Linear Acceleration Limit	90
4.3.3	Worst-Case Angular Velocity Limit	94
4.3.4	Stability Sensitivity Calculations	96
4.3.5	Combined Linear Acceleration and Angular Velocity Limits, Typical Case	98
4.4	Generalized Safe Kinematic Limits on Level Flat Terrain	100
4.4.1	Linear Acceleration Limit	100
4.4.2	Angular Velocity Limit	104
4.4.3	Simulation of Safety Limits	105
4.5	Mechanical Strength & Failure Analysis	107
4.6	Recommended Safe Operating Zones	110

Chapter 5. Integrated <i>Dreamer</i> Humanoid Robot	111
5.1 Design	111
5.1.1 Upper Body Summary	113
5.1.2 Mobile Base Summary	113
5.1.3 Power & Communication	114
5.2 Whole-Body Compliant Control (WBC)	116
5.3 Automatic Balancing	117
Chapter 6. Test Results	120
6.1 Component Calibration	120
6.1.1 Torque Limiters	120
6.1.2 Torque Cells	120
6.2 Investigation of Original Gearbox Failures	124
6.3 Whole-Body Compliant Control (WBC)	128
6.4 Auto-Balancing on Inclined Terrain	128
6.5 User Experience	129
Chapter 7. Design Evaluation & Method Recommendations	132
7.1 General <i>Dreamer</i> Evaluation	132
7.2 Proposed <i>Dreamer</i> and <i>Trikey</i> Applications	138
7.3 <i>Trikey</i> Design Evaluation	139
7.4 <i>Trikey</i> Redesign Avenues	142
7.4.1 Safety Improvements	142
7.4.2 Performance Improvements	146
7.4.3 User-Friendliness Improvements	148
7.4.4 Feature Additions	150
7.5 Method for Prioritizing Potential Redesigns	151
7.6 Method for Measuring Quality of Redesigns	154
7.7 Metrics of Human-Centeredness	156
7.8 Method for Designing a Human-Centered Robot	160

Chapter 8. New Design Concepts	164
8.1 Tracked Omniwheel Concept	164
8.1.1 Inner Layer	167
8.1.2 Outer Layer	168
8.1.3 Tracked Rollers	171
8.2 Suspension Concept	177
Appendices	183
Appendix A. CAD Files and Selected Drawings	184
Appendix B. Matlab Code for Kinematic Limit Simulation	201
Appendix C. Accessing Whole-Body Compliant Control Code	205
Index	207
Bibliography	210
Vita	217

List of Tables

1.1	Published specifications and abilities of Trikey base compared to similar recent omnidirectional wheeled bases. N/A = not applicable, N/I = not indicated in citation.	11
2.1	Function-feature list, Trikey Version 1	20
2.2	Function-feature list, Trikey Version 2	22
2.3	Function-feature list, Trikey Version 3	26
2.4	Function-feature list, Trikey Version 4	28
3.1	Function- and constraint-feature list, Trikey Version 5	37
3.2	List of Modules	45
3.3	Full Bill of Materials: Trikey Version 5	47
4.1	Worst-case mass distributions of Dreamer/Trikey robot in initial analyses. Parameters correspond to Figs. 4.8-4.10.	96
4.2	Worst-case kinematic limits of Dreamer/Trikey robot in initial analyses. Parameters correspond to Figs. 4.8-4.10.	97
4.3	Recommended safe operating limits for Trikey or Dreamer robot in standard body poses and no extra payload.	110
6.1	Calibration data for the three Trikey torque cells in March 2011, matching well with manufacturer data supplied in Summer 2010. . .	124
7.1	Published specifications and abilities of <i>Dreamer</i> robot versus similar recent human-centered robots. N/A = not applicable, N/I = not indicated in citation.	135

List of Figures

1.1	Front and side views of Spring 2012 version of the “Dreamer” human-centered robot at the University of Texas at Austin. The “Trikey” mobile base, or lower half of this robot, is the focus of this thesis.	1
1.2	Chain of goals for the Trikey and Dreamer projects. Achieving the end goals on the right call for prerequisite goals on the left. Work detailed in this thesis is highlighted in green. Concurrent projects headed by other HCRL team members are highlighted in yellow. Proposed or planned projects are highlighted red.	16
1.3	Timeline of tasks leading to the creation of the latest version of Trikey and Dreamer. The red “X” denotes that the task was discontinued from further development.	19
2.1	Trikey Version 1, in Dreamer concept.	21
2.2	Trikey Version 1, in Dreamer concept, with open walls.	21
2.3	Trikey Version 2A: inner-facing controllers.	23
2.4	Trikey Version 2B: outer-facing controllers.	23
2.5	In-house Human Centered Robotics Laboratory brushless DC motor controller (HCRL-BLDCMC), designed by Nick Paine.	24
2.6	Initial top-level power management system designed for Trikey Version 2, which was intended to be mostly custom-designed in-house.	25
2.7	Wheel module with new, higher torque motor and gearbox.	27
2.8	Trikey Version 4A: Higher waist, front facing a motor.	29
2.9	Trikey Version 4B: Lower waist, rear facing a motor.	29
2.10	Trikey Version 4 layout of batteries and electronics on the base.	31
2.11	Electronics module, version 1.	32
2.12	Electronics module, version 2.	33
2.13	Electronics module, version 3.	34
3.1	Dreamer Version 1: CAD.	38
3.2	Dreamer Version 1: Built.	38

3.3	CAD drafting of shortest possible height of the latest Trikey design at 28.6in above the floor. Dreamer is currently set atop Trikey with the waist at this height, in order to lower the center of gravity and improve balance.	39
3.4	CAD drafting of tallest possible height of the latest Trikey design at 30.6in above the floor. 29.6in tall is also possible.	40
3.5	Top-down views of the Trikey fixation plates, with Meka upper body base attached. Four main horizontal positions are possible for the Meka upper body, shown here. Assuming an upright upper body, the approximate center of mass of the upper body can lie 5.0in, 2.8in, 2.0in, and 0.0in in front of the geometric center of the Trikey mobile base.	41
3.6	Side view of an example extreme upper body configuration for Dreamer. Shown here is the most forward position of the Meka upper body (5.0in in front of the center of the Trikey base) and the tallest position (waist 30.6in above the floor). The center of mass in this configuration lies at waist-level denoted by the pink axes.	42
3.7	Drafting showing some measurements that may be useful for design analysis and for writing the control algorithm. Example measurements include the horizontal distance between the geometric center and the point of wheel contact with the floor.	43
3.8	Latest CAD of Trikey assembly.	44
3.9	Exploded view of Trikey main modules. See Table 3.2 for details. . .	45
3.10	Exploded view of the motor-wheel module. Refer to Table 3.3 for part designations.	56
3.11	Exploded view of the electronics module. Refer to Table 3.3 for part designations.	57
3.12	Exploded view of the BBB submodule that handled power input. The BBB PCB was held away from the plate with board spacers.	58
3.13	Exploded view of the PWR submodule that handles power distribution and communication. The PCB was held away from the plate using board spacers. The Crydom relay on the board helped to regulate power output.	59
3.14	Exploded view of the ELMO submodule that handles driving the motors. Four channels for motors are available with this setup (2 per PCB), although only three channels are used to control the three motors in Trikey. One significant design flaw that was only discovered after assembly and construction is that wiring ports at the bottom of part C9 are difficult to access with fingers and tools, given the limited space there. This occurred because of a lack of knowledge about the complete electronics design during the mechanical design phase. . .	60

3.15	Exploded view of the LOADCELL submodule that handled power, data acquisition, and signal conditioning for the torque cells.	61
3.16	The custom Trikey electronics were designed, built, and tested by Meka (San Francisco) concurrently with the latest mechanical re-designs of Trikey. They were shipped to UT for integration in Sep 2011. Photo supplied by Meka; annotation added by the author. . .	62
4.1	Kinematic model used for Dreamer design process. Top-down view of three-wheeled base. Image corrected from Gupta [15] so that the three generalized coordinates x , y , and θ are independent.	73
4.2	Function of the 3x3 rotation matrix \mathbf{R} that transforms vectors from the local xyz reference frame of the robot (left) to the global XYZ reference frame of the terrain (right). The Z -axis of the global frame points upward against the direction of gravity \vec{g} . The z -axis of the local frame is normal to the surface of the ground when all three wheels make contact with the ground.	76
4.3	Example dynamics simulation using Matlab code, assuming zero wheel inertia. Wheel torques are shown that correspond with a whole-body robot linear acceleration of 1 m/s^2 , in acceleration directions of 0 - 360° around the robot, on flat ground. Here a total mass of 100 kg was assumed for the robot and its payload, with a 0.112 m offset of the center of mass from the center of rotation. Whole-body Trikey rotational inertia about the center of rotation was estimated as 3.01 kg/m^2 , based on CAD model measurements and the parallel-axis theorem. The Meka upper body rotational inertia could not be estimated in the CAD model because of a lack of material property definitions from Meka Robotics, so it was assumed to be a fraction of the Trikey inertia, in the same proportion as the Meka upper body and Trikey masses (i.e. $I_{meka}/I_{trikey} = M_{meka}/M_{trikey} = 41 \text{ kg}/50 \text{ kg}$). The whole-body Dreamer rotational inertia was then taken as the sum of the Trikey and Meka upper body inertias.	79
4.4	Net wheel torque due to applied motor torque and ground reaction force.	80
4.5	Discrepancies between the maximum torques predicted by two dynamic models: one assuming zero wheel inertia, and one accounting for wheel inertia. Whole-body robot linear acceleration was assumed to be 1 m/s^2 . Discrepancies increase when the ratio of I_w/r_w increases, with the non-zero inertia model predicting slightly higher torques. .	84
4.6	3D free-body diagram of Trikey robot, seeing weight $m\vec{g}$ at the center of mass (CoM), and the tangential and normal ground reaction forces \vec{F}_i and \vec{N}_i at the wheel-ground contact points. The vectors \vec{r}_i denote the displacements from the CoM to the wheel-ground contact points. Section 4.1.2 discusses the rotation matrix used to transform vectors from the local to global coordinate systems.	85

4.7	Case 1: Dreamer configuration with likely “worst-case” mass distribution (waist 30.6in high, 5in forward offset), carrying a 7 lbs load in a laterally and frontally extended arm. Global coordinate system orientation denoted in lower left corner. Origin located directly below geometric center of Trikey baseplate at ground level.	91
4.8	Top-down diagram of the Dreamer center of mass in a worst-case balance condition.	92
4.9	Side view of the Dreamer center of mass in a worst-case balance condition.	93
4.10	Overhead view of the Dreamer center of mass in a worst-case balance condition, undergoing centripetal force.	95
4.11	Case 7: The configuration that is mostly likely to be seen in experimentation.	98
4.12	Simultaneous limits to safe linear acceleration a and angular velocity ω for the Dreamer robot in Case 7 (Table 4.2, Fig. 4.11).	99
4.13	Free-body diagram of example case of robot instability. If net body acceleration is large enough, the wheel in front of the acceleration direction sees no normal forces from the ground. A tipping moment may occur around the center of mass that causes robot liftoff from the ground.	101
4.14	Parameters for estimating safe accelerations of the robot center of mass. Top-right and bottom diagrams show directions of accelerations \vec{a} that are most likely to cause tipping over each ground-contact edge E_{pq}	102
4.15	Parameters used for calculating safe angular velocity limits, when the base rotates about its geometric center O on flat ground. These are in addition to the parameters shown in Figs. 4.13-4.14.	104
4.16	Safe linear acceleration limits versus acceleration direction, when Trikey/Dreamer center of mass is in an extreme position (Fig. 4.7). Acceleration direction refers to degrees counterclockwise from the front direction, when viewed overhead, as in Figs. 4.14-4.15.	106
4.17	Safe linear acceleration limits versus acceleration direction, when Trikey/Dreamer center of mass is in a more common position (Fig. 4.11). Acceleration direction refers to degrees counterclockwise from the front direction, when viewed overhead, as in Figs. 4.14-4.15.	107
4.18	FEA result for extreme loading on upper vertical plate (part B17). Maximum von Mises stresses were less than the yield strength for the 6061 aluminum material of 55 MPa.	109
5.1	Features of Dreamer robot.	112

5.2	Block diagram of Dreamer system wiring and electrical connections.	116
5.3	Block diagram of prioritized, closed-loop, whole-body compliant controller for Dreamer. Joint torque outputs are adjusted based on desired and actual CoM, hand, and posture positions, prioritized Jacobians, and controller gains, following the general linear control equation $\ddot{x} + K_p e + K_d \dot{x} = 0$. <i>Image courtesy of Kwan Suk Kim.</i>	118
6.1	Torque limiter limit test setup (top view).	121
6.2	Torque limiter limit test setup (side view).	121
6.3	Torque cell basic calibration test setup. The setup required a multi-meter, a 5 VDC power source (or the HCRL motor controllers, supplied with 24 VDC), custom test fixtures (see Appendix), the torque sensor and connector, 0.5 in square keys, rope, weights, S-hooks, 6 in C-clamps, and shim. An alternate, more robust calibration method would use a materials testing frame but would require more elaborate fixtures.	122
6.4	In-house raw calibration data for the three Trikey torque cells in March 2011, matching well with manufacturer data supplied in Summer 2010.	123
6.5	Original motor-gearbox assembly from Trikey 2 that exhibited poor mechanical performance.	125
6.6	Original planetary gearbox from Trikey Version 2, open and greased.	127
6.7	Demonstration of whole-body compliant control experiment. Dreamer body and posture position could be altered by a human (center) without altering the relative hand position (right). <i>Image courtesy of Luis Sentis and Josh Petersen.</i>	129
6.8	Example demonstration of automatic balancing. The torso adjusts to account for base tilting measured by an inertial measurement unit. <i>Image courtesy of Luis Sentis and Josh Petersen.</i>	130
6.9	Example demonstration of force-guided motion up a ramp, where Dreamer is led by a human. Tests were run tethered to AC power here.	130
7.1	Example design feature priority matrix. Feature ideas are on the left. Desired functions are at the top. Each cell scores how well a feature can achieve a function. For example adding rubber bumpers (1st row) can decrease damage in collisions (+2 score) but also increase robot mass (-1 score). The final score for each feature is the weighted sum of row scores. High-priority features are highlighted in yellow. Low-cost and low-development time features are highlighted in green.	153

7.2	Example “House of Quality” matrix for desired functional improvements in robot safety. Desired functions are on the left. Metrics of quality for these functions are at the top. The first function (1st row) of “decreasing damage caused by collisions” corresponds well with lower system mass, lower elastic moduli at the exterior, and lower stresses in crash tests, and hence scores 9 for those metrics.	155
8.1	CAD of tracked omniwheel concept.	165
8.2	Side view of concept wheel.	166
8.3	Front view of concept wheel.	166
8.4	Exploded view of wheel concept modules.	168
8.5	Inner layer of the wheel concept.	169
8.6	Exploded view of the inner layer of the wheel concept.	169
8.7	View of inner layer from the side, with the outer frame or ”spokes” removed to reveal the clamping fixtures.	170
8.8	Zoomed view of the inner layer from the side, showing clearance from the roller-tracks.	171
8.9	Front view of the inner layer frame and tracked-roller construct. The U-shaped upper part of the clamp connects the lower clamp and side frames together.	172
8.10	Exploded front view of the inner layer frame and tracked-roller construct.	173
8.11	Outer layer of the wheel concept.	173
8.12	Outer layer of the wheel concept, with plastic panels removed. . . .	174
8.13	Exploded view of the outer layer of the wheel concept, with plastic panels removed.	174
8.14	View from the inner direction of the outer layer of the wheel concept, with plastic panels removed.	175
8.15	Front view of the outer layer frame and tracked-roller construct. . .	175
8.16	Exploded front view of the outer layer frame and tracked-roller construct.	176
8.17	Exploded front view of the outer layer frame and tracked-roller construct.	177
8.18	Exploded front view of the outer layer frame and tracked-roller construct.	178
8.19	Independent wheel suspension concept module.	178
8.20	Side view of the suspension concept.	179

8.21	CAD of the suspension module, without a wheel.	180
8.22	Exploded side view of the suspension module, without a wheel. . .	180
8.23	Generic robot possible using the wheel and suspension concepts. . .	181
A.1	Electronics baseplate, part C1.	185
A.2	BBB PCB plate, part C2.	186
A.3	PWR PCB plate, part C5.	187
A.4	ELMO PCB plate, part C8.	188
A.5	Load cell PCB plate, part C13.	189
A.6	Ethercat hub plate, part E4.	190
A.7	Back panel, part F6.	191
A.8	Assembly of the following Meka upper body attachment fixtures. .	192
A.9	Top bracket for upper body fixation, part B19.	193
A.10	Upper vertical plate, part B17.	194
A.11	Main upper body fixation plate, part G1, sheet 1.	195
A.12	Main upper body fixation plate, part G1, sheet 2.	196
A.13	Main upper body fixation plate, part G1, sheet 3.	197
A.14	Front upper body fixation plate, part G2.	198
A.15	Left and right upper body fixation plates, parts G3 and G4. . . .	199
A.16	Motor-wheel module inner vertical plate, part B14	200
C.1	Sourceforge Stanford-WBC website, April 2012.	206
C.2	github Stanford_WBC website, April 2012.	206

Chapter 1

Introduction

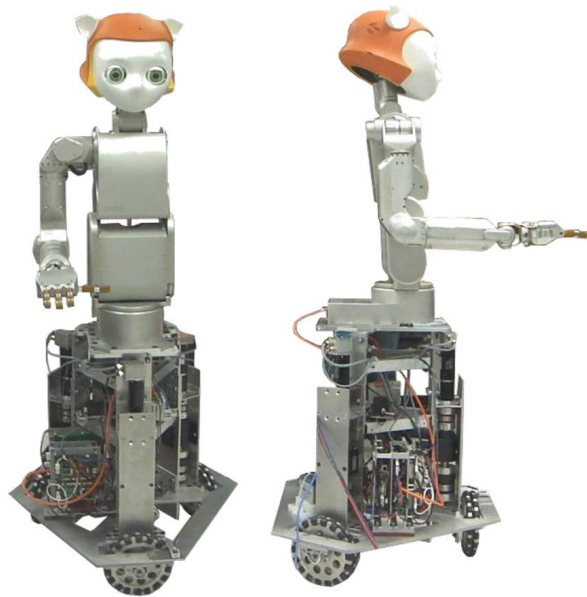


Figure 1.1: Front and side views of Spring 2012 version of the “Dreamer” human-centered robot at the University of Texas at Austin. The “Trikey” mobile base, or lower half of this robot, is the focus of this thesis.

What is a “human-centered” robot? Generally it is a robot that functions well around and with people, but that short description begs for more detail. How should such a robot look, move, and sense its surroundings? How should it be designed and built? What is its purpose? What is human-centeredness, why is it important, and when does a robot have it?

This thesis attempts to address these questions as it describes the creation of a real robot (Fig. 1.1) meant for all-purpose activities around people. This example provides insights into overarching principles of design, analysis, and project management for similarly complex robots. These insights can be applied to future robotics projects, in the hopes that those robots will match more closely a human-centered ideal.

1.1 Structure and Goals of This Work

Broadly speaking, this work attempts to facilitate the wider use of robots in human environments. To do this, I address two main goals: (1) improving safety of human-centered robots, and (2) offering more standard design and analysis methods for these robots. Each chapter contributes to both goals, as the two goals are intertwined. To justify these goals, **Chapter 1** gives the context of this project. It begins with a review of robot technology for working with or alongside humans in everyday situations in **Section 1.2**. Standard design recommendations for such robots are limited, and so the literature is first examined for guidance, with a focus on the need for physical safety in human-robot interactions. I argue that the next practical step in creating safer, more human-centered robots is to implement compliance in a humanoid with a wheeled, omnidirectional mobile base. **Section 1.3** then reviews the taxonomy of recently developed omnidirectional mobile bases to again find design guidance.

Given the technology trends for human-centered robots, **Section 1.4** describes some achievable next steps to enhance their safety and performance. Here I

detail the long- and short-term goals of my work, as well as how they fit with the work of my colleagues and robotics research in general. My short-term goals include developing a compliant, omnidirectional mobile robot, as recommended in **Section 1.2**. A human-centered robot is a complex system, maybe one day approaching that of a biological system. Its creation process is equally complex and cannot be ignored. For this reason I summarize the many tasks in this project in **Section 1.5**, which emphasizes the high importance of project management and people in the technical process. Failure of a development task can mean failure of the end system. Efforts to streamline development processes, such as team-based modular design, could promote success of future robots.

The iterative design evolution of the mobile base is summarized in **Chapter 2**, emphasizing function-based rather than feature-based design choices. The purpose of this chapter is to show the cyclic process of analysis, design, and testing needed to repeatedly identify design improvements. **Chapter 3** details the result of design iteration, the functions of the latest design, and the fabrication process, including a bill of materials. It emphasizes the importance of modular design, design for fabrication and assembly, and design for modification. Together, these chapters exemplify the heart of the design process for a human-centered robot.

The mathematical analyses influencing design and implementation decisions are given in **Chapter 4**. This chapter is another key example of a generalized mechanical design process for human-centered robots. Any such robot development process should consider modeling kinematics, dynamics, safety limits, strength, and lifetime, if possible. The kinematic and dynamic models here (**Sections 4.1** and

4.2) gave numbers that helped determine design parameters, such as motor sizes and sensor ranges. **Section 4.2.2** also shows that sometimes simplified models are sufficient for design purposes, such as when ignoring wheel inertias. Knowing when to simplify design analyses can streamline future design processes. Finally the safety and strength analyses in **Sections 4.3-4.6** are key for implementing a human-centered robot without hazards. They include algorithms to help keep a robot balanced and stable in **Section 4.4**. Fatigue experiments and modeling were not performed at this stage since the robot was not expected to see high amounts of cyclic loads, but such analysis should be included for robots where this is not the case. All these analyses ideally would take place *before* final implementation of another robot.

This design resulting from analytical models and iterative development was actually integrated with an upper body robot to create the humanoid robot Dreamer. A summary of the Dreamer system specifications and performance is given in **Chapter 5**. This section serves as a reference for how to integrate separate modules or systems into a humanoid robot under whole-body compliant control. It also compares recently developed similar robots for various traits. **Chapter 6** then describes the physical tests and experiments involved in robot development. It provides example calibration procedures, part failure investigations, and demonstrations of compliant control in an integrated robot. Whole-body compliant control is confirmed, as the results of the tests show. Future work can build off this achievement.

An evaluation of the design is given in **Chapter 7**. General successes and problems for the end design are given, particularly compared to existing human-

centered robots previously reviewed in **Chapters 1** and **5**. Its main success is implementing whole-body compliant control. Applications for the resulting safer, more compliant robot are described. Possible opportunities for redesigning the base and the integrated robot are listed in detail. Methods for organizing and evaluating the redesign of complex systems are given, with this robot as a case study. General conclusions are then drawn about designing specifically for human-centered robotic systems, which should always consider multiple aspects of safety and performance.

Some ideas for future redesign and experimentation are given in more detail in **Chapter 8**. This additional chapter focuses on design for better performance of wheeled robots in rough terrain, and hence gives ideas for wheel and suspension modules. It addresses safety only in terms of mobility on rough terrain, but is still relevant. Since the tracked omniwheel concept specifically is novel, it is shown in detail. The concepts are by no means fully tested, but they may inspire design ideas in future developers.

One last note must be said about units. This document switches back and forth between Imperial and SI units throughout. I hope this does not obfuscate data but rather gives additional information readers. The units show which measurement system was the primary one for a particular subject or physical component – for example CAD was mostly done in inches, while “original equipment manufacturer” (OEM) motors were mostly sized in metric units. Such details may be important for future reference.

1.2 Human-Centered Robotics

Historically robots were mainly used for industrial and manufacturing tasks. As robotics technology has improved, however, its use has expanded. Robots have growing potential to spread beyond industrial environments into more everyday, human-centered ones, based on broad trends over the last few decades [14]. Such human-centered robots (HCRs) should meet a hierarchy of simultaneous and dependent functional requirements, which range from safe mobility and manipulation to appropriate interaction with people. The vast scope of the design problem, detailed by Kemp [19], has led to numerous types of robots employing different approaches to good human-robot interaction. Ultimately an integrated approach is desired, which may consider basic platform design up to learning and artificial intelligence. Before implementing high-level concerns, though, fundamentals should be addressed.

Physical safety around humans is one of the most fundamental design requirements of a HCR with moving parts. A lack of safety renders a HCR risky and unusable, compromising any other traits or abilities it has. Safety can come from both *avoiding* and *reacting* to dangerous physical situations. For example, better perception and motion planning can help a robot avoid collisions [14]. Recently developed tools for this include potential-field sensing in static environments and human-sensitive navigation rules in dynamic environments [21]. These tools are useful assuming a robot can move with consistent stability, indicating that stability is also a prerequisite for safe mobility.

However, a robot should also be able to automatically react to or accommodate unexpected collisions and other disturbances in uncontrolled human envi-

ronments. Relevant strategies include light and flexible mechanical design, impact-safe material at manipulator interfaces [5], and compliantly controlled joints with variable-impedance actuators, as implemented recently in the upper-body humanoid Justin [2]. All these approaches can absorb energy from impacts but also can compromise robustness of control. Lighter, higher-bandwidth metallorheological actuators and clutches may partly resolve this conflict, and research in this area is ongoing [29].

Besides safety, less fundamental design considerations for HCRs include robot form and appearance. Altogether, form and appearance help moderate human expectations of what the robot can do and whether it is safe. Form refers to the general structure or skeleton of the robot, such as how many manipulators to include, or if it has legs or not. Since these robots are meant to function in human environments, being of human form and size has direct practical benefits, as Kemp [19] notes. For example a humanoid robot with normal limb sizes could theoretically reach objects on tables, open cabinets, step over curbs, climb stairs, and do many other household or office tasks just like a person. This form conveniently sets up the robot for everyday human environments, at the sacrifice of being more complicated to build.

Secondary to form, appearance refers to the visual character and quality of the form. It can include color, material, anthropomorphism, realism, and various subjective traits that influence how people perceive the robot. Robots that scare or psychologically harm humans are probably not ideal HCRs. The “uncanny valley” and, more recently, “uncanny cliff” [4] hypotheses advocate against creating

robots that are extremely human-like in appearance in order not to disturb people around it. In fact, evidence from Bartneck [4] suggests that anthropomorphic but obviously non-human robots are more likeable than robots with realistic-looking human faces. Nevertheless the evidence is inconclusive, and groups are attempting to make human-looking robots [17] [36]. Thus far, it is reasonable to conclude that likeable HCRs could take either humanoid or non-humanoid form, depending on appearance. Likeability should be considered and assessed for any new HCR after more fundamental concerns.

Although several safer, compliantly controlled robotic systems currently exist, few in the literature are mobile, and none are fully humanoid. Recent advancements in compliant mobile HCRs include the AZIMUT-3 guided platform [12] and Walbot assistive robot [32], which use wheeled, omnidirectional, and velocity-controlled bases in combination with load-sensing upper portions. These robots may show compliant and human-safe control, but they lack a multi-link humanoid structure. The Rollin' Justin robot [7] is closer to achieving humanoid compliant control, as it has a compliant humanoid upper body, but based on the available literature it does not control wheel movement in reaction to upper body loads [37]. A whole-body compliant control (WBC) algorithm for humanoids exists and performs well in multi-body contact simulations [28], but documentation of the practical implementation of WBC in a humanoid could not be found outside our lab during this thesis. Demonstrating WBC in a real humanoid was a feasible immediate next step toward creating a safe, compliant mobile robot. That in turn is a pivotal step in creating a more human-centered robot.

1.3 Omnidirectional Wheeled Robots

A mobile base can be a subsystem of a human-centered robot, but these bases also comprise a whole field of robotics in their own right. This work limits discussion of mobile base taxonomy to omnidirectional, wheeled bases, because early design decisions in the Dreamer project already settled on using this type of base. See Gupta [15] for a detailed review of both omnidirectional wheels and omnidirectional mobile robots, as well as for the original design decisions and justifications. Briefly, the omnidirectional, three-wheeled approach facilitated simpler control algorithms and faster mechanical construction, which in turn would lead to faster novel implementation of whole-body compliant control in a humanoid robot. An example of this is the convenient six-equation, six-unknown contact force system that results from simplified 3D free-body diagrams (see Section 4.2.3).

Even when limited to omnidirectional bases, many design approaches are possible. A comparison of recently developed omnidirectional mobile bases that inspired this work is shown in Table 1.1, which includes the bases cited by Gupta as well as additional relevant designs. Several of these robots are meant to interact with people or carry a humanoid robot (Justin base [13], ARMAR-III base [3], AZIMUT-3 [12], Walbot [32]) and could be considered human-centered. All these bases could conceivably be used in human environments if they implemented soft control algorithms and other safety features. The features that do exist so far suggest features to include in future bases. For example, consistent design patterns show that these bases presently can carry payloads greater than 20 kg and can move at speeds of 1-2 m/s. The desired Trikey design specifications were partly based on such

characteristics. The final Trikey design specifications are also shown in the first column of Table 1.1 for reference, but these details are discussed more fully in the following chapters.

Table 1.1: Published specifications and abilities of Trikey base compared to similar recent omnidirectional wheeled bases. N/A = not applicable, N/I = not indicated in citation.

Trait	Robot								
	Trikey (Dreamer base)	Justin base	ARMAR- III base	AZIMUT- 3	Walbot	ASOC- driven	OMR- SOW	Axebot	KUKA youBot base
Mass	50 kg	150 kg	N/I	N/I	N/I	35 kg	N/I	3.5 kg	20 kg
Height	0.727-	0.658-							
	0.777 m	0.728 m	0.700 m	N/I	N/I	0.39 m	0.420 m	0.100 m	0.140 m
Width	0.763 m	0.644-	N/I	N/I	N/I	1.12 m	N/I	0.178 m	0.380 m
Length	0.660 m	1.220 m	N/I	N/I	N/I	1.12 m	N/I	0.178 m	0.580 m
	0.283-	0.260 m	N/I	N/I	N/I	N/I	N/I	N/I	N/I
Height of center of mass/gravity	0.292 m								
Payload	>41 kg	>60 kg	30 kg	34 kg	N/I	N/I	>100 kg	N/I	20 kg
Max. rated velocity	1 m/s	1.5 m/s	1 m/s	1.47 m/s	N/I	2.2 m/s	N/I	N/I	0.8 m/s
Max. passable incline	10°	17°	N/I	N/I	N/I	N/I	10°	N/I	N/I
Max. passable bump height	untested	N/I	N/I	N/I	N/I	N/I	5 cm	N/I	N/I
Intended environ- ment	indoors, incline	indoors, incline	N/I	indoors	indoors	outdoors	N/I	indoors, flat	general research & education
Footprint	3 wheels	4 wheels	3 wheels	4 wheels	4 wheels	4 wheels	4 wheels	3 wheels	3 wheels
Wheel type	Omni	Caster	Omni	Caster	Omni	Caster, offset-split	Omni, offset- steerable	Omni	Mecanum
Total wheel actuators	3	8	3	8	4	8	5	3	4

Continued on next page...

Table 1.1 ...continued from previous page

Trait	Trikey (Dreamer base)	Justin base	ARMAR- III base	AZIMUT- 3	Walbot	ASOC- driven	OMR- SOW	Axeobot	KUKA youBot base
Driving actuator type	BLDC & gearbox	BLDC di- rect	N/I	BLDC, differential elastic	N/I	N/I	DC servo	N/I	N/I
Max wheel torque	9.6 Nm	30Nm	N/I	N/I	N/I	N/I	N/I	N/I	N/I
Physical brakes	-	N/I	N/I	✓	-	-	✓	N/I	N/I
Self-reconfigurable	-	✓	-	- (excluding casters)	-	- (excluding casters)	✓	-	N/I
Suspension	-	passive vertical	passive	passive horizontal	N/I	passive vertical	passive 4-bar linkage	N/I	N/I
Suspension travel	N/A	70 mm	N/I	N/I	N/I	N/I	N/I	N/I	N/I
Supply	internal/ external	internal	N/I	internal	N/I	N/I	N/I	N/I	internal
Input voltage	24VDC	48 VDC (40- 54VDC battery)	24VDC	N/I	N/I	N/I	N/I	N/I	24VDC
Rated max power	<1kW	3.7 kW	N/I	N/I	N/I	N/I	600 W	N/I	200 W
Batteries	Lead acid	Li- polymer	N/I	Ni-hybrid	N/I	N/I	N/I	N/I	Lead acid
Rated run-time on batteries	>15 min	3 hrs	8 hrs @25% drive	2-3 hrs	N/I	N/I	N/I	N/I	N/I
Processor/Computer	Quadcore i3 PC	4 MiniTX dualcore PC	PC, PC/104	MiniTX 2.0GHz Core 2 duo	N/I	Gumstix Overo Earth	N/I	Stargate Kit	MiniTX Atom Dualcore
Communication	EtherCAT	EtherCAT	Gigabit Ethernet	1 Mbps CAN bus	N/I	Xbee wire- less	N/I	N/I	EtherCAT

Continued on next page...

Table 1.1 ...continued from previous page

Trait	Trikey (Dreamer base)	Justin base	ARMAR- III base	AZIMUT- 3	Walbot	ASOC- driven	OMR- SOW	AxeBot	KUKA youBot base
Direct torque sense	✓	✓	N/I	✓	N/I	N/I	N/I	N/I	N/I
Control	torque/velocity	velocity	force- guided velocity	force- guided velocity	force- guided velocity	velocity	velocity	N/I	N/I
Publication dates	2012, 2011	2009	2006	2010	2011	2011, 2008	2006, 2004	2009	2011
Sources	Wong (present work), Gupta [15]	Fuchs [13]	Asfour [3]	Fremy [12]	Song [32]	Ishigami [16], Uden- gaard [34]	Byun [9], Song [31]	do Nasci- mento [11]	Bischoff [6]

1.4 Next Steps in Human-Centered Robotics

In order to advance the field of HCRs, including in safety, several people designed and built a mobile humanoid robotic system dubbed “Dreamer” (Fig. 1.1). It was meant to be a platform for testing new human-safe traits and behaviors. It takes an integrated approach toward human-centeredness and safety, considering control software, mobility, and general appearance, as recommended in Section 1.2. The more general purpose of Dreamer is to facilitate research and education in HCRs. Hence we intended to create a semi-modular system that could be used and upgraded by multiple student users over time. One major part of my work was the coordination of development tasks at the system level to meet these design requirements, midway through the project. Ideally such tasks should be organized at the start of any robotics project.

The immediate goal of the Dreamer project was to implement and refine safe WBC algorithms across all degrees of freedom of an entire mobile humanoid, based on newly detailed open-source software [25]. A wheeled structure was chosen for the initial design in order to avoid some stability problems and decrease the complexity of locomotion algorithms (see Section 1.3, [15]). As the WBC algorithms develop, these structures could be replaced with more complex wheeled designs, or with legged designs.

A secondary goal was then to investigate stabilizing behaviors to prevent tipping, essentially giving Dreamer artificial vestibular and proprioception systems and reflexes. This would let Dreamer adjust its body pose or accelerations automatically to keep balanced and stable on flat and inclined surfaces. It is hypothesized

that such features could help the robot in future forays into rougher or urban environments. Finally, the robot was to have additional features that would allow future studies in human-friendliness. A summary of the broad goals of this work is shown in Fig. 1.2.

My technical work focused specifically on the design of the Trikey mobile base, which is the lower half of the humanoid Dreamer robot, and on Trikey integration into Dreamer. The purpose of this Trikey project was to create a mobile base that would facilitate the longer-term goal of creating a safe legged robot. As such, it had to be sufficiently simple that it could be constructed within 1-2 years and used by multiple students, while retaining proper functionality. Functionality was redefined multiple times over the course of the project, but it always included payload-carrying capacity, mobility, and ease of designing its control algorithms. Quick construction would allow immediate testing of WBC algorithms that already exist, without waiting for completion of an alternate legged base. Finally the base had to be flexible enough in design so that it could be attached to another robot, modified, and detached fairly easily.

Past studies suggest numerous different characteristics help make a robot function well around people (see Section 1.2). Consequently the mobile base ideally could help test these characteristics and accommodate additional functions over time. Therefore a more open and modular system was targeted over a design that would be more difficult to change.

If a safer mobile humanoid robot could be developed, then the WBC software could be refined and improved. New mechanical and software development projects

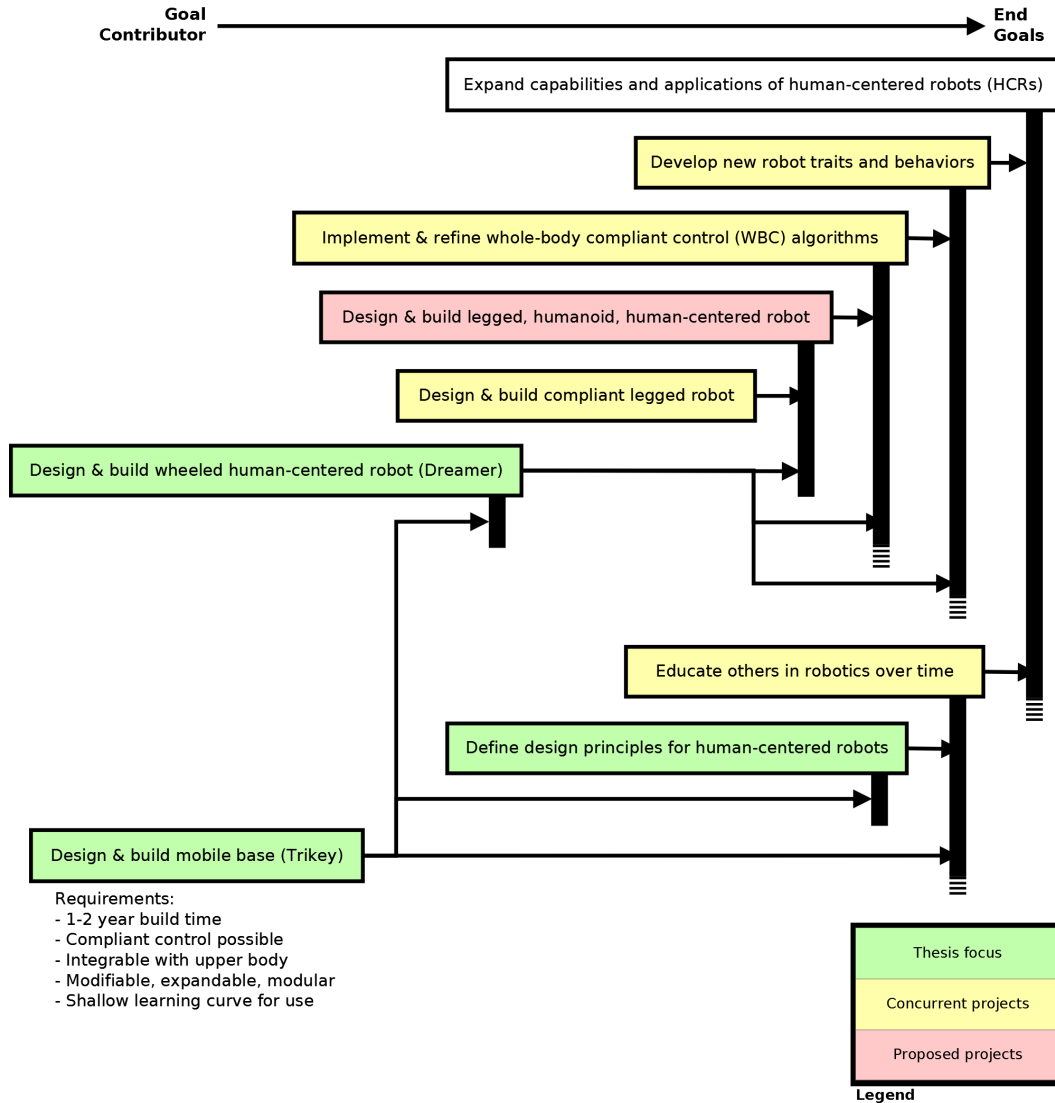


Figure 1.2: Chain of goals for the Trikey and Dreamer projects. Achieving the end goals on the right call for prerequisite goals on the left. Work detailed in this thesis is highlighted in green. Concurrent projects headed by other HCRL team members are highlighted in yellow. Proposed or planned projects are highlighted red.

then could follow that address even more aspects of human-centeredness. As an aid to any new mechanical design projects, standard design guidelines can be inferred from the present work.

1.5 Project Tasks & Timeline

Several people were involved in the Trikey project at the Human Centered Robotics Laboratory (HCRL) within the Department of Mechanical Engineering at the University of Texas at Austin (UT). A summary of the project timeline regarding the design up to Spring 2012 is shown in Fig. 1.3. The project was overseen by the head of the HCRL, Dr. Luis Sentis, and has been executed by multiple collaborators, as first documented by Somudro Gupta [15]. It began as an introductory group design project for local Austin high school students at a UT summer institute led by visiting undergraduate Frank Lima (University of Texas at Dallas) in Summer 2010. Lima constructed the first wood-and-metal prototype of the mechanical system with additional help from graduate students Gupta and Matt Gonzalez (UT Austin).

Since Fall 2010, Gupta and graduate student Pius Wong (UT Austin) redesigned Trikey in several iterations. The initial purposes of redesign were to incorporate three custom motor controller printed circuit boards (PCB) designed by graduate student Nick Paine and built by Paine, Wong, Gupta, and undergraduate Emily Chen (UT Austin). Testing showed that Trikey had to be more robust mechanically and easier to control. Later redesign headed by Gupta intended to replace the motors and gearboxes and make Trikey controllable with a Linux system PC.

Paine and visiting professor Sehoon Oh (University of Tokyo) also helped write control drivers at that time. The latest redesigns headed by Wong intended to integrate new electronics hardware from Meka Robotics (San Francisco, CA) to replace old hardware, and also to connect the humanoid robotic torso (Meka Robotics) on top of Trikey. Undergraduates Vansi Vallabhaneni (Carnegie Mellon University) and Alan Kwok (UT Austin) helped with machining and assembly of the latest version, while Gupta constructed electrical connectors and debugged the system with Meka Robotics.

Several persons already mentioned contributed to the multiple design reviews up to this point. Somudro Gupta has documented [15] design details particularly for Trikey versions 1 and 3, while focusing on basic modeling and control algorithms for the robot. Algorithms based on Dr. Sentis's past research were implemented by Josh Petersen in Fall 2011 (UT Austin, Imperial College London) and are still being refined. The work conducted by Wong specifically between Fall 2010 and Spring 2012 is detailed here, which focuses on the electromechanical design and evaluation of Trikey versions 2, 4, and 5. Trikey Version 5 has been joined with another robotic humanoid torso in the Dreamer project, which is being taken over by UT doctoral candidate Kwan Suk Kim.

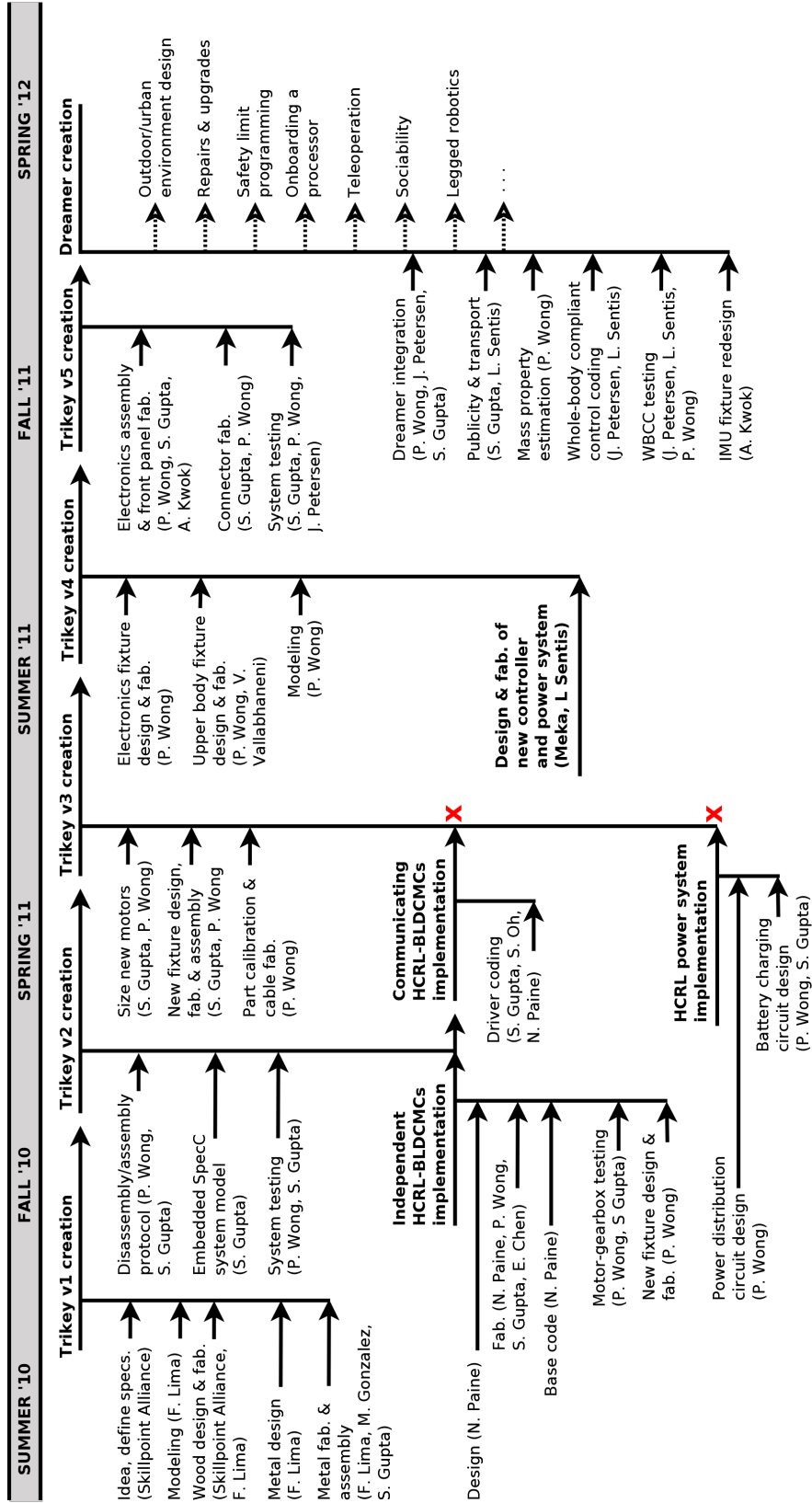


Figure 1.3: Timeline of tasks leading to the creation of the latest version of Trikey and Dreamer. The red “X” denotes that the task was discontinued from further development.

Chapter 2

Design History

Since its beginning, the Trikey design has been modified significantly to improve and expand its functions. Its history was first documented by Gupta [15] and is summarized here with additional details on Trikey Versions 2 and 4, leading into the current design of Trikey 5 and Dreamer. All files were created in SolidWorks 2010 or 2011 (Dassault Systèmes SolidWorks Corp, Waltham, MA) with a temporary student license.

2.1 *Trikey* Version 1

Version 1 was designed (Summer-Fall 2010) for the following functions, performed by certain features (Table 2.1).

Table 2.1: Function-feature list, Trikey Version 1

Function	Performed by Feature
• Allow omnidirectional translation	• Three holonomic omniwheels
• Allow simpler controls	• Three holonomic omniwheels
• Carry payloads, Meka upper body (>100 lbs)	• Metal baseplate, overdesigned joints
• House an undetermined amount of electronics and low-cost motors	• Extra internal space

The Meka upper body was to rest on a wooden outer frame (Fig. 2.1). Spaces for batteries are shown as three large blocks. A shelf for holding electronics was

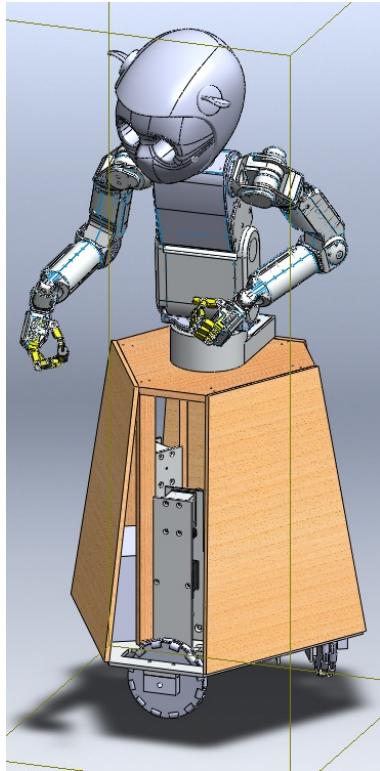


Figure 2.1: Trikey Version 1, in Dreamer concept.

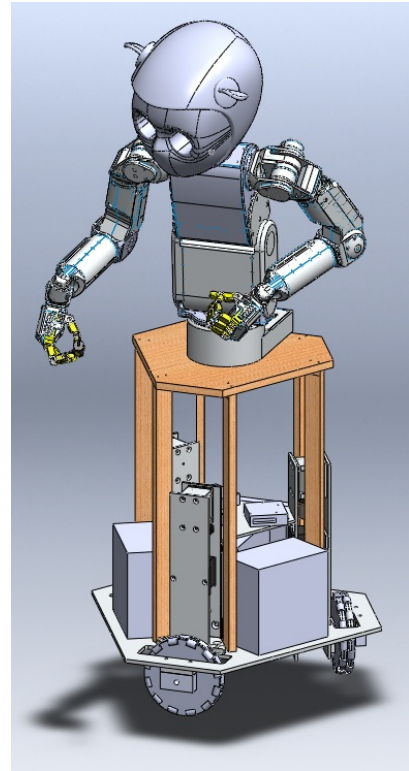


Figure 2.2: Trikey Version 1, in Dreamer concept, with open walls.

included in the middle. Everything in this design was physically constructed except the batteries and shelf. The Meka upper body was available but not connected to the wooden shell.

Three wheel modules fit into the main baseplate. The modules included a hobbyist brushless DC motor and planetary gearbox (Moog, via eBay, unknown rated torque, 66:1 gear ratio), torque cell (500 in-lbs, Sensor Developments, Lake Orion, MI), torque limiter (60 Nm, R+W, Bensenville, IL), and omnidirectional wheel (Banebots, Loveland, CO). This design set the base size and geometry of Trikey, to be modified later.

2.2 *Trikey* Version 2

Version 2 was redesigned for the following functions, with changes italicized (Table 2.2).

Table 2.2: Function-feature list, Trikey Version 2

Function	Performed by Feature
<ul style="list-style-type: none"> • Allow omnidirectional translation • Allow simpler controls • Carry payloads, Meka upper body (>100 lbs) • <i>House custom motor controllers, low-cost motors, additional undetermined electronics</i> 	<ul style="list-style-type: none"> • Three holonomic omniwheels • Three holonomic omniwheels • Metal baseplate, overdesigned joints • <i>Motor controller fixation plates, extra internal space</i>

Placement of the motor controllers on the base varied as shown in Figs. 2.3 and 2.4. Version 2A was constructed and not 2B, in order to protect the electronics more on the inside of the robot. By this time three custom HCRL brushless DC

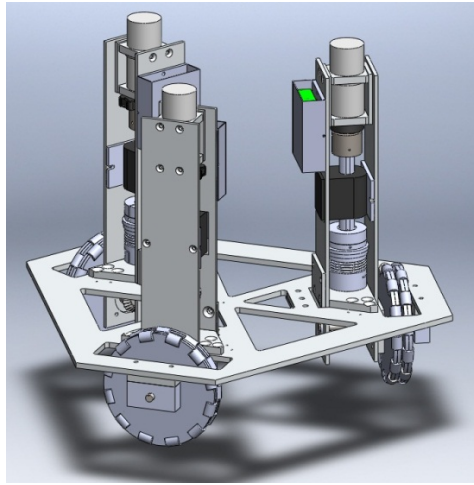


Figure 2.3: Trikey Version 2A: inner-facing controllers.

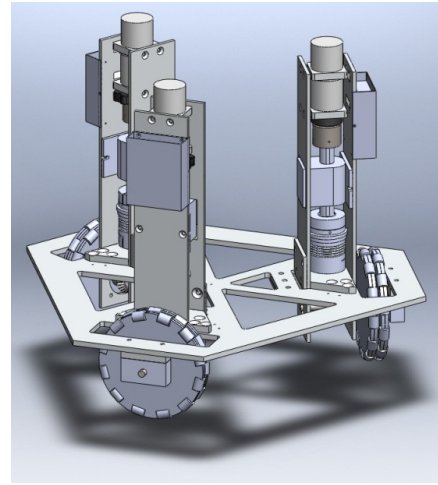


Figure 2.4: Trikey Version 2B: outer-facing controllers.

motor controllers (HCRL-BLDCMC, Fig. 2.5) were designed, soldered together, tested, and integrated into the mechanical system. Testing and calibration of the motor controllers, torque cells, and torque limiters was performed together with the HCRL-BLDCMCs (see Section 6.1).

At the time (Fall 2011), significant work was also done to explore the possibility of installing a custom AC-DC and battery-charging circuit using robust commercial hardware (Vicor Power, Andover, MA). One draft higher-level design of this circuitry is shown in Fig. 2.6. Additional details on this power management system are not given here since, after this design review, it was decided to outsource its design and construction.

Testing of the complete base at this time (Spring 2010) indicated that these lower-cost motor-wheel modules were not sufficiently robust. Backlash, friction, and susceptibility to shaft misalignment all reduced the ease of control of the wheels

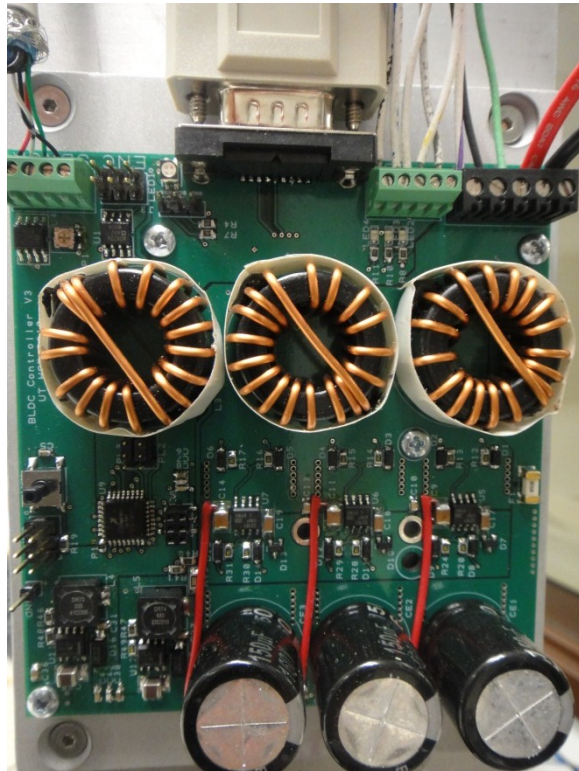


Figure 2.5: In-house Human Centered Robotics Laboratory brushless DC motor controller (HCRL-BLDCMC), designed by Nick Paine.

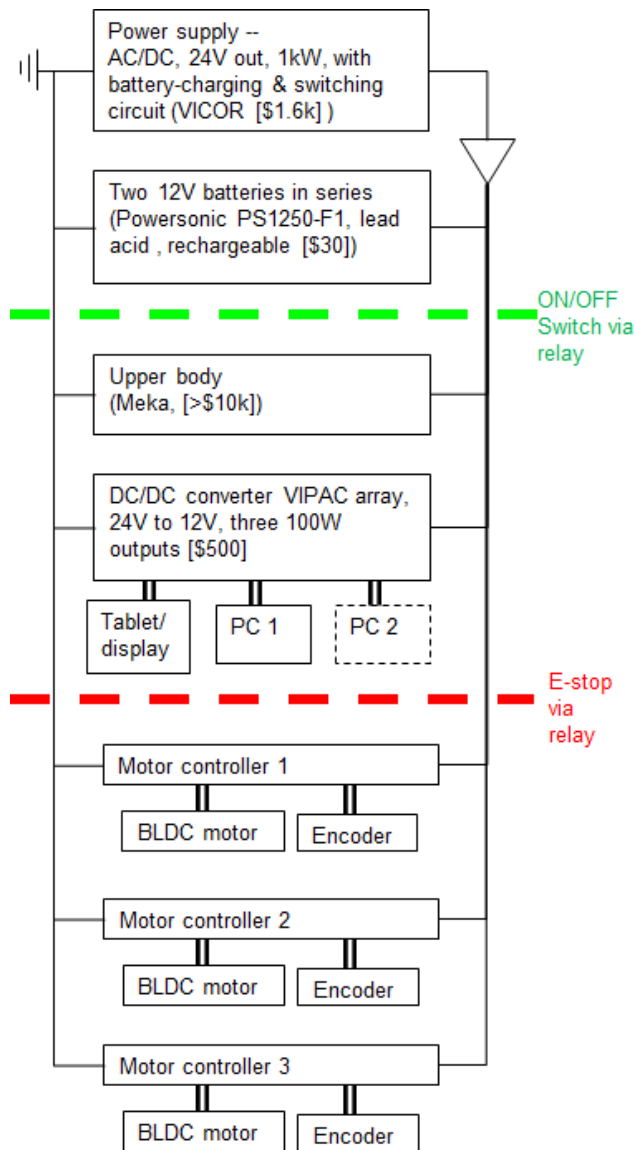


Figure 2.6: Initial top-level power management system designed for Trikey Version 2, which was intended to be mostly custom-designed in-house.

(see Section 6.2). Ultimately the next version had to accommodate newer industrial motors and gearboxes. Meka Robotics (San Francisco, CA) was chosen to head the power system design, since it was important to have the same team that designed the upper body deal with the electronics for the lower body. The UT HCRL in turn upgraded the hardware, as described in the next version.

2.3 *Trikey* Version 3

Version 3 was a modification of Version 2, designed (Spring 2011) for the following functions, with changes from the previous design italicized (Table 2.3).

Table 2.3: Function-feature list, *Trikey* Version 3

Function	Performed by Feature
<ul style="list-style-type: none"> • Allow omnidirectional translation • Allow simpler controls • Carry payloads, Meka upper body (>100 lbs) • House custom motor controllers, <i>OEM motors</i>, additional undetermined electronics • <i>Allow some motor axis misalignment</i> 	<ul style="list-style-type: none"> • Three holonomic omniwheels • Three holonomic omniwheels • Metal baseplate, overdesigned joints • Motor controller fixation plates, <i>new custom motor fixtures</i>, extra internal space • <i>Additional coupler between torque cell and motor</i>

The less robust MOOG motors were replaced with more robust Maxon brushless DC (BLDC) motors and gearboxes (EC-45-13610, 240 W, Sachseln, Switzerland). The fixation mechanisms were updated appropriately for the retrofit. Each of the three wheel modules were redesigned as shown in Fig. 2.7, with new fixation structures. New motor controllers were not yet available, and so these modules were tested using the same electronics as in Version 2. A full justification of part selection

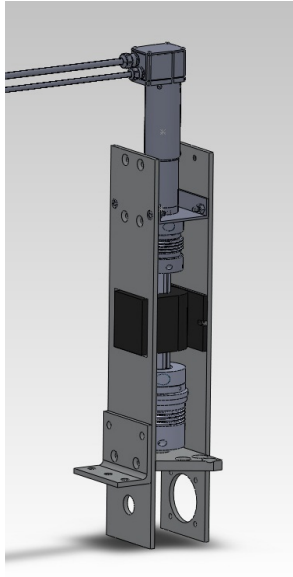


Figure 2.7: Wheel module with new, higher torque motor and gearbox.

is given by Gupta [15].

2.4 *Trikey* Version 4

Version 4 added the new functional requirement of securing the Meka upper body at an as-yet undefined position over the base, while incorporating Meka electronics. At the time of design (Summer 2011), the desired applications of the complete robot (*Trikey* + upper body, or *Dreamer*) were still being defined. For example, the *Dreamer* robot could be designed to work in an assembly-line manufacturing environment in front of a table, or it could be designed for an outdoor environment picking up objects off the ground. These different goals would alter key design characteristics, such as height or center of balance. At the same time, delaying the design was harmful to the long-term viability of the project, since fund-

ing depended on progress to date. Some design decisions had to be made despite uncertainties. This reflects some industry design dilemmas.

To deal with the uncertainty in design goals, two alternative designs to Version 4 were drafted to allow multiple functions for the upper body. Close communication with Meka was required to design fixtures for the electronics, which had not yet been fully designed nor fabricated. The electronics fixtures were intended to comprise a single module that could be moved within (or removed from) Trikey as a single unit.

The desired functions in Trikey version 4 were as follows, with additions italicized (Table 3.1).

Table 2.4: Function-feature list, Trikey Version 4

Function	Performed by Feature
• Allow omnidirectional translation	• Three holonomic omniwheels
• Allow simpler controls	• Three holonomic omniwheels
• Carry payloads, Meka upper body (>100 lbs)	• Metal baseplate, overdesigned joints
• House OEM motors <i>and controllers</i> , additional undetermined electronics	• Custom motor fixtures, extra internal space
• Allow some motor axis misalignment	• Additional coupler between torque cell and motor
• <i>House 4 Meka PCBs, other electronics</i>	• <i>Electronics module at base</i>
• <i>Run on battery power</i>	• <i>2 nylon holders for 2 batteries each</i>
• <i>House Beckhoff EtherCAT-compatible PC</i>	• <i>Fixtures in central shelf equidistant to wheels</i>
• <i>Fix upper body at multiple heights</i>	• <i>Vertical plates with multiple fixation holes</i>
• <i>Allow multiple discrete forward-backward placements of upper body</i>	• <i>Horizontal plates with multiple fixation holes</i>

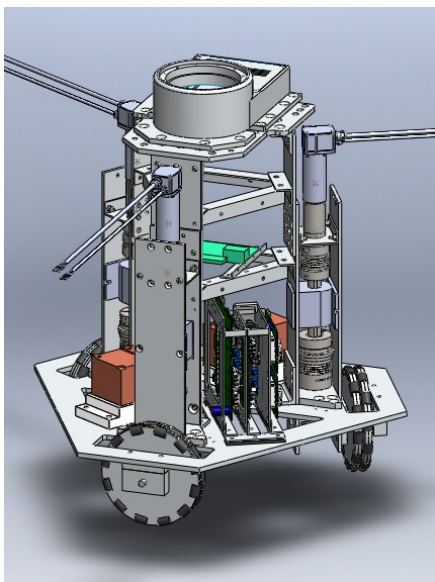


Figure 2.8: Trikey Version 4A: Higher waist, front facing a motor.

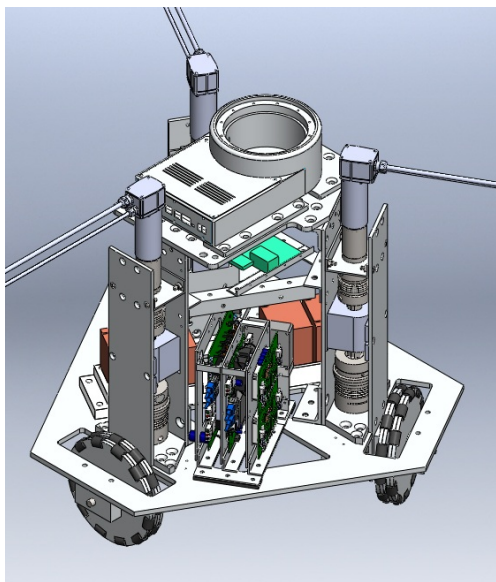


Figure 2.9: Trikey Version 4B: Lower waist, rear facing a motor.

Trikey Version 4A (Fig. 2.8) allowed placement of the upper body at heights greater than approximately 28 in from the ground, whereas Version 4B (Fig. 2.9) allowed only a fixed height of 22.5 in. Version 4A also allowed a greater amount of forward offset of the upper body, since none of the wheel modules obstructed the upper body. Version 4B had limited forward-backward positioning variability since the modules would block the upper body from moving too far forward.

The main advantage of Version 4B was the closer reach to the ground and possible increase in stability due to a lower center of mass (CoM). However, Version 4A was chosen for proceeding designs, since 4B could still not guarantee the ability of the Dreamer robot to touch the floor, which was the purpose of 4B in the first place. Version 4A would have more flexible capabilities.

In both alternate designs, the general layout of the electronics and batteries modules was the same (Fig. 2.10). The layout attempted to fit new electronics compactly into the existing space.

2.4.1 Electronics Module Version 1

The electronics module also saw multiple design iterations in this phase. The intention of the module was to house multiple pieces of electronics hardware from Meka, remain lightweight and lower-cost, fit within the existing Trikey frame, and be easy to put together and access for a user.

At first, the electronics module was designed to allow variable positioning of all the electronics boards (Fig. 2.11), since the designs of the electronics were not complete yet and could change. Design review deemed this first setup too difficult

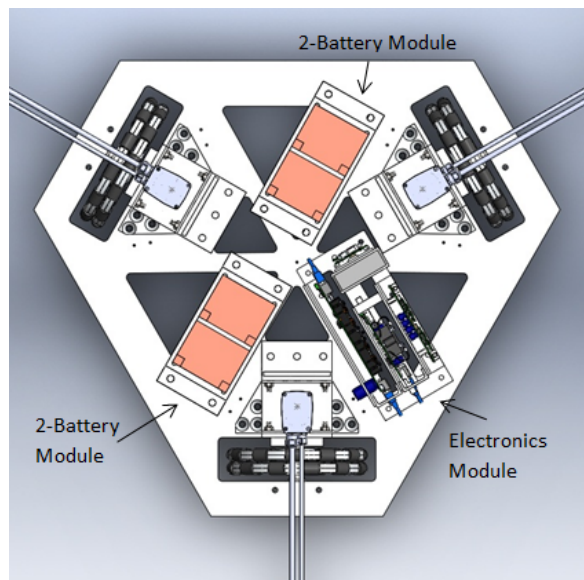


Figure 2.10: Trikey Version 4 layout of batteries and electronics on the base.

to assemble and access, with too many parts. Furthermore although certain parts were OEM, the cost was excessive.

The first design was improved to reduce the number of parts, at the cost of less flexibility in positioning of the electronics. Less flexibility in positioning was acceptable, based on the assumption that Meka has good experience designing electronics; if Meka designed a good system, we would not need to replace, troubleshoot, or access the PCBs frequently. Lab experience with the Meka upper body supported this assumption.

2.4.2 Electronics Module Version 2

Version 2 of the electronics module (Fig. 2.12) has fewer parts than version 1. It also incorporates better mechanisms for cooling the PCBs (fan, metal surfaces

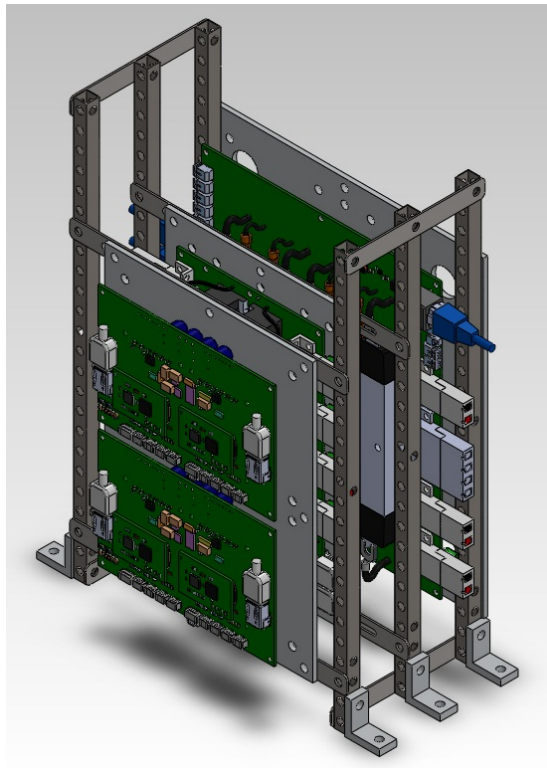


Figure 2.11: Electronics module, version 1.

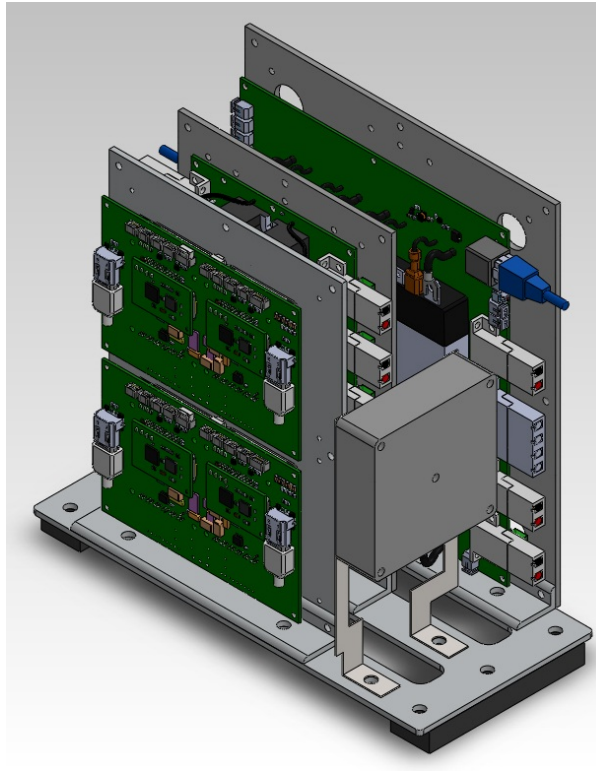


Figure 2.12: Electronics module, version 2.

for heat dissipation, space for thermal pads). Cooling was recommended mostly for the motor driver PCB, whose MOSFETS could see significant heat according to communications with Meka. Special attention was given to allowing hand and finger access to the various ports on all the PCBs. Fabrication of some parts, including the PCB fixation plates, was performed in the UT machine shop. The PCB fixation plates were 1/8" (6.35 mm) thick aluminum plates to allow for a stiff support for the plastic PCBs, but with holes in the center to make room for large capacitors and reduce weight. Rubber feet were added on the bottom to reduce vibration into the electronics module.

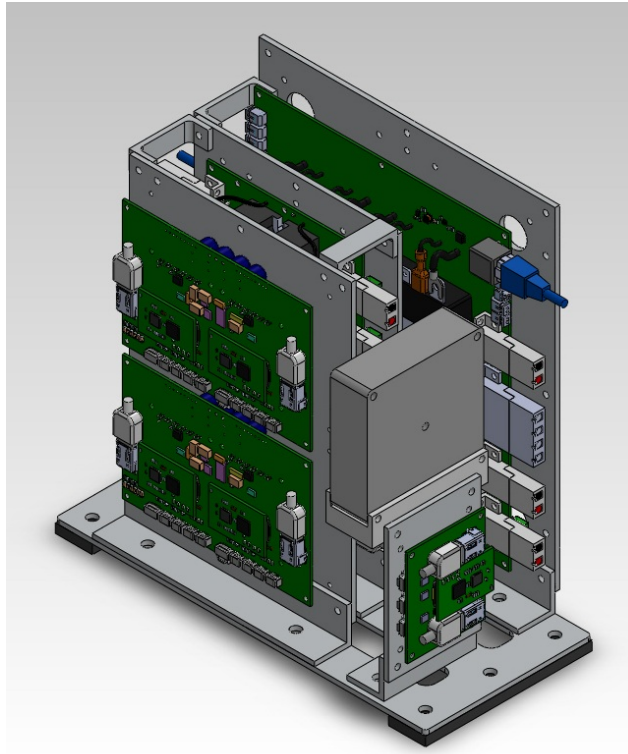


Figure 2.13: Electronics module, version 3.

2.4.3 Electronics Module Version 3

Midway during the fabrication process of the electronics module (Summer 2011), the electronics system had to be modified to also include hardware for an Attitude Heading Reference System (AHRS) , which was an inertial measurement unit or accelerometer-compass. Incorporating the AHRS was an unforeseen design change. This was integrated into the existing design, leading to Version 3 of the module (Fig. 2.13). Additional structures that joined the PCB support plates were added to improve resistance to torsion and vibration on the module. Version 3 ended up continuing into the next design revisions of Trikey and Dreamer overall.

These electronics were controlled via UBUNTU with RealTime Application Interface (RTAI) and M3 control software from Meka Robotics. The controller is currently in development, concurrent with design of future upgrades to the mechanical system.

Chapter 3

Implemented Design: *Trikey* Version 5

3.1 Functions

The latest revision (*Trikey* Version 5) was designed with the following functions, with specifications for individual OEM components listed in Gupta [15]. From this point onward (Sep 2011), the *Trikey* project was pipelined into the overall Dreamer project (see Chapter 5).

The three omniwheels are oriented around the center of the base, allowing three degrees of freedom of motion on a surface. Because omniwheels instead of caster wheels were used, motion can begin without having to orient any wheels, thereby simplifying the control algorithm. Also, each wheel has a load capacity of 100 lbs, giving a theoretical total weight limit for Dreamer of 300 lbs, which dictated the more conservative 250 lbs weight limit during initial design calculations.

Trikey is intended to hold at least a 100 lbs (45 kg) payload, which corresponds with the approximate mass of the Meka upper body. Gupta [15] documented the finite element analysis (FEA) that was performed to verify the strength of the large bottom aluminum baseplate for sustaining such a vertical load in addition to the weight of *Trikey*, itself. Additional FEA was performed to verify the strength of other parts predicted to see the highest stresses during worst-case movements or configurations of the Dreamer robot (see Chapter 4).

Table 3.1: Function- and constraint-feature list, Trikey Version 5

Function	Performed by Feature
<ul style="list-style-type: none"> • Allow omnidirectional translation • Allow simpler controls • Carry payloads, Meka upper body (>100 lbs) • Weight limit of 250 lbs (110 kg) 	<ul style="list-style-type: none"> • Three holonomic omniwheels • Three holonomic omniwheels • Metal baseplate, overdesigned joints
<ul style="list-style-type: none"> • House OEM motors and controllers • Allow some motor axis misalignment 	<ul style="list-style-type: none"> • Light aluminum material, empty space/holes • Custom motor fixtures
<ul style="list-style-type: none"> • Allow some motor axis misalignment 	<ul style="list-style-type: none"> • Additional coupler between torque cell and motor
<ul style="list-style-type: none"> • House 5 Meka PCBs, other electronics • Run on battery power • House Beckhoff EtherCAT-compatible PC 	<ul style="list-style-type: none"> • Electronics module at base • 2 nylon holders for 2 batteries each • Space for PC in upper shelves
<ul style="list-style-type: none"> • Fix upper body at multiple heights 	<ul style="list-style-type: none"> • Vertical plates with multiple fixation holes
<ul style="list-style-type: none"> • Allow multiple discrete forward-backward placements of upper body 	<ul style="list-style-type: none"> • Horizontal plates with multiple fixation holes
<ul style="list-style-type: none"> • Allow clear space 	<ul style="list-style-type: none"> • Vertical plates with multiple fixation holes

The design incorporates OEM components into independent modules within the base where possible. Most of the electronics were designed by Meka Robotics (see Section 2.4). Cable holders were fixed to Trikey Version 5 to route interconnecting wires cleanly through the base. Another change from Trikey Version 4 to 5 includes moving the AHRS/IMU from the center, away from the motor winding magnetic fields, and onto the outer portion of the main baseplate.

Trikey Version 5 allows discretely variable positioning of its payload – i.e. the Meka upper body can rest on top of Trikey in multiple positions (Figs. 3.3-3.6).

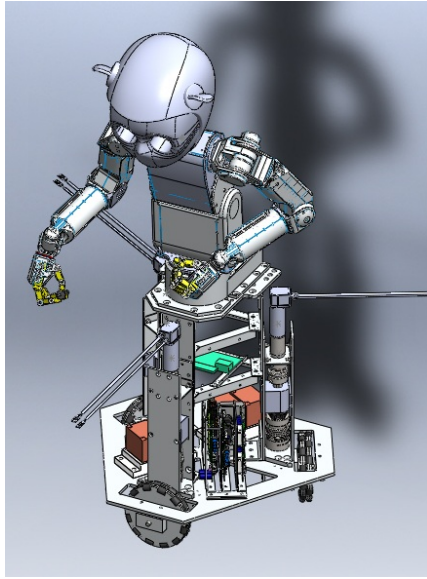


Figure 3.1: Dreamer Version 1: CAD.

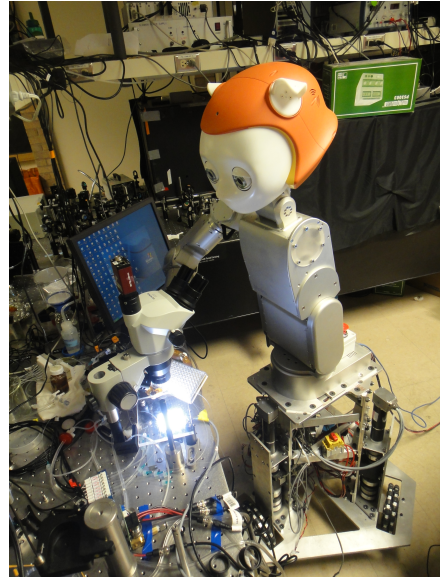


Figure 3.2: Dreamer Version 1: Built.

This function was addressed by adding additional parts to the original wheel-motor module, rather than making entirely new modules, in order to reduce fabrication time and meet project deadlines.

Not all the fixation holes available in the plates may be used to secure the Meka upper body at a given position. More intermediate positions are possible than shown in Fig. 3.5, but at such intermediate positions the upper body is less secure, since even fewer fixation holes may be used. This positioning flexibility accommodates some uncertainty in the ultimate function of the Dreamer robot. A zero-offset position may be more balanced and stable, while a 5 in.-offset position may give better grasping range.

Some key geometric measurements that are important for devising the control algorithm and for analyzing different loading conditions are shown in Fig. 3.7.

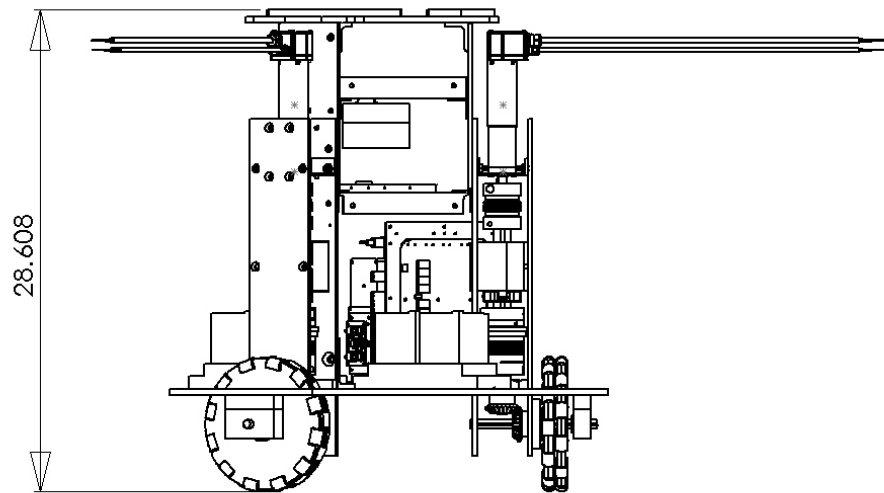


Figure 3.3: CAD drafting of shortest possible height of the latest Trikey design at 28.6in above the floor. Dreamer is currently set atop Trikey with the waist at this height, in order to lower the center of gravity and improve balance.

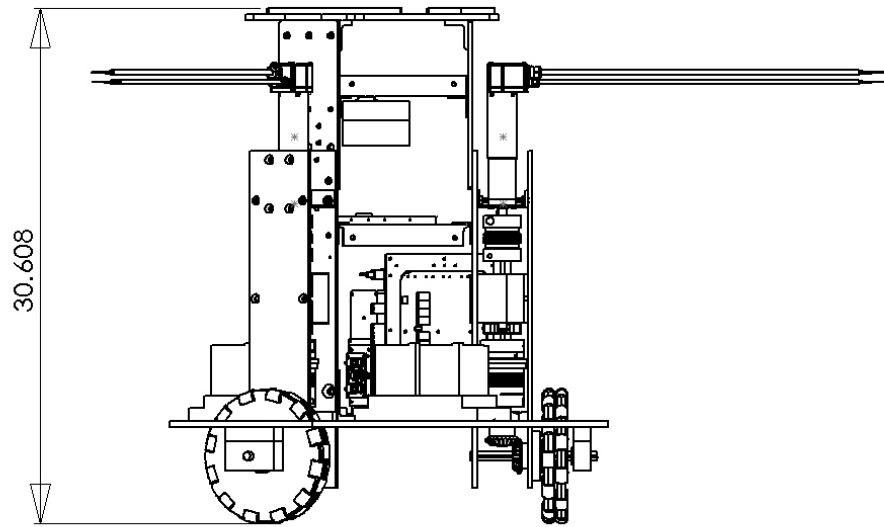


Figure 3.4: CAD drafting of tallest possible height of the latest Trikey design at 30.6in above the floor. 29.6in tall is also possible.

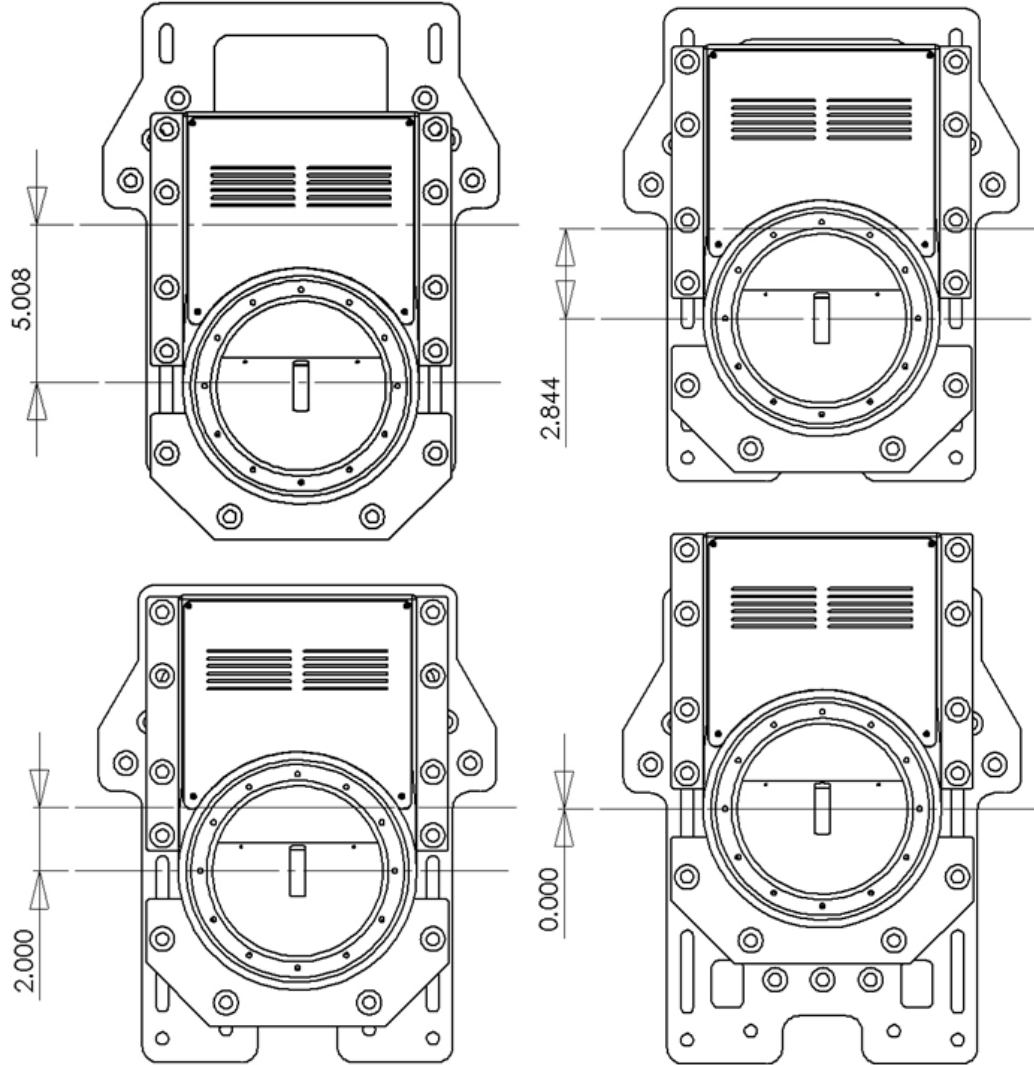


Figure 3.5: Top-down views of the Trikey fixation plates, with Meka upper body base attached. Four main horizontal positions are possible for the Meka upper body, shown here. Assuming an upright upper body, the approximate center of mass of the upper body can lie 5.0 in, 2.8 in, 2.0 in, and 0.0 in in front of the geometric center of the Trikey mobile base.

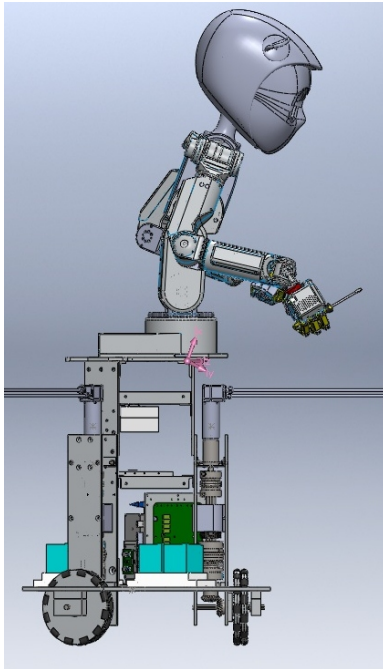


Figure 3.6: Side view of an example extreme upper body configuration for Dreamer. Shown here is the most forward position of the Meka upper body (5.0 in in front of the center of the Trikey base) and the tallest position (waist 30.6 in above the floor). The center of mass in this configuration lies at waist-level denoted by the pink axes.

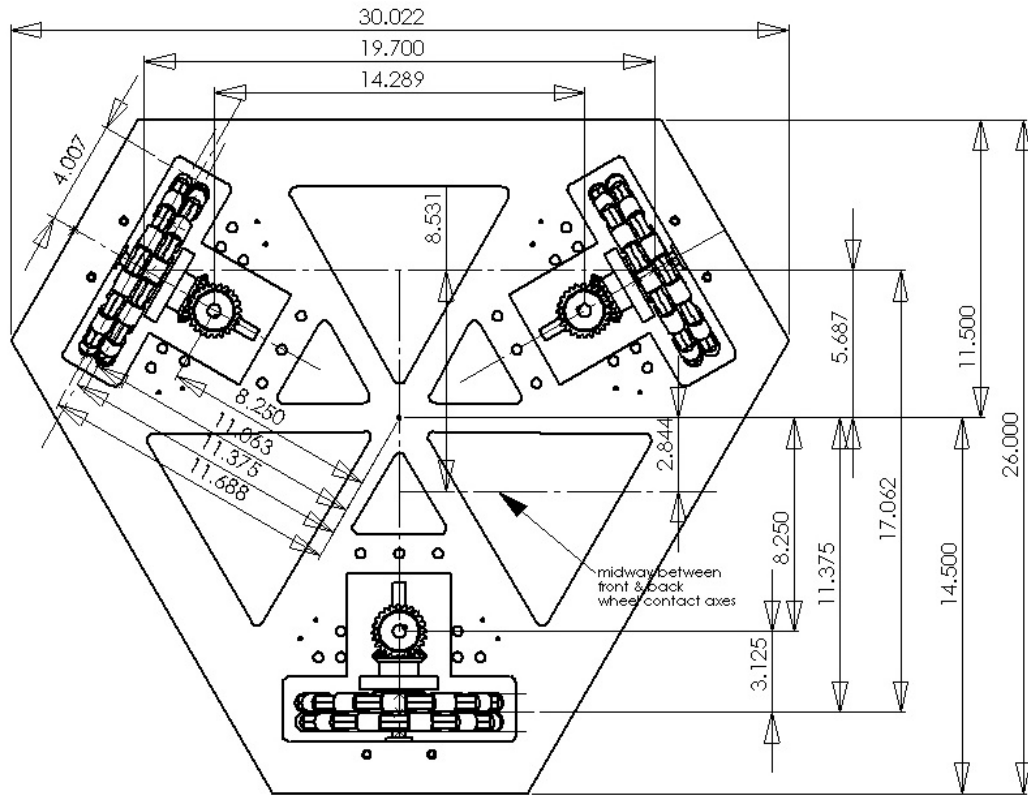


Figure 3.7: Drafting showing some measurements that may be useful for design analysis and for writing the control algorithm. Example measurements include the horizontal distance between the geometric center and the point of wheel contact with the floor.

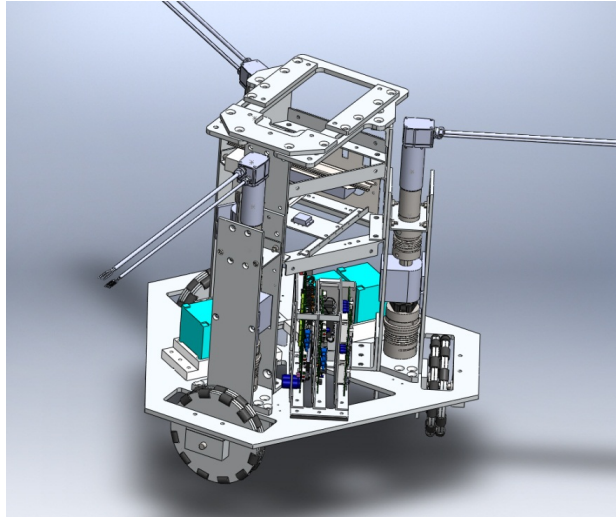


Figure 3.8: Latest CAD of Trikey assembly.

3.2 Modules

The seven main modules of the Trikey base (Fig. 3.8) are (A) the baseplate and lower frame, (B) the three wheel-motor modules, (C) the electronics module, (D) the two double-battery modules, (E) the EtherCAT hub module, (F) the mid-shelf module, and (G) the upper body fixation module (Fig. 3.9). (H) is an eighth “module” made of miscellaneous parts that were not directly modeled. Additional fasteners are not shown. Each module was mostly designed as an independent unit that can be changed later without altering other modules.

The approximate cost of building Trikey Version 5 is, at minimum, \$24k, based on spending records (Table 3.2). This does not completely cover miscellaneous costs such as taxes, shipping, tools, labor, and unused components of previous designs, and so real costs likely exceed this estimate.

Table 3.2: List of Modules

Label	Module	Description	Qty	Total mass (kg)	Total cost (est)	Cost density (\$/kg)
A	Baseplate & lower frame	basic support and frame	1	6.3	\$360	\$57
B	Wheel-motor module	drives movement	3	22.7	\$13,211	\$583
C	Electronics module	houses most electronics	1	2.7	\$8,675	\$3,259
D	Double-battery module	houses batteries	2	7.2	\$103	\$14
E	EtherCAT hub module	houses communications hardware	1	0.2	\$319	\$1,733
F	Mid-shelf module	mechanical support, storage, panel	1	1.5	\$390	\$266
G	Upper body fixation module	attaches to Meka upper body	1	2.3	\$572	\$251
H	Additional miscellaneous parts	Fasteners, wires, connectors, etc.	1	6.8	\$268	\$39
TOTAL				49.6	\$23,898	\$481

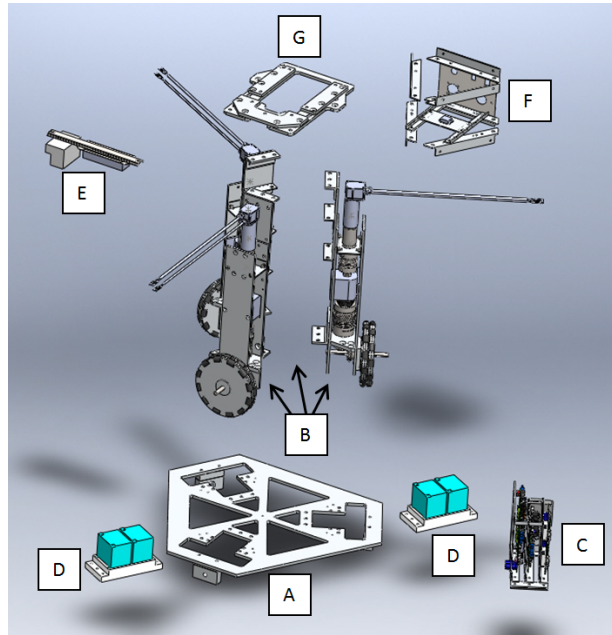


Figure 3.9: Exploded view of Trikey main modules. See Table 3.2 for details.

3.3 Bill of Materials

A bill of materials is provided in Table 3.3. Module H is not a true module but rather includes fasteners, wires, and other miscellaneous necessary parts.

Table 3.3: Full Bill of Materials: Trikey Version 5

Mod-Part ule no.	Part	Description/ Mfegr. part no.	Qty. per mod.	Maker/ Mfegr.	Mat./ Prod. Vendor	Material	Mass (kg)	Unit price	Total Total qty. mass price (kg)	Price
A Baseplate & Lower frame (1)										
A 1	Baseplate	base sup- port	1	laser- cutter	metals4u .com	Aluminum	5.3	\$300.00	1 5.3 \$300.00	estimate
A 2	Bearing block	supports axle	3	unknown	unknown	Steel	0.1	\$10.00	3 0.3 \$30.00	estimate
A 3	Spacer block	supports bearing	3	F. Lima	metals4u .com	Aluminum	0.2	\$10.00	3 0.7 \$30.00	estimate
B Wheel-motor module (3)										
B 1	BLDC Mo- tor	EC-45, 24VDC, #136207	1	Maxon	Maxon	Steel, others	0.3	\$1,604.60	3 0.9 \$4,813.80	includes shipping
B 2	Gearbox	43:1 Plan- etary, #203120	1	Maxon	Maxon	Steel, others	0.8	NA	3 2.3 NA	included with B1
B 3	Gearbox mount	U-plate holding gearbox	1	S. Gupta	McMaster- Carr	Aluminum	0.1	\$30.00	3 0.3 \$90.00	estimate
B 4	Shaft cou- pler	BKL30	1	R+W	R+W	Steel	0.3	\$250.00	3 0.8 \$750.00	estimate
B 5	Torque sen- sor	01324-052	1	Sensor Develop- ments	Sensor Develop- ments	unknown	0.4	\$1,642.50	3 1.3 \$4,927.50	excluding shipping
B 6	2500 ppr Encoder Kit	E6-2500- 1000-ISHTB	1	US Digi- tal	US Digi- tal	Poly- carbonate	0.0	\$94.29	3 0.0 \$282.87	excluding shipping
B 7	Torque lim- iter/ Clutch	SK2/60/10/D/ 12.7PFN	1	R+W	R+W	Steel	1.0	\$394.91	3 3.0 \$1,184.73	excluding shipping
B 8	Bearing mount, upper	holds verti- cal shaft	1	F. Lima	unknown	Aluminum	0.3	\$50.00	3 1.0 \$150.00	estimate

Continued on next page...

Table 3.3 ...continued from previous page

Mod-Part ule no.	Part	Description/ Mfgr. part no.	Qty. per mod.	Maker/ Mfgr.	Mat./ Prod. Vendor	Material	Mass (kg)	Unit price	Total qty.	Total mass (kg)	Total price	Price
B 9	Miter gear, upper	6529K22	1	unknown	McMaster- Carr	Steel	0.3	\$26.71	3	0.8	\$80.13	excluding shipping estimate
B 10	Vertical shaft	holds miter gear	1	unknown	McMaster- Carr	Steel	0.1	\$10.00	3	0.3	\$30.00	estimate
B 11	Horizontal shaft	holds miter gear	1	unknown	McMaster- Carr	Steel	0.2	\$15.00	3	0.5	\$45.00	estimate
B 12	Miter gear, lower	6529K22, shortened	1	unknown	McMaster- Carr	Steel	0.3	\$26.71	3	0.8	\$80.13	estimate
B 13	Vertical plate, outer	supports module	1	F. Lima	unknown	Aluminum	0.8	\$40.00	3	2.5	\$120.00	estimate
B 14	Vertical plate, inner	supports module	1	F. Lima	unknown	Aluminum	0.8	\$40.00	3	2.3	\$120.00	estimate
B 15	Bearing mount, lower	holds hori- zontal shaft	1	F. Lima	unknown	Aluminum	0.2	\$20.00	3	0.5	\$60.00	estimate
B 16	Omniwheel	am-0559	1	AndyMark	AndyMark	Aluminum, 1.0 Rubber	1.0	\$107.00	3	2.9	\$321.00	excluding shipping estimate
B 17	Vertical plate, upper	8975K424	1	P. Wong	McMaster- Carr	Aluminum	0.4	\$10.16	3	1.3	\$30.49	excluding shipping estimate
B 18	L-bracket, large	base-module connection	1	F. Lima	unknown	Aluminum	0.2	\$10.00	3	0.6	\$30.00	estimate
B 19	L-bracket, top	8982K344	1	UT ME shop	McMaster- Carr	Aluminum	0.1	\$11.88	3	0.4	\$35.64	excluding shipping estimate
B 20	L-bracket, small	anodized	2	P. Wong	McMaster- Carr	Aluminum	0.1	\$10.00	6	0.3	\$60.00	estimate
C	Electronics module (1)											

Continued on next page...

Table 3.3 ...continued from previous page

Mod-Part ule no.	Part	Description/ Mfgr. part no.	Qty. per mod.	Maker/ Mfgr.	Mat./ Prod. Vendor	Material	Mass (kg)	Unit price	Total qty.	Total mass (kg)	Total price	Price
C 1	Electronics baseplate	8975K923	1	P. Wong	McMaster- Carr	Aluminum	0.2	\$20.00	1	0.2	\$20.00	estimate
C 2	BBB plate	89015K18	1	P. Wong	McMaster- Carr	Aluminum	0.2	\$29.05	1	0.2	\$29.05	excluding ship- ping, labor
C 3	BBB bracket	support	1	P. Wong	McMaster- Carr	Aluminum	0.1	\$10.00	1	0.1	\$10.00	estimate
C 4	BBB PCB for DC-DC	has Vicor Megamod	1	Meka Robotics	Meka Robotics	various	0.9	\$2,000.00	1	0.9	\$2,000.00	estimate
C 5	PWR plate	8975K923	1	P. Wong	McMaster- Carr	Aluminum	0.1	\$20.00	1	0.1	\$20.00	estimate
C 6	PWR PCB	power & comm.	1	Meka Robotics	Meka Robotics	various	0.4	\$2,000.00	1	0.4	\$2,000.00	estimate
C 7	PWR bracket	support	1	P. Wong	McMaster- Carr	Aluminum	0.1	\$10.00	1	0.1	\$10.00	estimate
C 8	ELMO plate	8975K923	1	P. Wong	McMaster- Carr	Aluminum	0.1	\$20.00	1	0.1	\$20.00	estimate
C 9	ELMO PCB	motor am- plifier, driver	2	Meka Robotics	Meka Robotics	various	0.2	\$2,000.00	2	0.3	\$4,000.00	estimate
C 10	ELMO bracket	support	1	P. Wong	McMaster- Carr	Aluminum	0.1	\$10.00	1	0.1	\$10.00	estimate
C 11	Fan	DC12V, FD8025B12W7	1	Cooltron	UT Physics store	Poly- ethylene	0.0	\$5.60	1	0.0	\$5.60	discount
C 12	Foot	support	2	unknown	McMaster- Carr	Rubber	0.0	\$5.00	2	0.0	\$10.00	estimate
C 13	Load plate	cell 8975K923	1	P. Wong	McMaster- Carr	Aluminum	0.0	\$10.00	1	0.0	\$10.00	estimate

Continued on next page...

Table 3.3 ...continued from previous page

Mod-Part ule no.	Part	Description/ Mfcgr. part no.	Qty. per mod.	Maker/ Mfcgr.	Mat./ Prod. Vendor	Material (kg)	Mass Unit price	Total qty.	Total mass price (kg)	Price
C	14	Load cell PCB Load cell support bracket	1	Meka Robotics	Meka Robotics	various	0.0	1	0.0	\$500.00 \$500.00 estimate
C	15	Load cell support bracket	1	P. Wong Robotics	McMaster- Carr	Aluminum	0.0	1	0.0	\$10.00 \$10.00 estimate
C	16	Fan fixture	1	P. Wong	McMaster- Carr	Poly- ethylene	0.0	1	0.0	\$5.00 \$5.00 estimate
C	17	Strut	3	P. Wong	unknown	Aluminum	0.0	3	0.0	\$15.00 \$15.00 estimate
D	Double-battery module (2)									
D	1	Battery holder	1	P. Wong, V. Val- labha- neni	McMaster- Carr	Poly- ethylene	0.4	2	0.8	\$20.00 \$40.00 estimate
D	2	Battery, 12V, 5A-hr	2	Powersonic	Allied Elec- tronics	various	1.6	4	6.4	\$15.72 \$62.88 excluding shipping
D	3	Zip tie(s)	1	unknown	unknown	Poly- ethylene	0.0	2	0.0	\$0.05 \$0.10 estimate
E	EtherCat hub module (1)									
E	1	DIN rail 3	1	unknown	McMaster- Carr	Steel	0.2	1	0.2	\$8.84 \$8.84 estimate
E	2	EtherCat hub	1	Beckhoff	Meka Robotics	various	0.0	1	0.0	\$200.00 \$200.00 estimate
E	3	Step up- down con- verter	1	unknown	Meka Robotics	various	0.0	1	0.0	\$100.00 \$100.00 estimate
E	4	Sheet metal for at- taching converter	1	A. Kwok	unknown	aluminum	0.0	1	0.0	\$10.00 \$10.00 estimate

Continued on next page...

Table 3.3 ...continued from previous page

Mod-Part ule no.	Part	Description/ Mfgr. part no.	Qty. per mod.	Maker/ Mfgr.	Mat./ Prod. Vendor	Material	Mass (kg)	Unit price	Total qty.	Total mass (kg)	Total price	Price
F	Mid-shelf module (1)											
F	1	Shelf bar, lower	3	P. Wong	McMaster- Carr	Aluminum	0.1	\$10.00	3	0.4	\$30.00	estimate
F	2	Shelf bar, upper	3	P. Wong	McMaster- Carr	Aluminum	0.1	\$10.00	3	0.3	\$30.00	estimate
F	3	Shelf rail	2	P. Wong	McMaster- Carr	Aluminum	0.1	\$3.00	2	0.1	\$6.00	estimate
F	4	Center plate for IMU attachment	1	A. Kwok	unknown	Aluminum	0.1	\$10.00	1	0.1	\$10.00	estimate
F	5	Inertial Meas. Unit	1	MicroStrain	Meka Robotics	various	0.0	\$200.00	1	0.0	\$200.00	estimate
F	6	Back panel	1	A. Kwok, P. Wong	McMaster- Carr	Steel	0.5	\$34.39	1	0.5	\$34.39	excluding ship- ping, labor
F	7	Charge Box 7POS Conn	1	unknown	Meka Robotics	various	0.0	\$10.00	1	0.0	\$10.00	estimate
F	8	DPST power switch	1	unknown	Meka Robotics	various	0.0	\$20.00	1	0.0	\$20.00	estimate
F	9	E-stop, base	1	unknown	Meka Robotics	various	0.0	\$15.00	1	0.0	\$15.00	estimate
F	10	E-stop, re-mote	1	unknown	Meka Robotics	various	0.0	\$15.00	1	0.0	\$15.00	estimate
F	11	RJ45 jack	1	unknown	Meka Robotics	various	0.0	\$10.00	1	0.0	\$10.00	estimate
F	12	DPWR switch	1	unknown	Meka Robotics	various	0.0	\$10.00	1	0.0	\$10.00	estimate
G	Upper body fixation module (1)											

Continued on next page...

Table 3.3 ...continued from previous page

Mod-Part ule no.	Part	Description/ Mfgr. part no.	Qty. per mod.	Maker/ Mfgr.	Mat./ Prod. Vendor	Material	Mass (kg)	Unit price	Total qty.	Total mass (kg)	Total price	Price
G 1	Plate, waist	CNC- machined, 89155K28	1	UT ME shop	McMaster- Carr	Aluminum	1.4	\$571.53	1	1.4	\$571.53	includes labor
G 2	Plate, front	89155K28	1	UT ME shop	McMaster- Carr	Aluminum	0.4	NA	1	0.4	NA	included with G1
G 3	Plate, left	89155K28	1	UT ME shop	McMaster- Carr	Aluminum	0.2	NA	1	0.2	NA	included with G1
G 4	Plate, right	89155K28	1	UT ME shop	McMaster- Carr	Aluminum	0.2	NA	1	0.2	NA	included with G1
H	Additional miscellaneous parts & fasteners											
H 1	Bearings	6384K361	9	unknown	McMaster- Carr	Steel	0.0	\$8.52	9	0.2	\$76.68	excluding shipping estimate
H 2	Bolt, 3/8- 16, 1/2" or 3/4"	for frame	50	various	various	Steel	0.0	\$0.05	50	1.0	\$2.50	
H 3	Bolt, 3/8-16 1" flat	for frame	30	various	various	Steel	0.0	\$0.05	30	0.6	\$1.50	estimate
H 4	Bolt, 1/4-20 3/4"	for frame	100	various	various	Steel	0.0	\$0.05	100	2.0	\$5.00	estimate
H 5	Bolt, 1/4-20 5/8"	for frame	20	various	various	Steel	0.0	\$0.05	20	0.4	\$1.00	estimate
H 6	Bolt, 1/4-20 1-3/8"	for frame	10	various	various	Steel	0.0	\$0.05	10	0.2	\$0.50	estimate
H 7	Bolt, #6-32, 1/2", socket	for electron- ics module	14	various	UT Physics store	Steel	0.0	\$0.03	14	0.0	\$0.42	estimate
H 8	Bolt, #6-32, 3/8", socket	for electron- ics module	5	various	various	Steel	0.0	\$0.03	5	0.0	\$0.15	estimate
H 9	Bolt, #6-32 1-1/2"	for electron- ics module	2	various	various	Steel	0.0	\$0.03	2	0.0	\$0.06	estimate

Continued on next page...

Table 3.3 ...continued from previous page

Mod-Part ule no.	Part	Description/ Mfgr. part no.	Qty. per mod.	Maker/ Mfgr.	Mat./ Prod. Vendor	Material	Mass (kg)	Unit price	Total qty.	Total mass (kg)	Total price	Price
H 10	Bolt, #4-40, 1", socket	for electron- ics module	5	various	McMaster- Carr	Steel	0.0	\$1.00	5	0.0	\$5.00	estimate
H 11	Bolt, #4-40, 5/8" socket	for electron- ics module	10	various	various	Steel	0.0	\$0.05	10	0.1	\$5.00	estimate
H 12	Bolt, #2-56, 1", socket	91251A109	8	unknown	McMaster- Carr	Steel	0.0	\$0.03	8	0.0	\$0.24	estimate
H 13	Bolt, #2-56, 1/2", socket	for IMU	4	unknown	McMaster- Carr	Steel	0.0	\$0.03	4	0.0	\$0.12	estimate
H 14	Bolt, M8 15mm flat	for fixing Meka torso	7	unknown	McMaster- Carr	Steel	0.0	\$0.03	7	0.0	\$0.21	estimate
H 15	Nut, 1/4-20		130	various	various	Steel	0.0	\$0.03	130	0.1	\$3.90	estimate
H 16	Locknut, 1/4-20		20	various	various	Steel	0.0	\$0.03	20	0.0	\$0.60	estimate
H 17	Nut, 3/8-16		60	various	various	Steel	0.0	\$0.03	60	0.1	\$1.80	estimate
H 18	Nut, #6-32		20	various	various	Steel	0.0	\$0.03	20	0.0	\$0.60	estimate
H 19	Nut, #4-40		20	various	various	Steel	0.0	\$0.03	20	0.0	\$0.60	estimate
H 20	Nut, #2-56		10	various	various	Steel	0.0	\$0.03	10	0.0	\$0.30	estimate
H 21	Spacer, #4, 5/8"	9908-625	13	Bivar Inc	Digikey	Nylon	0.0	\$0.08	13	0.0	\$1.04	excluding shipping
H 22	Spacer, #4, 1/4"	492-1074- ND	5	Bivar Inc	Digikey	Nylon	0.0	\$0.07	5	0.0	\$0.35	excluding shipping
H 23	Snap rings	98585A109	6	unknown	McMaster- Carr	Steel	0.0	\$2.17	6	0.0	\$13.02	excluding shipping
H 24	Thermal pad, 0.40"	GP1500- 0.040-02- 0404	2	Bergquist	Digikey	polymer	0.0	\$8.25	2	0.0	\$16.50	excluding shipping
H 25	Torque cell connector	PT06E-12- 10S(SR)	3	Amphenol	Allied Elec- tronics	various	0.0	\$29.10	3	0.0	\$87.30	excluding shipping
H 26	Washers, various		50	various	various	Steel			50	0.5	\$5.00	estimate

Continued on next page...

Table 3.3 ...continued from previous page

Mod-Part ule no.	Part	Description/ Mfgr. part no.	Qty. per mod.	Maker/ Mfgr.	Mat./ Prod. Vendor	Material	Mass (kg)	Unit price	Total qty.	Total mass (kg)	Total price	Price
H 27	Wires			various	various	various				1.0	\$20.00	estimate
H 28	Solder			various	various	various			0	0.5	\$10.00	estimate
H 29	Set screws	various	15	various	various	various			15	0.0	\$1.00	estimate
H 30	Square keys, 1/4"	over- and undersized	15	various	various	various			15	0.0	\$1.00	estimate
H 31	Cable carri- ers		10	various	various	various			10	0.0	\$7.00	estimate

3.4 Exploded Views

Exploded views of the two most complex modules with many parts - the wheel-motor module and the electronics module - are given in Figs. 3.10 and 3.11. Fastener types are indicated in the original draftings (see Appendix 1 for file information).

The electronics module included submodules for housing printed circuit boards (PCBs) that handled powering, communicating with, and driving the Trikey motors and sensors. The “BBB” PCB submodule (Fig. 3.12) took in the input voltage from an AC-DC converted and included commercial power management hardware, including the Vicor Megamod and output the DC voltage to the next “PWR” submodule. The PWR submodule (Fig. 3.13) distributed 24VDC to the next motor driver PCBs or “ELMO” PCBs (Fig. 3.14), and it also communicated with the load cell conditioners (Fig. 3.15) and with a computer via a connected EtherCAT hub.

Each supporting plate for the PCBs were designed to be lightweight but rigid. Large cutouts in the BBB and PWR plates allow airflow and aid cooling. Gaps between parts were designed to allow finger and wrench access. The ELMO plate had no cutouts, as it could be cooled via conduction. A fan circulates air through this module, blowing inward. Nylon board spacers or standoffs are meant to hold the PCBs away from the plates, so as not to interfere with the electronics and to reduce the effect of any hole misalignment. Holes were not threaded, which could also help decrease the stresses in the PCBs associated with any possible hole misalignment. Additional holes around the edge were machined to allow fixation

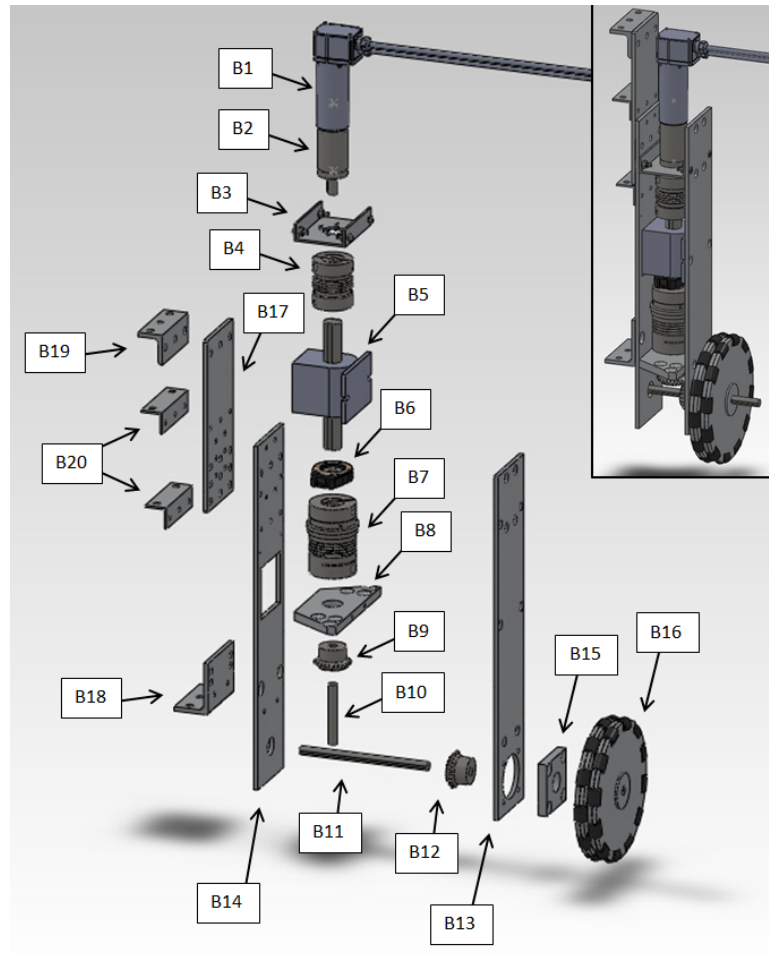


Figure 3.10: Exploded view of the motor-wheel module. Refer to Table 3.3 for part designations.

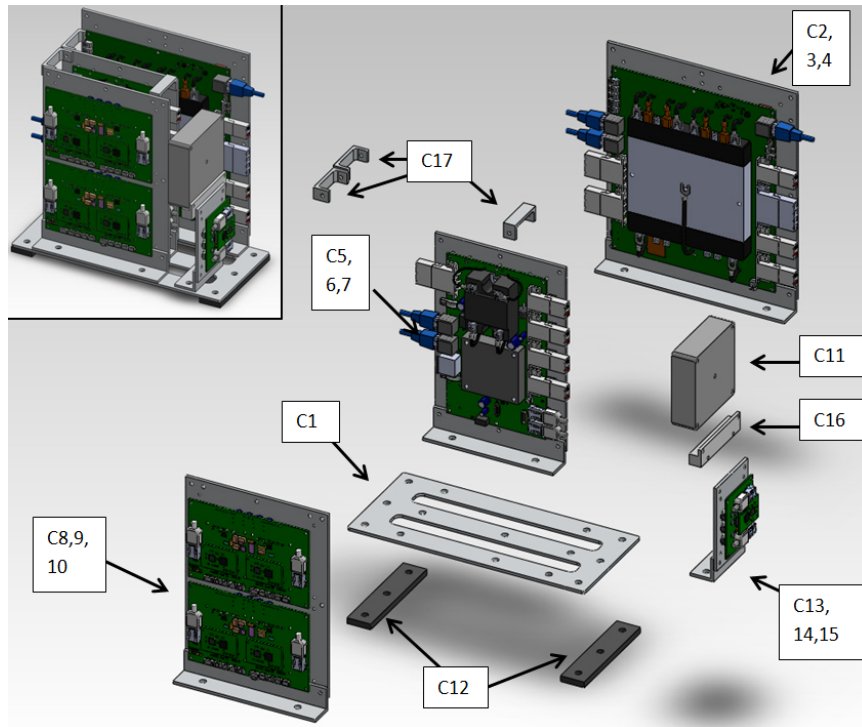


Figure 3.11: Exploded view of the electronics module. Refer to Table 3.3 for part designations.

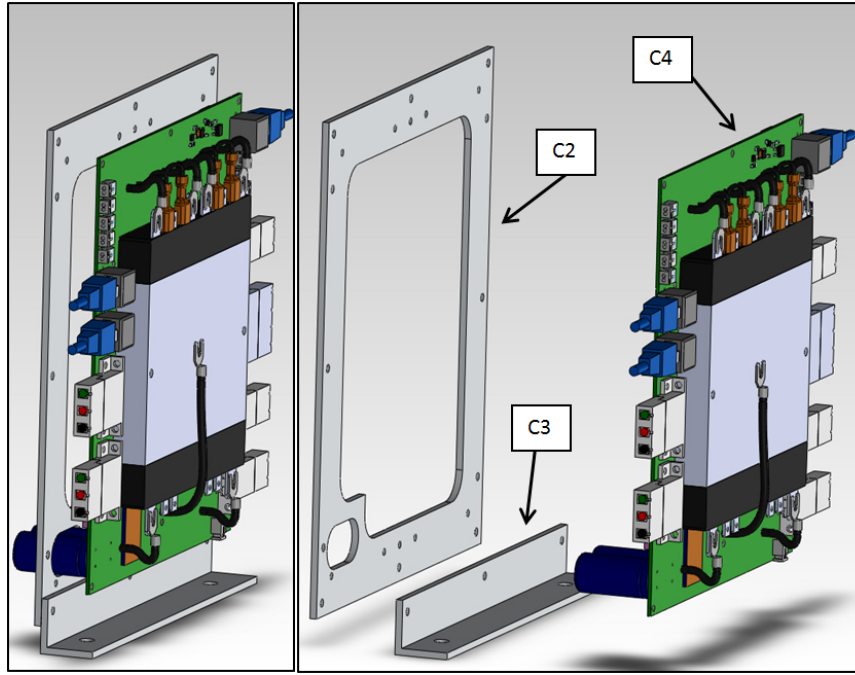


Figure 3.12: Exploded view of the BBB submodule that handled power input. The BBB PCB was held away from the plate with board spacers.

struts between plates.

The electronics (Fig. 3.16) were tested outside the mechanical system by Meka outside UT. The main parts corresponding with the Bill of Materials are denoted.

3.5 Component Selection

OEM component selection throughout the design history is more fully documented by Gupta [15]. Parts were chosen based on desired kinematics and dynamics of the overall base, while trying to minimize size and cost. Any custom parts were designed to house these OEM parts and use standard fasteners where possible. Load-

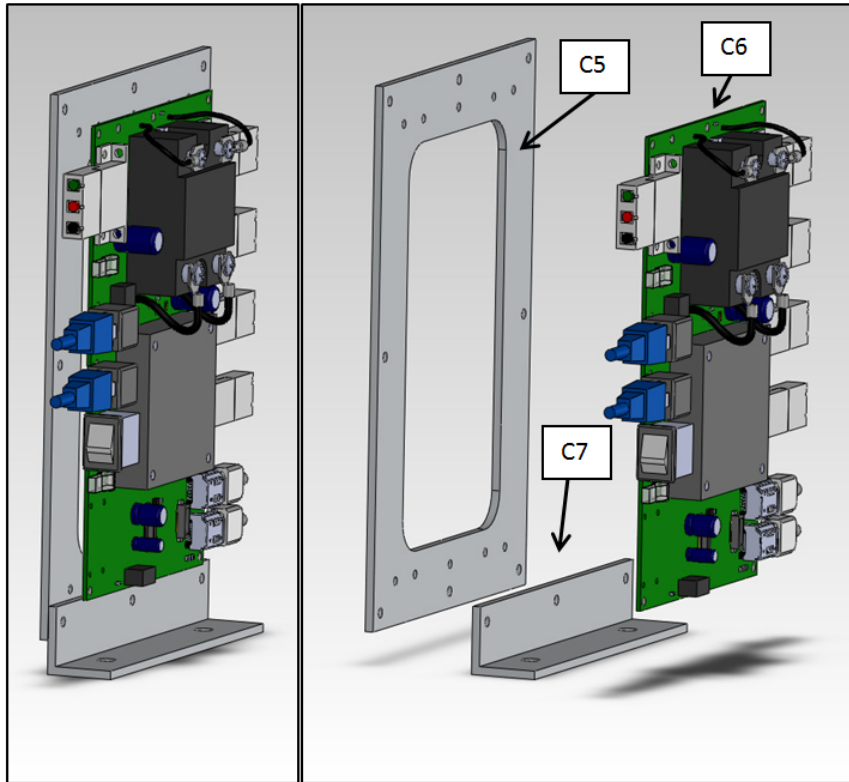


Figure 3.13: Exploded view of the PWR submodule that handles power distribution and communication. The PCB was held away from the plate using board spacers. The Crydom relay on the board helped to regulate power output.

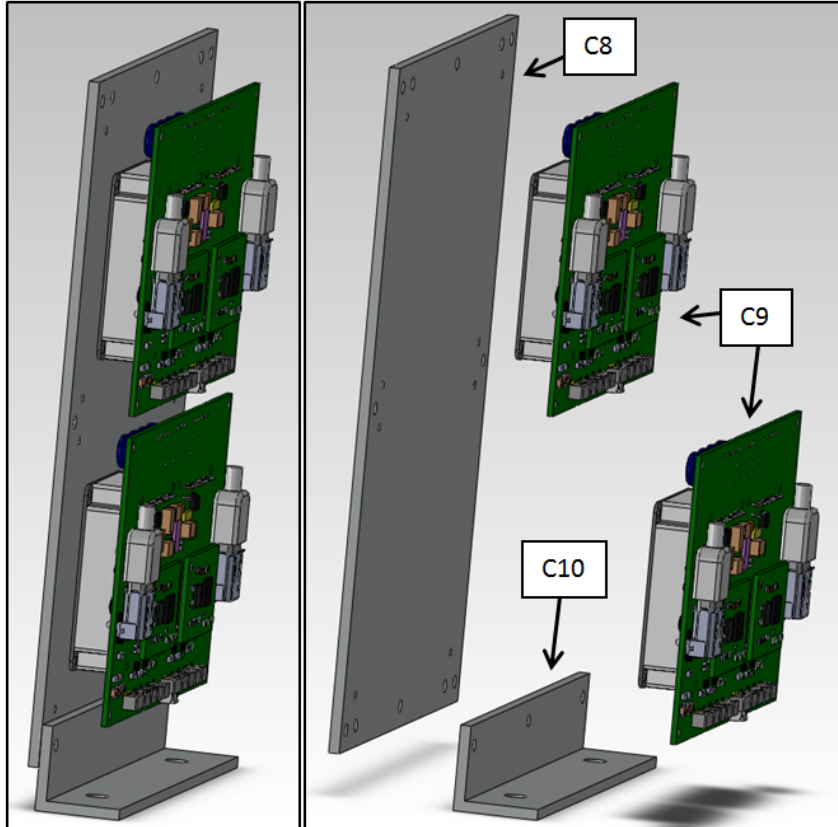


Figure 3.14: Exploded view of the ELMO submodule that handles driving the motors. Four channels for motors are available with this setup (2 per PCB), although only three channels are used to control the three motors in Trikey. One significant design flaw that was only discovered after assembly and construction is that wiring ports at the bottom of part C9 are difficult to access with fingers and tools, given the limited space there. This occurred because of a lack of knowledge about the complete electronics design during the mechanical design phase.

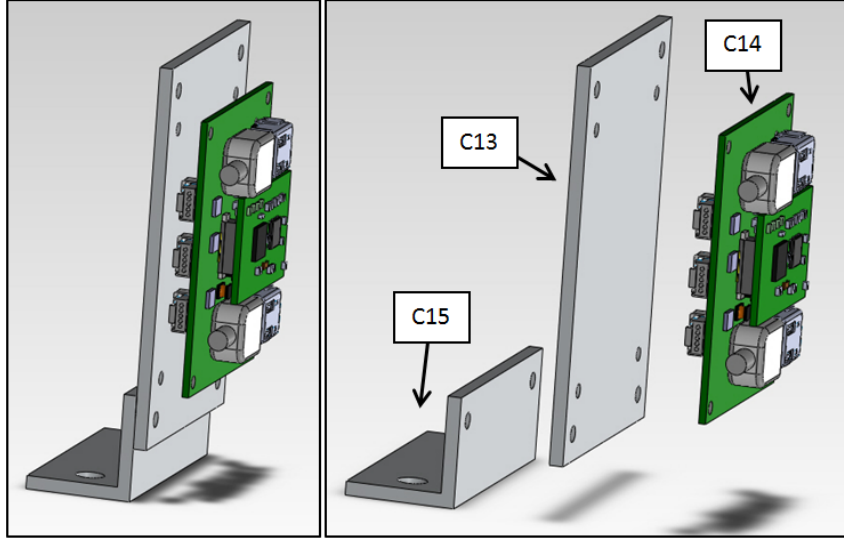


Figure 3.15: Exploded view of the LOADCELL submodule that handled power, data acquisition, and signal conditioning for the torque cells.

bearing components generally used aluminum material due to its relative strength, lower weight, lower cost, and ease of machinability.

The current base was initially designed to move at a maximum speed of 1 m/s and maximum acceleration of 1 m/s^2 , in any direction. The desired speed limit matches with a comfortable walking speed for humans, since the typical walk-run transition speed for healthy adult males is 1.88 m/s [33], and the desired acceleration limit was arbitrarily chosen as reasonable for a daily indoors robot. This would allow Trikey (or Dreamer) to move with some humanlike speeds and accelerations. Gupta [15] documents how this acceleration is associated with a 70 N resultant horizontal force on the base, assuming a mass above the wheels of 70 kg . Based on these assumptions, kinematic and dynamic models led to the selection of the particular Maxon motors and gearboxes used here.

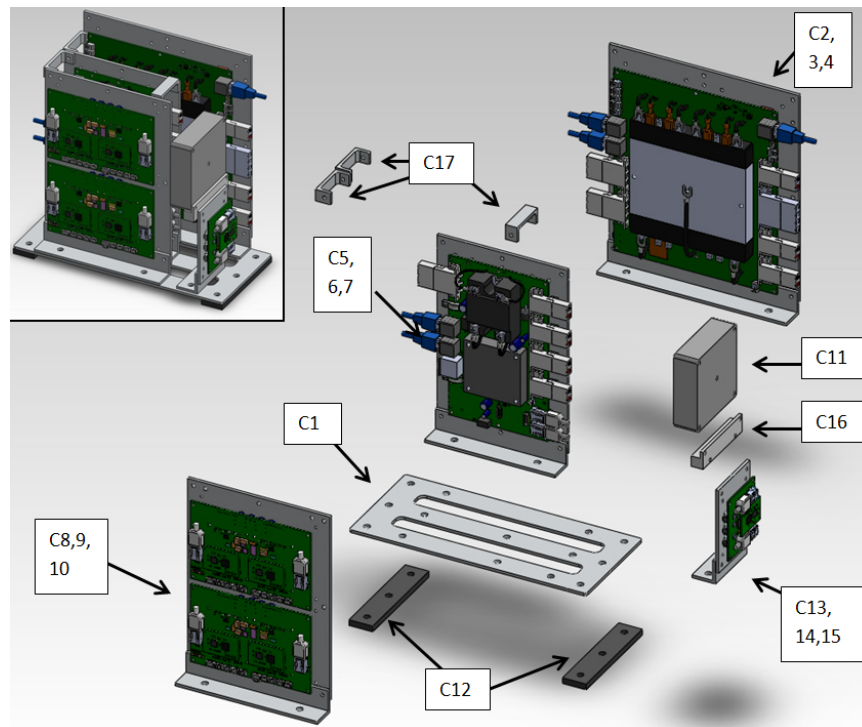


Figure 3.16: The custom Trikey electronics were designed, built, and tested by Meka (San Francisco) concurrently with the latest mechanical redesigns of Trikey. They were shipped to UT for integration in Sep 2011. Photo supplied by Meka; annotation added by the author.

The torque limiter was set to a 25 Nm limit, to accommodate the maximum torque allowable for the Maxon gearbox, which was the weakest electronic component in the wheel-motor module. Both the torque limiter and the coupler helped accommodate any misalignment in the driving axis of the module.

3.6 Fabrication

Approximately 74 custom-designed parts for Trikey Version 5 were machined (see Appendix 2 for selected drawings). Of these, approximately 66 parts were machined by HCRL students at the UT mechanical engineering machine shop. The parts were fabricated in waves, with the bulk of machining for all these parts occurring in August 2010, January 2011, and August-September 2011. Most of these parts were plates made from general-purpose 6061 aluminum alloy or similar, requiring only basic use of the mill with two-flute endmills, standard drill bits, and alignment, tap, and deburring tools. The exceptions were the monoblock plastic battery holders (part D1), which were designed to be easy to machine, and the steel rods (parts B10,11) and back panel (part F6). The large circular holes in the back panel could be made using an electronics hole punch tool, while the rectangular holes could be made with very small endmills. Steel parts were machined with four-flute endmills and nitride-coated drill bits.

Machining tolerances for most dimensions were ± 0.010 in (± 0.25 mm), which was sufficient for the purposes of this prototype, allowing some freedom in alignment. Only especially long pieces, such as the wheel-motor module plates, required careful use of the indicator tool to keep angular alignment and dimensions within

the tolerances. The modules that were most sensitive to wide tolerances were the wheel-motor modules and the electronics module, and these concerns were addressed separately. The wheel-motor module had shaft couplers that allowed for misalignment of parts, and so this module could keep the relatively slack tolerances of ± 0.010 in and still function properly. The holes in the electronics module plates, however, were located with tighter tolerances of ± 0.002 in, in order to prevent any fixation stresses on the PCBs in this module caused by hole misalignment.

Large custom parts, such as the back panel (part F6) and BBB plate (part C2) required more time and tooling to fabricate. Generally if a part had two perpendicular dimensions greater than 6 in, it would not fit into the vises of the UT machine shop mills and had to be directly mounted to the table with a custom setup of strap clamps and blocks. Then the alignment had to be verified with the indicator tool. Large or complicated parts were better machined by the UT machine shop or outside vendors either by laser-/water-cutter or computer-numerical controlled (CNC) mill. When possible, parts were designed to be smaller to avoid outside machining costs.

Sending drawings and draftings to outside vendors sometimes required file translation of the original SolidWorks files, either due to version incompatibility or restrictions on the student license for the software. When needed, SolidWorks drawings were converted to general parasolid files (.x_t format), which eliminate design histories in the CAD but which preserve the final geometry and are readable by most CAD software today.

3.7 Assembly & Disassembly

Because Trikey and Dreamer are educational in purpose, several users are expected to interact with them and most likely breakdown or modify them, as well. For this reason assembly and disassembly steps for the robots should be clear and easy when possible. Trikey 1 and the Meka upper body may not have been explicitly designed for easy assembly/disassembly, but later additions to Trikey considered this important characteristic. Based on experience with Trikey 5, assembly steps are given below; disassembly steps can follow the reverse order. Criticisms of the assembly steps are in Chapter 7.

Figs. 3.9-3.14 indicate the general assembly orientations of the parts that comprise the Trikey modules. All parts were assembled with imperial or SI bolts, except the encoder-torque cell assembly joined with adhesive, and the battery assembly which was secured with plastic zip ties.

3.7.1 General Assembly Steps for Trikey/Dreamer

1. Assemble the three individual motor-wheel modules (B-module), and attach them one at a time to the main bottom plate (A-module) (detailed below).
2. Fix the mid-shelf module (F-module) to the three motor-wheel modules (B-module) using the appropriate nuts and bolts.
3. Attach the electronics (C-module) and batteries (D-modules) to the bottom plate using the appropriate nuts and bolts. Include the rubber feet between the electronics module and the baseplate, and remember to electrically short the

aluminum frame of the module with the Trikey frame. The batteries should be secured in their holders with zip ties before fixing them to the baseplate. The electronics module should already be assembled (detailed below).

4. Secure the EtherCAT hub (E-module) to the midshelf-module (F-module). Align the module such that it does not interfere with required wires.
5. Attach *only* the bottom main plate of the upper body fixation module (part G1, Appendix 2) to the top of the structure with the appropriate nuts and bolts.
6. If attaching the Meka upper body, then rest the upper body on a soft surface, exposing its bottom metal plate. Attach the transition plates (parts G2-4) to the bottom of the Meka upper body first, using the appropriate metric bolts for countersunk holes. The bolts should be flush to or below the surface of the plates. Then place the Meka upper body upright atop the Trikey base and secure with appropriate bolts (job of two people).
7. Make the remaining electrical connections between the electronics module and the motors, sensors, batteries, EtherCAT hub, computer, front panel buttons, and emergency stops according to wiring diagrams (Fig. 5.2), Meka manuals, and Gupta [15]. Wires can be secured in cable holders fixed along the mid-shelf module.

3.7.2 Assembly Steps for Motor-Wheel Modules

1. Attach encoder (B6) to torque sensor (B5) according to encoder manufacturer instructions. This requires fixing the encoder housing to the torque sensor housing with manufacturer-provided adhesive and alignment tool, and attaching the rotary disk to the torque sensor rod with a set screw.
2. Attach the torque sensor (B5) to the main, outer vertical plate (B13). Attach the torque limiter (B7) to the torque sensor (B5) shaft, using a square key. Tighten the clamp screws on the limiter. Hold the unsupported end of the limiter so as not to bend the sensor.
3. Secure the trapezoidal plate (B8) to the the main plate (B13). Attach the vertical axle (B10) to the torque limiter through the bearing in the trapezoidal plate (B8). Secure the corresponding clamp screw on the torque limiter after making sure the exposed length of the axle rod is sufficient for miter gear placement. Secure the miter gear (B9) to the axle rod with square key and set screw.
4. Attach the motor mounting plate (B3) to the motor gearbox (B2), which is already connected to the motor (B1). Use four metric bolts and locking washers to prevent loosening. Be sure to align the plate such that the wires of the motor would point *away* from the central body upon final integration. This way, there is no impingement with the upper vertical plate (B17) later.
5. Attach the coupler (B4) to the torque cell (B6) at the rod. Then attach the gearbox (B2) shaft to the upper part of the coupler, with the fixation plate

already attached to the gearbox. Align the motor-gearbox so the wires point away from the vertical plate. Secure the motor gearbox mounting plate (B3) to the main plate (B13).

6. Attach the inner vertical plate (B14) to the bottom trapezoidal plate (B8) and motor mounting plate (B3). Be sure to use the appropriate low-profile bolts to attach the motor mounting plate, so that they lie flush to or below the surface of the vertical inner plate.
7. Attach the upper vertical plate (B17) to the inner vertical plate (B14) at the desired height, using five bolts/nuts for increased strength of the attachment. For stability reasons, the recommended height is the shortest height, although taller heights are acceptable, as detailed in Chapter 4. Taller heights may also complicate attaching the front panel of the mid-shelf module later.
8. Attach the inner brackets (B18-B20) to the inner vertical plates (B14, B17).
9. Align the partly-assembled module vertically over the opening in the main Trikey baseplate (A1), ensuring that it faces the correct direction. Secure the module to the baseplate through the trapezoidal plate (B8) and bottom bracket (B18).
10. Attach the spacer block (B15) to the outer plate (B13).
11. Turn the module-baseplate assembly on its side, so that the remaining horizontal axle (B11) can be inserted through the vertical plates (B13, B14) without

falling out due to gravity. Slide the axle through the outer plate (B13) bearing, a free-floating plastic spacer, the free-floating horizontal miter gear (B12), and the inner plate (B14) bearing. Without securing anything yet, attach the wheel (B16) to the outer part of the axle.

12. Place the outer wheel bearing (A2) over the exposed outer part of the horizontal axle, and align it with the appropriate holes on the main baseplate (A1). Attach the bearing holders to the bearing. Squeeze the bearing spacer block (A3) between the bearing holders and the main baseplate.
13. Align all these unsecured parts of the horizontal wheel assembly so that the horizontal and vertical miter gears mesh appropriately. Then secure these parts with keys, set screws, and snap rings on the axles. Secure the outer wheel bearing and spacer block with long bolts.

3.7.3 Assembly Steps for Electronics Module

Refer to Figs. 3.11-3.15 for more details of part placement.

1. Assemble the BBB submodule. Use 1 in #4-40 bolts to fix the BBB PCB (C4) to the BBB plate (C2), such that the capacitors fit through the appropriate corner hole in the plate. Use 5/8 in long nylon spacers around the bolts to space the plate and PCB, and secure with nuts and locking washers to prevent loosening. Attach the plate (C2) to the appropriate bracket (C3) with #6-32 bolts as oriented in Fig. 3.12.
2. Assemble the PWR submodule. Use 5/8 in #4-40 bolts to fix the PWR PCB

(C6) to the BBB plate (C5). Use 1/4in long nylon spacers around the bolts to space the plate and PCB, and secure with nuts and locking washers to prevent loosening. Attach the plate (C5) to the appropriate bracket (C7) with #6-32 bolts as oriented in Fig. 3.13.

3. Assemble the ELMO submodule. Afix compressible thermal pad material of thickness 0.020-0.040in onto the flat side of the metal ELMO amplifier components. Then use 1 in #2-56 bolts to fix the two ELMO PCBs (C9) to the ELMO plate (C8), such that the thermal pad can conduct heat directly from amplifier to plate. Use 5/8in long nylon spacers around the bolts to space the plate and PCB, and secure with nuts and locking washers to prevent loosening. Attach the plate (C5) to the appropriate bracket (C7) with #6-32 bolts as oriented in Fig. 3.14.
4. Assemble the LOADCELL submodule. Use Use 5/8in #4-40 bolts to fix the load cell PCB (C14) to its plate (C13). Use 1/4in long nylon spacers around the bolts to space the plate and PCB, and secure with nuts and locking washers to prevent loosening. Attach the plate (C13) to the appropriate bracket (C15) with #6-32 bolts as oriented in Fig. 3.15.
5. Attach in order the BBB, PWR, ELMO, and LOADCELL submodules to the main electronics baseplate (C1) in the correct positions and orientations as shown in Fig. 3.11.
6. Attach the nylon fan mount (C16) to the load cell plate (C13), and then the fan (C11) to the mount.

7. Bolt three support struts (C17) to the tops of the upright plates so that the structure can better resist twisting and vibration. One can fit between the BBB and PWR plates, and two can fit between the PWR and ELMO plates.
8. Make the intra-module electrical connections with the appropriate wires, as described by Gupta [15]. If an appropriate power source is available, also connect the fan to power.
9. When attaching the module to the main Trikey base (A1), remember to include the rubber feet (C12) between the bottom of the main electronics plate (C1) and the Trikey baseplate (A1) to cushion the ride of the module slightly. Also remember to electrically connect the aluminum frame of the electronics module with the frame of Trikey.

Chapter 4

Design Analysis

During development, simplified analytical models of Trikey physical behaviors helped in the sizing and design of parts. They also gave early indicators of safety limitations of the robot, which is necessary for any robot meant to work around people.

Ideally all the analyses described below would be performed before design completion and construction; however, time and resources constrained what could be done. In practice, the simplified models and worst-case scenario calculations were performed early, so that design could proceed without significant delay, and more complex analyses that were not critical to immediate design could be performed as design progressed.

4.1 Kinematics Models

4.1.1 Level Flat Terrain Kinematics

The general kinematic and dynamic models for a 3-wheeled omnidirectional holonomic base on flat ground were previously described by Kim [20] and detailed for Dreamer by Gupta [15]. The updated models here adopt the convention where the front and left of Dreamer are the positive x - and y -axes, respectively, of the local xyz robot reference frame, and angular velocity $\dot{\theta}$ is around the geometric top-down

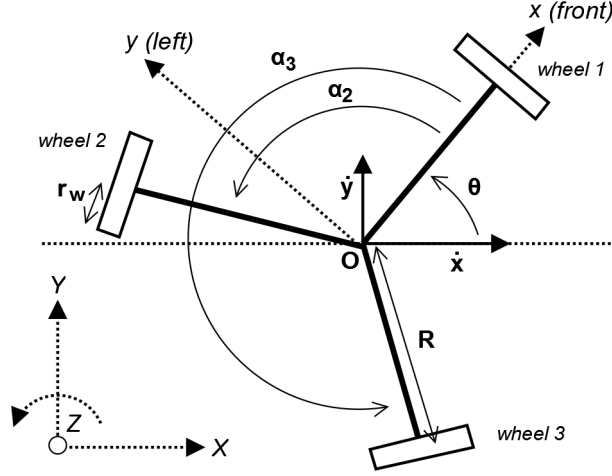


Figure 4.1: Kinematic model used for Dreamer design process. Top-down view of three-wheeled base. Image corrected from Gupta [15] so that the three generalized coordinates x , y , and θ are independent.

center of the base O (Fig. 4.1). Also the present model has positive wheel rotations correspond with a counterclockwise rotation of the Trikey body as a whole; i.e. the positive wheel rotation vector points inward toward the center of the base, following the right-hand-rule. This accounts for the sign changes compared to the previous equations from Gupta [15]. This idealized model assumes no slip between wheel and ground.

Based on the kinematic analysis of Gupta [15], the following equation can be derived. Given a velocity vector $\vec{v} = [\dot{x}, \dot{y}, \dot{\theta}]^T$, which is the desired whole-body linear and angular velocity of body O in the global XYZ coordinate system, the required rotational velocity of the i th wheel $\dot{\phi}_i$ is estimated as:

$$\dot{\phi}_i = \frac{1}{r_w} (-\dot{x} \sin(\theta + \alpha_i) + \dot{y} \cos(\theta + \alpha_i) + R\dot{\theta}) \quad (4.1)$$

where r_w is the 0.102 m wheel radius, R is the 0.289 m wheel distance from the

geometric center of the base, and α_i is the angle offset of the i th wheel module in the horizontal plane relative to the x -axis (0° , 120° , and 240°) (some measurements shown in Chapter 3). Eq. 4.1 says that the total angular velocity of an individual wheel is just the sum of \dot{x} and \dot{y} projected onto the wheel orientation, plus the tangential velocity due to $\dot{\theta}$.

Eq. 4.1 leads to matrix equations relating the whole-body velocity vector \vec{v} to the wheel velocity vector $\vec{\phi} = [\dot{\phi}_1, \dot{\phi}_2, \dot{\phi}_3]^T$:

$$\vec{v} = r_w \mathbf{J} \vec{\phi} \quad \text{or} \quad \vec{\phi} = \frac{1}{r_w} \mathbf{J}^{-1} \vec{v} \quad (4.2)$$

where matrix \mathbf{J}^{-1} is given by:

$$\mathbf{J}^{-1} = \begin{bmatrix} -\sin(\theta + \alpha_1) & \cos(\theta + \alpha_1) & R \\ -\sin(\theta + \alpha_2) & \cos(\theta + \alpha_2) & R \\ -\sin(\theta + \alpha_3) & \cos(\theta + \alpha_3) & R \end{bmatrix} \quad (4.3)$$

Matrix \mathbf{J}_0 is \mathbf{J} when letting $\theta = 0^\circ$. \mathbf{J}_0 then relates the wheel velocities to the body velocity in the local robot reference frame xyz and is given by:

$$\mathbf{J}_0^{-1} = \begin{bmatrix} 0 & 1 & R \\ -\frac{\sqrt{3}}{2} & -\frac{1}{2} & R \\ \frac{\sqrt{3}}{2} & -\frac{1}{2} & R \end{bmatrix} \quad \mathbf{J}_0 = \begin{bmatrix} 0 & -\frac{\sqrt{3}}{3} & \frac{\sqrt{3}}{2} \\ \frac{2}{3} & -\frac{1}{3} & -\frac{1}{3} \\ \frac{1}{3R} & \frac{1}{3R} & \frac{1}{3R} \end{bmatrix} \quad (4.4)$$

Wheel motor-gearbox-sensor assemblies were chosen partly based on the required wheel velocities resulting from this model. The results of the Matlab simulation of this model is detailed by Gupta [15].

4.1.2 Inclined Flat Terrain Kinematics

A general strategy for modeling kinematics over inclined flat ground is given below. Although Trikey was designed for level flat ground, the potential for moving

on inclined flat ground was explored after it was built. The motivation for this was twofold: to test the functionality limits of the current robot, and to help generate design ideas for new robots moving in rougher terrains. Sections 6.3-6.4 describe proof-of-concept tests of the robot on inclined terrain. Future wheeled mobile bases for inclined terrains can follow a similar modeling strategy as follows before construction, in order to select and size components more accurately.

First note that the Attitude Heading Reference System (AHRS) inertial sensor on board Trikey provides real-time data of the direction of gravity, in the form of a 3x3 rotation matrix \mathbf{R} (Fig. 4.2). Matrix \mathbf{R} contains the orthogonal unit vectors that form a basis for describing vectors in the local Trikey reference frame, or local coordinate system. One unit vector is normal to the ground, if all wheels contact the ground, while the other two unit vectors are related to the relative rotational orientation of Trikey on the ground. A vector in the local coordinate system of Trikey, when pre-multiplied by \mathbf{R} , transforms to the global coordinate system of the ground. Likewise, vectors in the global frame, pre-multiplied by \mathbf{R}^{-1} , transform to the local frame.

The model for level flat terrain presented in Section 4.1.1 is the starting point for the simple inclined flat terrain model. Given a desired set of body velocities \dot{x} , \dot{y} , and $\dot{\theta}$ in the local Trikey frame, parallel to the ground surface, the same Eqs. 4.1-4.4 apply, with the caveat that all calculations remain in the local frame.

Therefore, given a set of Trikey wheel velocities, and using the same notation as in Section 4.1.1, the local body velocity vectors can be calculated from Eq. 4.2 as $\dot{x}\hat{\mathbf{i}}$, $\dot{y}\hat{\mathbf{j}}$, and $\dot{\theta}\hat{\mathbf{k}}$. Then the global body velocity vectors will just be the transformed

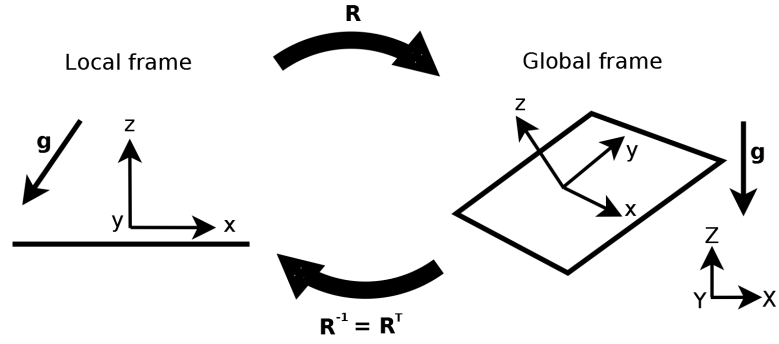


Figure 4.2: Function of the 3x3 rotation matrix \mathbf{R} that transforms vectors from the local xyz reference frame of the robot (left) to the global XYZ reference frame of the terrain (right). The Z -axis of the global frame points upward against the direction of gravity \vec{g} . The z -axis of the local frame is normal to the surface of the ground when all three wheels make contact with the ground.

vectors $\mathbf{R}\hat{i}$, $\mathbf{R}\hat{j}$, and $\mathbf{R}\hat{k}$.

In the other direction, given a generic desired body velocity in the global frame \vec{V} , it transforms to the local frame as $\mathbf{R}^{-1}\vec{V}$. Then $\mathbf{R}^{-1}\vec{V}$ can be broken down into local x - and y -components (local z -components are not possible). The components are used in Eq. 4.2 to find required wheel velocities.

4.2 Dynamics Models

4.2.1 Level Flat Terrain Dynamics, Zero Wheel Inertia

Dynamics on level flat ground were modeled similarly to the kinematics (see Section 4.1.1) by resolving the total body inertial forces into the components on each wheel. The omniwheels can only apply torques around their main axes of rotation. The net x - and y -forces and moment about the z -axis for the whole base at point O (Fig. 4.1) come from summing the relevant individual force components from each

wheel. This gives the dynamic balance equations:

$$\begin{aligned}\sum F_x &= M\ddot{x} = \sum_{i=1}^3 -F_i \sin(\theta + \alpha_i) \\ \sum F_y &= M\ddot{y} = \sum_{i=1}^3 F_i \cos(\theta + \alpha_i) \\ \sum M_z &= I\ddot{\theta} = \sum_{i=1}^3 F_i R\end{aligned}\tag{4.5}$$

where M is the total mass of the base plus its payload, I is the mass moment of inertia about O in the z -direction, and R is the distance between the wheels and robot base center (same R as in Eq. 4.1).

Assuming no wheel inertias, the applied motor-wheel torque equals the moment caused by the horizontal ground reaction force, or $\tau_i = r_w F_i$. Then from Eq. 4.5 the matrix equation relating the whole-body acceleration vector $\vec{a} = [\ddot{x}, \ddot{y}, \ddot{\theta}]^T$ in the global frame to the wheel torque vector $\vec{\tau} = [\tau_1, \tau_2, \tau_3]^T$ is:

$$\mathbf{M}\vec{a} = \frac{1}{r_w}\mathbf{K}\vec{\tau} \quad \text{or} \quad \vec{\tau} = r_w\mathbf{K}^{-1}\mathbf{M}\vec{a}\tag{4.6}$$

where matrix \mathbf{K} is:

$$\mathbf{K} = \begin{bmatrix} -\sin(\theta + \alpha_1) & -\sin(\theta + \alpha_1) & -\sin(\theta + \alpha_3) \\ \cos(\theta + \alpha_1) & \cos(\theta + \alpha_2) & \cos(\theta + \alpha_3) \\ R & R & R \end{bmatrix}\tag{4.7}$$

The idealized inertial matrix \mathbf{M} is the diagonal matrix:

$$\mathbf{M} = \begin{bmatrix} M & 0 & 0 \\ 0 & M & 0 \\ 0 & 0 & I \end{bmatrix}\tag{4.8}$$

where M is the total robot mass and I is the mass moment of inertia of the robot around the vertical z -axis. This equation was used for initial basic estimates of design parameters, adjusting M and I as the robot CAD evolved. An example simulation of Eq. 4.6 is shown below (Fig. 4.3). The individual wheel torques required

to produce a whole-body linear acceleration of 1 m/s^2 depend on the acceleration direction. This example assumes a center of mass that is not perfectly centered over the base, and a total robot mass of 100 kg.

Besides indicating the minimum torque requirements of the motors, data like this would help in the future if the robot were ever to perform repetitive tasks. Fatigue tests could be performed on parts using the worst-case numbers estimated in this simulation. This would in turn aid redesign decisions.

4.2.2 Level Flat Terrain Dynamics, Nonzero Wheel Inertia

A slightly more realistic model relating robot accelerations \vec{a} to wheel torques $\vec{\tau}$ assumes nonzero wheel inertia. However, the inertia may not have a significant effect on design calculations. To check if wheel inertia is important, a dynamic model including it was derived and compared to the zero-inertia model.

In this case the net torque on the i th wheel $\sum T_i$ is the applied torque from the motor-gearbox assembly τ_i minus the moment caused by the horizontal ground reaction force F_i , assuming no slip with the ground (Fig. 4.4). From classical mechanics:

$$\sum T_i = I_w \ddot{\phi}_i = \tau_i - F_i r_w \quad (4.9)$$

where r_w again is the wheel radius (see Eq. 4.1), and I_w is the wheel mass moment of inertia about its principal axis of rotation. For Trikey Version 5 the three wheels were estimated to each have inertias I_w of $0.00913 \text{ kg}\cdot\text{m}^2$ as measured in SolidWorks. $\ddot{\phi}$ is the wheel angular acceleration. This gives an equation for F_i :

$$F_i = \frac{1}{r_w} (\tau_i - I_w \ddot{\phi}_i) \quad (4.10)$$

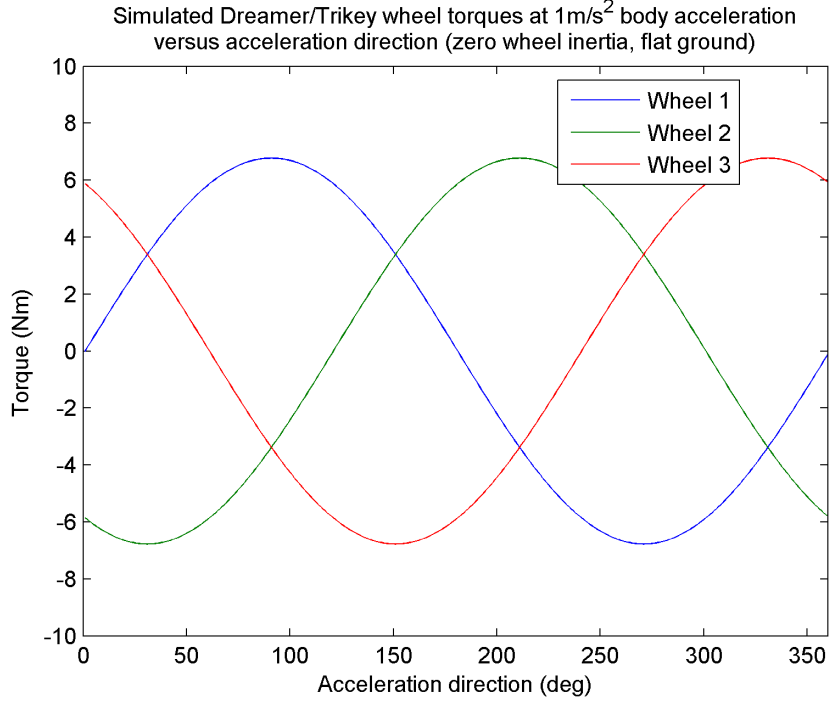


Figure 4.3: Example dynamics simulation using Matlab code, assuming zero wheel inertia. Wheel torques are shown that correspond with a whole-body robot linear acceleration of 1 m/s^2 , in acceleration directions of $0\text{-}360^\circ$ around the robot, on flat ground. Here a total mass of 100 kg was assumed for the robot and its payload, with a 0.112 m offset of the center of mass from the center of rotation. Whole-body Trikey rotational inertia about the center of rotation was estimated as 3.01 kg/m^2 , based on CAD model measurements and the parallel-axis theorem. The Meka upper body rotational inertia could not be estimated in the CAD model because of a lack of material property definitions from Meka Robotics, so it was assumed to be a fraction of the Trikey inertia, in the same proportion as the Meka upper body and Trikey masses (i.e. $I_{mek}/I_{trikey} = M_{mek}/M_{trikey} = 41 \text{ kg}/50 \text{ kg}$). The whole-body Dreamer rotational inertia was then taken as the sum of the Trikey and Meka upper body inertias.

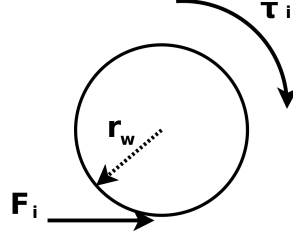


Figure 4.4: Net wheel torque due to applied motor torque and ground reaction force.

Wheel angular acceleration $\ddot{\phi}_i$ is obtained from the time derivative of Eq. 4.1 as:

$$\ddot{\phi}_i = \frac{1}{r_w} [-\dot{x}\dot{\theta} \cos(\theta + \alpha_i) - \ddot{x} \sin(\theta + \alpha_i) - \dot{y}\dot{\theta} \sin(\theta + \alpha_i) + \ddot{y} \cos(\theta + \alpha_i) + R\ddot{\theta}] \quad (4.11)$$

Letting $s_i = \sin(\theta + \alpha_i)$ and $c_i = \cos(\theta + \alpha_i)$, Eq. 4.11 can be written in shorthand as:

$$\ddot{\phi}_i = \frac{1}{r_w} [-\dot{x}\dot{\theta}c_i - \ddot{x}s_i - \dot{y}\dot{\theta}s_i + \ddot{y}c_i + R\ddot{\theta}] \quad (4.12)$$

Substituting Eq. 4.12 into Eq. 4.10, then Eq. 4.10 into Eq. 4.5, rearranging, and grouping terms, gives the system of dynamic balance equations below.

$$\begin{aligned} M\ddot{x} &= \sum_{i=1}^3 -\frac{1}{r_w} (\tau_i - I_w (\frac{1}{r_w} (-\dot{x}\dot{\theta}c_i - \ddot{x}s_i - \dot{y}\dot{\theta}s_i + \ddot{y}c_i + R\ddot{\theta})))s_i \\ M\ddot{y} &= \sum_{i=1}^3 \frac{1}{r_w} (\tau_i - I_w (\frac{1}{r_w} (-\dot{x}\dot{\theta}c_i - \ddot{x}s_i - \dot{y}\dot{\theta}s_i + \ddot{y}c_i + R\ddot{\theta})))c_i \\ I\ddot{\theta} &= \sum_{i=1}^3 \frac{R}{r_w} (\tau_i - I_w (\frac{1}{r_w} (-\dot{x}\dot{\theta}c_i - \ddot{x}s_i - \dot{y}\dot{\theta}s_i + \ddot{y}c_i + R\ddot{\theta}))) \\ M\ddot{x} &= \sum_{i=1}^3 [-\frac{\tau_i}{r_w} s_i - \frac{I_w}{r_w^2} \dot{x}\dot{\theta}s_i c_i - \frac{I_w}{r_w^2} \ddot{x}s_i^2 - \frac{I_w}{r_w^2} \dot{y}\dot{\theta}s_i^2 + \frac{I_w}{r_w^2} \ddot{y}s_i c_i + \frac{I_w R}{r_w^2} \ddot{\theta}s_i] \\ M\ddot{y} &= \sum_{i=1}^3 [\frac{\tau_i}{r_w} c_i + \frac{I_w}{r_w^2} \dot{x}\dot{\theta}c_i^2 + \frac{I_w}{r_w^2} \ddot{x}s_i c_i + \frac{I_w}{r_w^2} \dot{y}\dot{\theta}s_i c_i - \frac{I_w}{r_w^2} \ddot{y}c_i^2 - \frac{I_w R}{r_w^2} \ddot{\theta}c_i] \\ I\ddot{\theta} &= \sum_{i=1}^3 [\frac{R\tau_i}{r_w} + \frac{I_w R}{r_w^2} \dot{x}\dot{\theta}c_i + \frac{I_w R}{r_w^2} \ddot{x}s_i + \frac{I_w R}{r_w^2} \dot{y}\dot{\theta}s_i - \frac{I_w R}{r_w^2} \ddot{y}c_i - \frac{I_w R^2}{r_w^2} \ddot{\theta}] \end{aligned}$$

$$\begin{aligned}
(M + \sum_{i=1}^3 \frac{I_w}{r_w^2} s_i^2) \ddot{x} - (\sum_{i=1}^3 \frac{I_w}{r_w^2} s_i c_i) \ddot{y} - (\sum_{i=1}^3 \frac{I_w R}{r_w^2} s_i) \ddot{\theta} &= \sum_{i=1}^3 (\frac{\tau_i}{r_w} s_i - \frac{I_w}{r_w^2} \dot{x} \dot{\theta} s_i c_i - \frac{I_w}{r_w^2} \dot{y} \dot{\theta} s_i^2) \\
(-\sum_{i=1}^3 \frac{I_w}{r_w^2} s_i c_i) \ddot{x} + (M + \sum_{i=1}^3 \frac{I_w}{r_w^2} c_i^2) \ddot{y} + (\sum_{i=1}^3 \frac{I_w R}{r_w^2} c_i) \ddot{\theta} &= \sum_{i=1}^3 (\frac{\tau_i}{r_w} c_i + \frac{I_w}{r_w^2} \dot{x} \dot{\theta} c_i^2 + \frac{I_w}{r_w^2} \dot{y} \dot{\theta} s_i c_i) \\
(-\sum_{i=1}^3 \frac{I_w R}{r_w^2} s_i) \ddot{x} + (\sum_{i=1}^3 \frac{I_w R}{r_w^2} c_i) \ddot{y} + (I + \sum_{i=1}^3 \frac{I_w R^2}{r_w^2}) \ddot{\theta} &= \sum_{i=1}^3 (\frac{R \tau_i}{r_w} + \frac{I_w R}{r_w^2} \dot{x} \dot{\theta} c_i + \frac{I_w R}{r_w^2} \dot{y} \dot{\theta} s_i)
\end{aligned}$$

In matrix form, this becomes:

$$\begin{bmatrix} M + \sum_{i=1}^3 \frac{I_w}{r_w^2} s_i^2 & -\sum_{i=1}^3 \frac{I_w}{r_w^2} s_i c_i & -\sum_{i=1}^3 \frac{I_w R}{r_w^2} s_i \\ -\sum_{i=1}^3 \frac{I_w}{r_w^2} s_i c_i & M + \sum_{i=1}^3 \frac{I_w}{r_w^2} c_i^2 & \sum_{i=1}^3 \frac{I_w R}{r_w^2} c_i \\ -\sum_{i=1}^3 \frac{I_w R}{r_w^2} s_i & \sum_{i=1}^3 \frac{I_w R}{r_w^2} c_i & I + \sum_{i=1}^3 \frac{I_w R^2}{r_w^2} \end{bmatrix} \begin{bmatrix} \ddot{x} \\ \ddot{y} \\ \ddot{\theta} \end{bmatrix} =$$

$$\begin{bmatrix} -\frac{s_1}{r_w} & -\frac{s_2}{r_w} & -\frac{s_3}{r_w} \\ \frac{c_1}{r_w} & \frac{c_2}{r_w} & \frac{c_3}{r_w} \\ \frac{R}{r_w} & \frac{R}{r_w} & \frac{R}{r_w} \end{bmatrix} \begin{bmatrix} \tau_1 \\ \tau_2 \\ \tau_3 \end{bmatrix} + \begin{bmatrix} -\sum_{i=1}^3 \frac{I_w}{r_w^2} s_i c_i & -\sum_{i=1}^3 \frac{I_w}{r_w^2} s_i^2 & 0 \\ \sum_{i=1}^3 \frac{I_w}{r_w^2} s_i c_i^2 & \sum_{i=1}^3 \frac{I_w}{r_w^2} s_i c_i & 0 \\ \sum_{i=1}^3 \frac{I_w R}{r_w^2} c_i & \sum_{i=1}^3 \frac{I_w R}{r_w^2} s_i & 0 \end{bmatrix} \begin{bmatrix} \dot{x} \dot{\theta} \\ \dot{y} \dot{\theta} \\ 0 \end{bmatrix}$$

Factoring out the common terms, this can alternately be written as:

$$\begin{bmatrix} M + \sum_{i=1}^3 \frac{I_w}{r_w^2} s_i^2 & -\sum_{i=1}^3 \frac{I_w}{r_w^2} s_i c_i & -\sum_{i=1}^3 \frac{I_w R}{r_w^2} s_i \\ -\sum_{i=1}^3 \frac{I_w}{r_w^2} s_i c_i & M + \sum_{i=1}^3 \frac{I_w}{r_w^2} c_i^2 & \sum_{i=1}^3 \frac{I_w R}{r_w^2} c_i \\ -\sum_{i=1}^3 \frac{I_w R}{r_w^2} s_i & \sum_{i=1}^3 \frac{I_w R}{r_w^2} c_i & I + \sum_{i=1}^3 \frac{I_w R^2}{r_w^2} \end{bmatrix} \begin{bmatrix} \ddot{x} \\ \ddot{y} \\ \ddot{\theta} \end{bmatrix} =$$

$$\frac{1}{r_w} \begin{bmatrix} -s_1 & -s_2 & -s_3 \\ c_1 & c_2 & c_3 \\ R & R & R \end{bmatrix} \begin{bmatrix} \tau_1 \\ \tau_2 \\ \tau_3 \end{bmatrix} + \frac{I_w}{r_w^2} \begin{bmatrix} -\sum_{i=1}^3 s_i c_i & -\sum_{i=1}^3 s_i^2 & 0 \\ \sum_{i=1}^3 c_i^2 & \sum_{i=1}^3 s_i c_i & 0 \\ R \sum_{i=1}^3 c_i & R \sum_{i=1}^3 s_i & 0 \end{bmatrix} \begin{bmatrix} \dot{x} \dot{\theta} \\ \dot{y} \dot{\theta} \\ 0 \end{bmatrix}$$

(4.13)

Eq. 4.13 gives an alternative dynamic equation to Eq. 4.6 as follows:

$$\mathbf{M}_1 \vec{a} = \frac{1}{r_w} \mathbf{K}_1 \vec{\tau} + \frac{I_w}{r_w^2} \mathbf{K}_2 \vec{u} \quad (4.14)$$

where the matrices and vectors in Eq. 4.14 are defined as in Eq. 4.13 above. Note that inertial matrix \mathbf{M}_1 becomes diagonal when I_w is zero, reducing to the idealized case. Also the Jacobian \mathbf{K}_1 is the same as \mathbf{K} in Eq. 4.7. It equals the transpose of wheel angular velocity matrix \mathbf{J}^{-1} (Eq. 4.3), which is typical for kinematic and dynamic Jacobians for a multi-jointed system. Lastly, note that the last term in Eq. 4.14 is a Coriolis term related to the wheel inertia and products of the generalized velocities. These expected features help verify the derivation of this equation.

Alternately, constants can be factored out of the inertial matrix and canceled, giving the equation:

$$\frac{I_w}{r_w} \mathbf{M}_2 \vec{a} = \mathbf{K}_1 \vec{\tau} + \frac{I_w}{r_w} \mathbf{K}_2 \vec{u} \quad (4.15)$$

where Coriolis vector $\vec{u} = [\dot{x}\dot{\theta}, \dot{y}\dot{\theta}, 0]^T$, and \mathbf{K}_1 is the same as in Eq. 4.7. inertial matrix \mathbf{M}_2 is:

$$\mathbf{M}_2 = \begin{bmatrix} \frac{Mr_w^2}{I_w} + \sum_{i=1}^3 s_i^2 & -\sum_{i=1}^3 s_i c_i & -\sum_{i=1}^3 R s_i \\ -\sum_{i=1}^3 s_i c_i & \frac{Mr_w^2}{I_w} + \sum_{i=1}^3 c_i^2 & \sum_{i=1}^3 R c_i \\ -\sum_{i=1}^3 R s_i & \sum_{i=1}^3 R c_i & \frac{Ir_w^2}{I_w} + \sum_{i=1}^3 R^2 \end{bmatrix} \quad (4.16)$$

and \mathbf{K}_2 is:

$$\mathbf{K}_2 = \begin{bmatrix} -\sum_{i=1}^3 s_i c_i & -\sum_{i=1}^3 s_i^2 & 0 \\ -\sum_{i=1}^3 c_i^2 & \sum_{i=1}^3 s_i c_i & 0 \\ \sum_{i=1}^3 R c_i & \sum_{i=1}^3 R s_i & 0 \end{bmatrix} \quad (4.17)$$

When this model was simulated in Matlab for the actual robot, the resulting wheel torque curves were nearly identical to the curves assuming zero wheel inertia, such as those in Fig. 4.3. The maximum discrepancy between the two models was 0.090 Nm, or 1% of the maximal wheel torque value calculated in the nonzero-inertia model. This shows that the simpler method of assuming zero wheel inertia was sufficient for design considerations in this case.

However, some future plans to replace the wheel system should consider this model. It may be important if the ratio of I_w to r_w is unusually large, and if the absolute maximum expected wheel torque is small. This most likely would occur for either heavy-wheeled robots or for lightweight robots, whose wheels may take up a proportionally larger mass of the whole robot. For example, the model shows larger discrepancies from the zero-inertia model as the wheel radius is decreased, while holding inertia constant (Fig. 4.5). This means that wheel inertia is more important as wheel size decreases, if inertia stays the same.

One final note for this model concerns the motor and gearbox inertia. These kinematics and dynamics equations are used for calculating *wheel* torques, not motor torques. Section 4.2.4 accounts for this, or for the difference between torques before and after the gearbox. However, an alternative to Section 4.2.4 is to treat the torques τ_i in these equations as *motor* torques, and treat I_w as the combined rotational

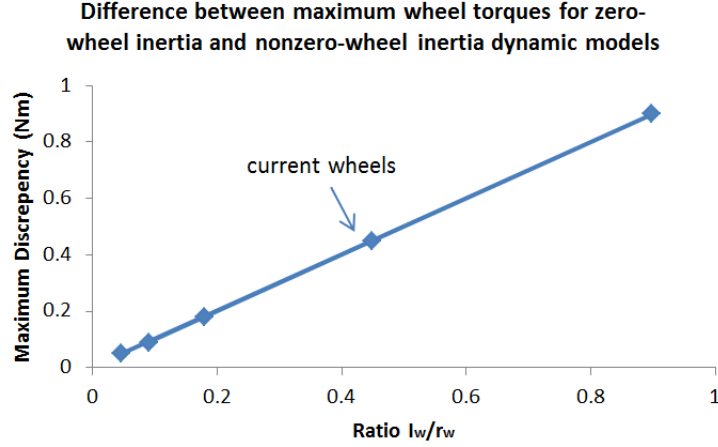


Figure 4.5: Discrepancies between the maximum torques predicted by two dynamic models: one assuming zero wheel inertia, and one accounting for wheel inertia. Whole-body robot linear acceleration was assumed to be 1 m/s^2 . Discrepancies increase when the ratio of I_w/r_w increases, with the non-zero inertia model predicting slightly higher torques.

inertia of the wheel plus all other spinning components between the motor and wheel, including the gearbox inertia, which is significant. The kinematics and dynamics equations in the previous sections would need to be updated to account for the gearbox reduction factor. Then the resulting new forms of Eqs. 4.14 and 4.15 would likely find that the new I_w is important. This alternative model was not necessary for this work, but other researchers could formulate it as desired for future work.

4.2.3 Inclined Flat Terrain Dynamics, Zero Wheel Inertia

As explained in Section 4.1.2, movement on inclined flat terrain was explored after the Trikey design and construction process. A corresponding simple 3D dynamic model was sought, as this could not be found in the literature. This could give an explicit solution for the ground reaction forces, given a desired whole-

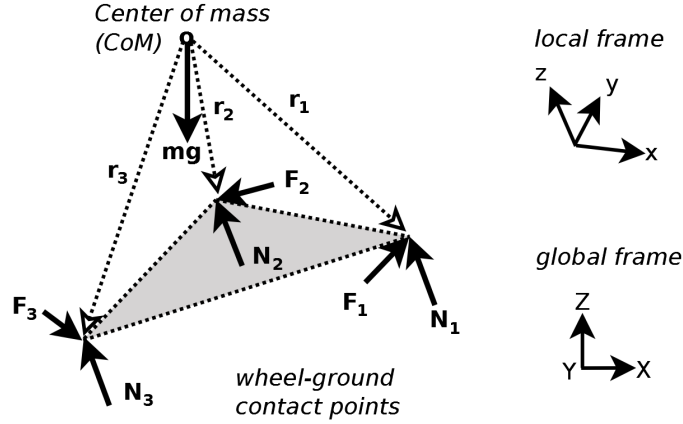


Figure 4.6: 3D free-body diagram of Trikey robot, seeing weight $m\vec{g}$ at the center of mass (CoM), and the tangential and normal ground reaction forces \vec{F}_i and \vec{N}_i at the wheel-ground contact points. The vectors r_i denote the displacements from the CoM to the wheel-ground contact points. Section 4.1.2 discusses the rotation matrix used to transform vectors from the local to global coordinate systems.

body acceleration. Also the whole-body compliant control algorithm implemented in Trikey/Dreamer addresses 3D dynamics numerically rather than with an explicit model, and it does not give the same insights as an explicit solution. Just as with the kinematics model, future designs of wheeled robots can follow a similar modeling strategy as outlined below, before construction, to better select and design components.

The system dynamics can be represented by a 3D free-body diagram (Fig. 4.6), where ground reaction forces are composed of both tangential forces \vec{F}_i and normal forces \vec{N}_i . Force vector \vec{F}_i has magnitude F_i and corresponds with the tangential forces on level ground in Eq. 4.5. The normal forces are in the same direction as the local z -axis, whose orientation is known from the rotation matrix \mathbf{R} from the AHRS sensor (Fig. 4.2, Section 4.1.2). The ground reaction forces in

the local xyz frame then are defined by:

$$\vec{F}_i = -F_i \sin(\theta + \alpha_i) \hat{\mathbf{i}} + F_i \cos(\theta + \alpha_i) \hat{\mathbf{j}} \quad (4.18)$$

$$\vec{N}_i = N_i \hat{\mathbf{k}} \quad (4.19)$$

where θ and α_i again are defined according to Fig. 4.1, also in the local xyz frame.

Dynamic balance equations for the forces and moments about the CoM in the local xyz coordinate system of the robot are:

$$\sum \vec{F} = m\vec{a} = m\vec{g} + \sum_{i=1}^3 (\vec{F}_i + \vec{N}_i) \quad (4.20)$$

$$\sum \vec{M} = \mathbf{I}_c \vec{\alpha}_c = \vec{H} = \sum_{i=1}^3 (\vec{r}_i \times (\vec{F}_i + \vec{N}_i)) \quad (4.21)$$

where $m\vec{a}$ and $\mathbf{I}_c \vec{\alpha}_c$ are the sums of forces and moments, respectively, on the system. Scalar m is the system mass. Vector \vec{g} is gravitational acceleration. Expressed in terms of the local xyz frame, $\vec{g} = -g\mathbf{R}^{-1}\hat{\mathbf{k}} = g_x\hat{\mathbf{i}} + g_y\hat{\mathbf{j}} + g_z\hat{\mathbf{k}}$, where g is the magnitude of gravitational acceleration and \mathbf{R}^{-1} is the global-to-local rotation matrix from the AHRS sensor (Fig. 4.2). Vector $\vec{a} = a_x\hat{\mathbf{i}} + a_y\hat{\mathbf{j}} + a_z\hat{\mathbf{k}}$ and is the acceleration of the CoM in the local xyz frame. Matrix \mathbf{I}_c is the inertia matrix of the robot about the CoM and aligned with the robot xyz frame, not the robot principal axes of rotational inertia; \mathbf{I}_c can be estimated through the CAD model. Vector $\vec{\alpha}_c = \alpha_x\hat{\mathbf{i}} + \alpha_y\hat{\mathbf{j}} + \alpha_z\hat{\mathbf{k}}$ is the robot angular acceleration about the local xyz axes. Vector $\vec{H} = \dot{H}_x\hat{\mathbf{i}} + \dot{H}_y\hat{\mathbf{j}} + \dot{H}_z\hat{\mathbf{k}}$ is the time derivative of angular momentum and is another representation of the total moments $\mathbf{I}_c \vec{\alpha}_c$ on the system. \vec{F}_i and \vec{N}_i are defined as in Eqs. 4.18 and 4.19.

Moment arm vector \vec{r}_i is the displacement from the CoM to the i th wheel-ground contact point (Fig. 4.6). The local ground contact point positions are

known based on robot geometry. If the position of the CoM is known in the local frame, for example from CAD models or real-time sensing, then the components of \vec{r}_i in the local xyz frame can be readily calculated. Here it is represented as $\vec{r}_i = r_{ix}\hat{\mathbf{i}} + r_{iy}\hat{\mathbf{j}} + r_{iz}\hat{\mathbf{k}}$.

If given a set of accelerations of the CoM and angular accelerations about the CoM, the left side of Eqs. 4.20 and 4.21 are known. Then they result in six equations that can be solved for the six unknown ground reaction variables – a benefit of having a three-wheeled base. Using the vector and scalar definitions above, and letting $s_i = \sin(\theta + \alpha_i)$ and $c_i = \cos(\theta + \alpha_i)$, the system becomes:

$$\begin{aligned}
ma_x &= -F_1s_1 - F_2s_2 - F_3s_3 + mg_x \\
ma_y &= F_1c_1 + F_2c_2 + F_3c_3 + mg_y \\
ma_z &= N_1 + N_2 + N_3 + mg_z \\
\dot{H}_x &= r_{1y}N_1 - r_{1z}F_1c_1 + r_{2y}N_2 - r_{2z}F_2c_2 + r_{3y}N_3 - r_{3z}F_3c_3 \\
\dot{H}_y &= -r_{1x}N_1 - r_{1z}F_1s_1 - r_{2x}N_2 - r_{2z}F_2s_2 - r_{3x}N_3 - r_{3z}F_3s_3 \\
\dot{H}_z &= r_{1x}F_1c_1 + r_{1y}F_1s_1 + r_{2x}F_2c_2 + r_{2y}F_2s_2 + r_{3x}F_3c_3 + r_{3y}F_3s_3
\end{aligned} \tag{4.22}$$

This can be rewritten in matrix notation as:

$$\begin{bmatrix} m(a_x - g_x) \\ m(a_y - g_y) \\ m(a_z - g_z) \\ \dot{H}_x \\ \dot{H}_y \\ \dot{H}_z \end{bmatrix} =$$

$$\begin{bmatrix}
-s_1 & -s_2 & -s_3 & 0 & 0 & 0 \\
c_1 & c_2 & c_3 & 0 & 0 & 0 \\
0 & 0 & 0 & 1 & 1 & 1 \\
-r_{1z}c_1 & -r_{2z}c_2 & -r_{3z}c_3 & r_{1y} & r_{2y} & r_{3y} \\
-r_{1z}s_1 & -r_{2z}s_2 & -r_{3z}s_3 & -r_{1x} & -r_{2x} & -r_{3x} \\
r_{1x}c_1 + r_{1y}s_1 & r_{2x}c_2 + r_{2y}s_2 & r_{3x}c_3 + r_{3y}s_3 & 0 & 0 & 0
\end{bmatrix}
\begin{bmatrix}
F_1 \\
F_2 \\
F_3 \\
N_1 \\
N_2 \\
N_3
\end{bmatrix}
\quad (4.23)$$

The reaction forces magnitude matrix on the right of Eq. 4.23 can be solved when the local CoM position, local robot angular position, local whole-body accelerations, mass properties, and ground inclination of the system are known or given. Since Section 4.2.2 showed that wheel inertia is likely not a major factor for the dynamics of this robot, the wheel inertias will be ignored here. Therefore, the solved reaction forces here can be used with the equations in Section 4.2.1 to calculate the corresponding wheel torques. For the rarer cases where wheel inertia becomes important, the equations in Section 4.2.2 could be used instead.

One important note is that negative solutions for any of the normal force magnitudes N_i are impossible, since normals only apply force in one direction. A negative solution would indicate instability or wheel liftoff from the ground. These concepts could be explored further in future robot studies where inclined terrain may be more crucial.

4.2.4 Transmission Losses

The required motor torque τ_m to produce a given wheel torque τ was assumed to follow the relation:

$$\tau = \tau_m GE - \tau_f \quad (4.24)$$

where G is the gearbox multiplier, E is rated efficiency related to motor-gearbox inertia and friction, and τ_f represents other frictional torque losses in the components between the gearbox and wheels. This relation also models the forces applied on the motor when the wheels are backdriven. We chose robot components partly based on the torque requirements resulting from this model.

4.3 Worst-Case Analysis of Safe Kinematic Operating Limits on Flat Ground

At early development stages, a limited number of extreme cases of unstable mass distributions for the Trikey/Dreamer robot were considered. This led to a fast estimate of safe operating limits for the robot. After physical implementation of Dreamer, a more detailed analysis of the safe acceleration limits was performed (see Section 4.4). The initial limited analysis is given here.

Several simplified “worst-case” or “corner case” mass distributions of the Dreamer robot were progressively analyzed to determine safe operating velocities and accelerations, where “worst-case” refers to the most likely configurations to be encountered that would result in loss of balance or tipping over. The actual Dreamer that was built had only one right arm and one battery module, so this was modeled in the following analyses. (*NOTE: The coordinate systems, variables, and notation for this Worst-Case Analysis section are different from in other sections, since it was performed much earlier.*)

4.3.1 Extreme Configuration

The least stable Dreamer configuration is the tallest, most far-forward configuration (waist 30.6 in high, 5 in forward offset), with the electronics module placed on the right side, since this places the center of mass (CoM) higher up and closer to the edge of the wheel support. Since the Dreamer robot is intended to manipulate objects, this case can be made even more extreme by extending the arm forward and laterally 45° from the torso and placing a 7 lb weight at the end of the arm (see figure below). This is Case 1.

For this extreme case, the CAD model estimated the total system mass to be 94.6 kg and the CoM to lie at the coordinate $(x,y,z) = (-0.058, 0.781, 0.172)$ meters, where the origin (0,0,0) lies directly below the geometric center of the Trikey main baseplate at floor level, the x -axis points to the left, the y -axis points up, and the z -axis points to the front. This is different from the kinematics coordinate system described previously (see note at the beginning of Section 4.3).

4.3.2 Worst-Case Linear Acceleration Limit

The limit to safe linear acceleration was estimated given the known geometry and mass properties of the system. Looking from the top down at the system, the tipping moment arm d is the shortest distance in the xz -plane between the CoM and the closest wheel axis (Fig. 4.8).

Essentially gravity g and moment arm d induces a stabilizing moment, while force associated with the acceleration from the motor-wheel modules F and the system height Y induce a destabilizing moment (Fig. 4.9).

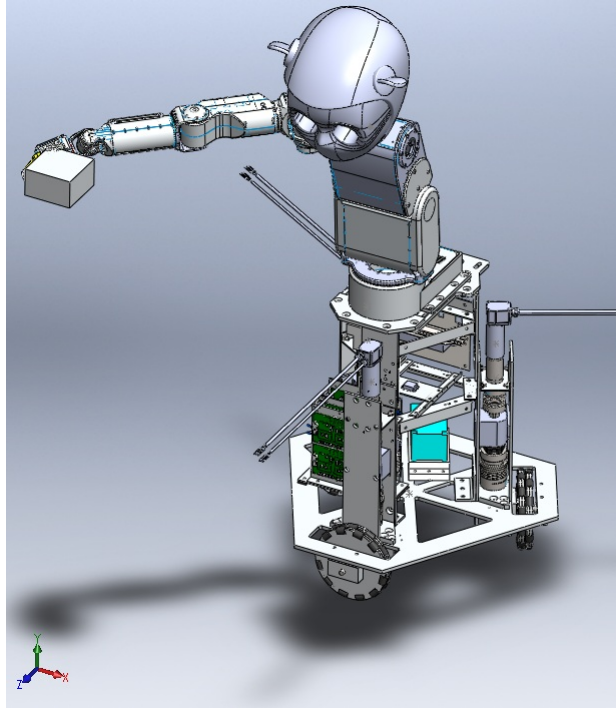


Figure 4.7: Case 1: Dreamer configuration with likely “worst-case” mass distribution (waist 30.6in high, 5in forward offset), carrying a 7lbs load in a laterally and frontally extended arm. Global coordinate system orientation denoted in lower left corner. Origin located directly below geometric center of Trikey baseplate at ground level.

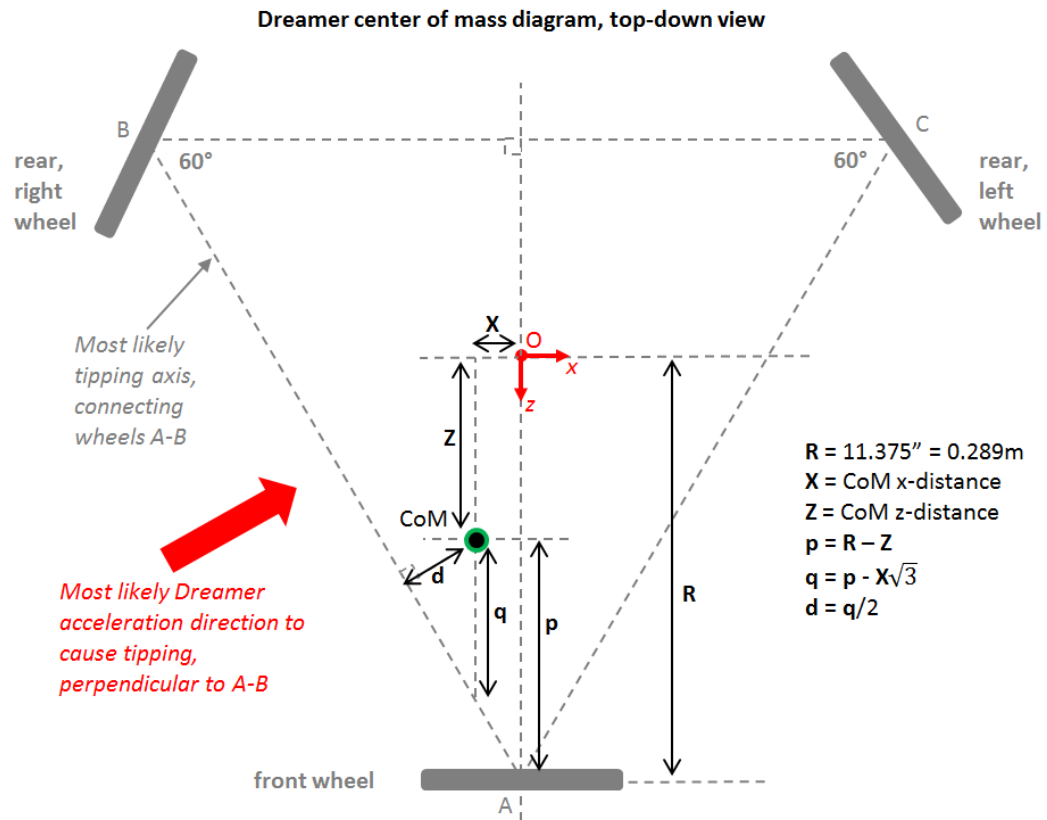


Figure 4.8: Top-down diagram of the Dreamer center of mass in a worst-case balance condition.

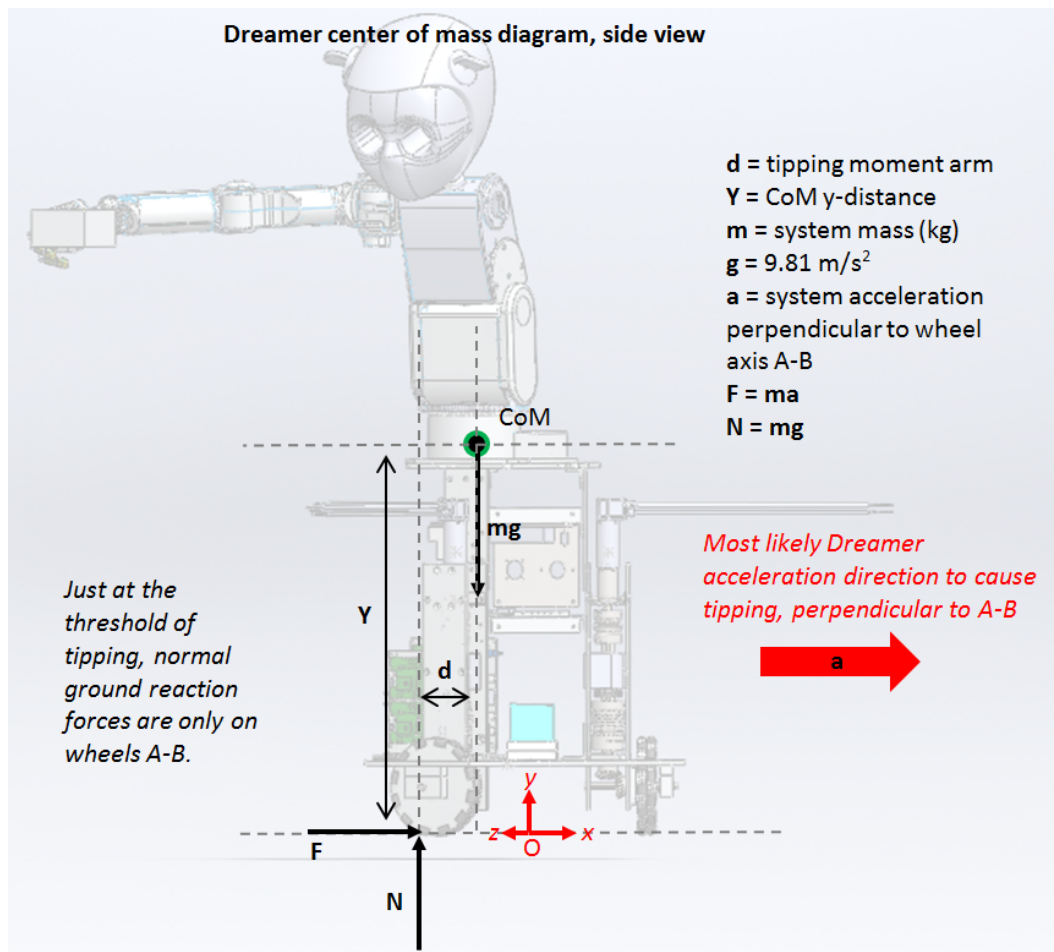


Figure 4.9: Side view of the Dreamer center of mass in a worst-case balance condition.

This simple model of stability was analyzed by assuming that, just at the threshold of tipping over, the total moment around the CoM equaled zero, or $FY = Nd$. Then when there is only linear acceleration a , $F = ma$, and $N = mg$. The worst-case limit to acceleration is determined by $maY = mgd$, giving:

$$a = gd/Y \quad (4.25)$$

where g = the acceleration of gravity and Y = the height of the CoM above the floor.

In extreme Case 1, the tipping moment arm $d = 0.008$ m, and the estimated maximum stable acceleration is 0.1 m/s^2 . Acceleration in other directions should have a higher safe limit. This number was considered in initial tests of Trikey with the Meka upper body attached.

4.3.3 Worst-Case Angular Velocity Limit

For a simple model of safe angular velocities, when there is no linear acceleration, similar assumptions were made as in the previous section. However, here F was determined from the centripetal force F_c associated with the system rotating about the y -axis, which contributes to tipping (Fig. 4.10).

Now $F = F_c \sin(\alpha + \beta)$ and $F_c = mr\omega^2$, where $(\alpha + \beta)$ equals the angle describing the direction of the centripetal force vector F_c (Fig. 4.10). At the tipping threshold the normal force $N = mg$. Then the worst-case limit to angular velocity is:

$$mr\omega^2 \sin(\alpha + \beta)Y = mgd \quad (4.26)$$

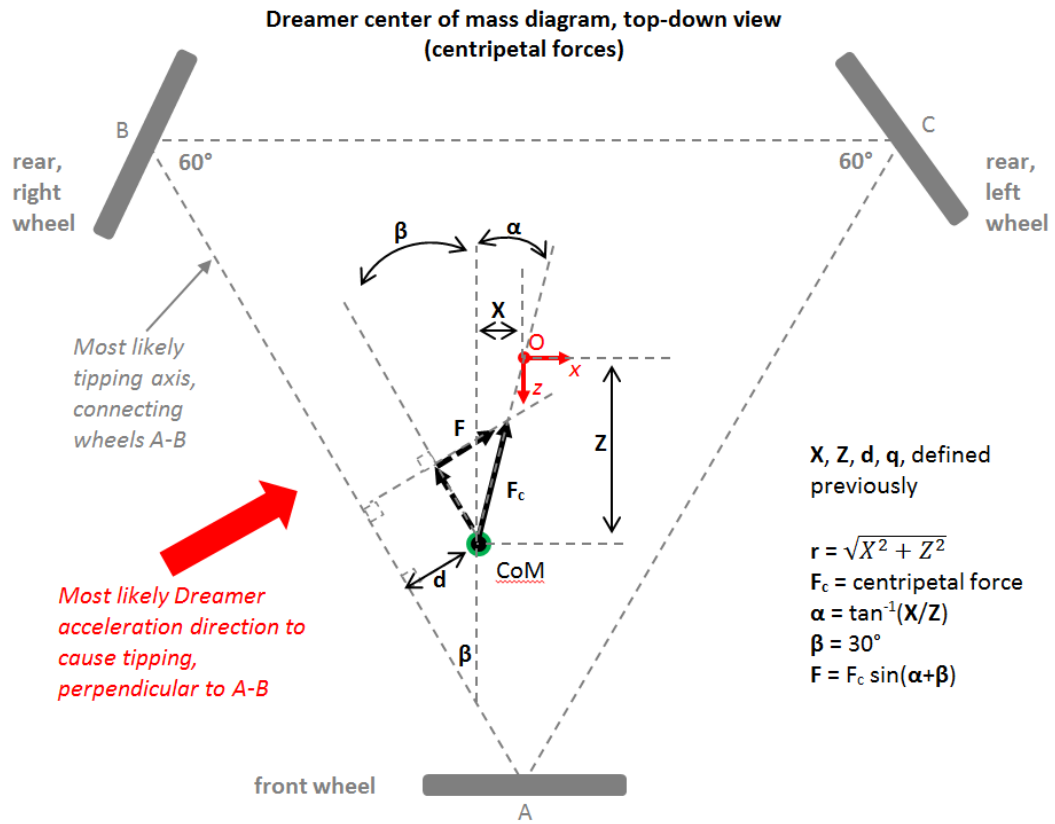


Figure 4.10: Overhead view of the Dreamer center of mass in a worst-case balance condition, undergoing centripetal force.

Table 4.1: Worst-case mass distributions of Dreamer/Trikey robot in initial analyses. Parameters correspond to Figs. 4.8-4.10.

Dreamer configuration					Mass distribution properties ^a						
Case	Robot height ^b	Waist offset (in)	Arm reach	With 7lbs mass?	m (kg)	X (m)	Y (m)	Z (m)	r (m)	α (°)	d (m)
1	tall	5	far	yes	94.7	0.058	0.781	0.172	0.182	18.7	0.008
2	short	5	far	yes	94.7	0.058	0.753	0.171	0.181	18.8	0.008
3	tall	5	far	no	91.3	0.038	0.764	0.153	0.157	13.8	0.036
4	short	5	far	no	91.3	0.038	0.738	0.153	0.157	13.8	0.036
5	short	0	far	no	91.3	0.038	0.738	0.094	0.101	21.8	0.065
6	short	2.8	far	no	91.3	0.038	0.738	0.127	0.132	16.5	0.049
7	short	2.8	close	no	91.3	0.022	0.724	0.117	0.119	10.6	0.067

^aCoordinate system here differs from outside Section 4.3. See note at beginning of Section 4.3.

^b“Tall” and “short” refer to a waist that is 30.6 in and 28.6 in high above the floor, respectively.

where $\omega = \sqrt{\frac{gd}{Yr \sin(\alpha+\beta)}}$; $r = \sqrt{X^2 + Z^2}$, $\alpha = \tan^{-1}(X/Z)$, and $\beta=30^\circ$. r is the radius of the whole-body rotation around O , and X , Y , and Z are the distances of the CoM from the origin as defined above. In extreme Case 1, the safe angular velocity limit, when there is no linear acceleration, is 0.865 rad/s^2 (0.138 rps). Less extreme configurations should allow faster angular velocities.

4.3.4 Stability Sensitivity Calculations

The linear acceleration and angular velocity limits were estimated for several more cases more likely to be seen in actual experiments. First the relevant variables describing the mass distributions were calculated using the same procedures as described above (Table 4.1).

Then the corresponding worst-case limits to linear acceleration and angular velocity were calculated (Table 4.2). As shown in Cases 1 to 4, changing the robot height from the tallest to the shortest configuration does not affect the safe limits

Table 4.2: Worst-case kinematic limits of Dreamer/Trikey robot in initial analyses. Parameters correspond to Figs. 4.8-4.10.

Dreamer configuration					Kinematic limits ^c		
Case	Robot height ^d	Waist offset (in)	Arm reach	With 7lbs mass?	a (m/s ²)	ω (°/s)	ω (rpm)
1	tall	5	far	yes	0.102	49.6	8.26
2	short	5	far	yes	0.108	51.0	8.50
3	tall	5	far	no	0.457	117.3	19.6
4	short	5	far	no	0.473	119.3	19.9
5	short	0	far	no	0.863	188.8	31.5
6	short	2.8	far	no	0.646	148.8	24.8
7	short	2.8	close	no	0.904	195.4	32.6

^cLimits to linear acceleration a alone, and angular velocity ω alone

^d“Tall” and “short” refer to a waist that is 30.6 in and 28.6 in high above the floor, respectively.

much. However, a 7 lb load in the grasp of the Dreamer greatly affects the limits; removing the 7 lb weight increased the safe linear acceleration nearly 5x and the angular velocity more than 2x. Finally, as shown in Cases 4-6, the horizontal waist offset also has a strong effect on the safe kinematic limits.

The final Case 7 is the configuration most likely to be observed in Dreamer experiments, with a short height, an intermediate 2.8 in horizontal offset, and an arm that is closer to the body (Fig. 4.11). Its worst-case acceleration limit is 0.904 m/s², which is close to the intended 1 m/s² acceleration limit for the Trikey design.

The overall conclusion of this initial analysis was that stability of the Dreamer robot in its current state is most sensitive to the horizontal positioning of the upper body over Trikey, the amount of arm extension, and whether or not there is a payload. These must be considered when setting up and running the system.

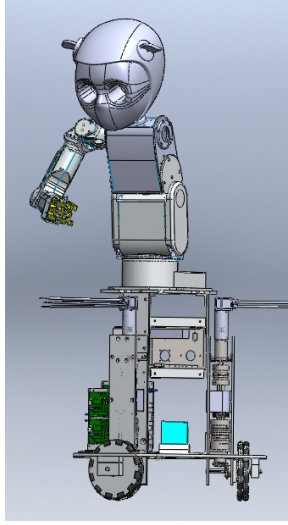


Figure 4.11: Case 7: The configuration that is mostly likely to be seen in experimentation.

4.3.5 Combined Linear Acceleration and Angular Velocity Limits, Typical Case

If the CoM of the Dreamer is known at a given point in time, a rough estimate can be made of the safe zone for simultaneous linear acceleration and angular velocity, using the simple models above. Let F equal the sum of the horizontal forces associated with both translation and rotation of the robot CoM, or $F = ma + mr\omega^2 \sin(\alpha + \beta)$. Then based on the parameters previously defined (Figs. 4.8-4.10), at the tipping threshold the stabilizing and destabilizing moments are equal:

$$(ma + mr\omega^2 \sin(\alpha + \beta))Y = mgd \quad (4.27)$$

Solving Eq. 4.27 for ω , the maximum allowable angular velocity given a

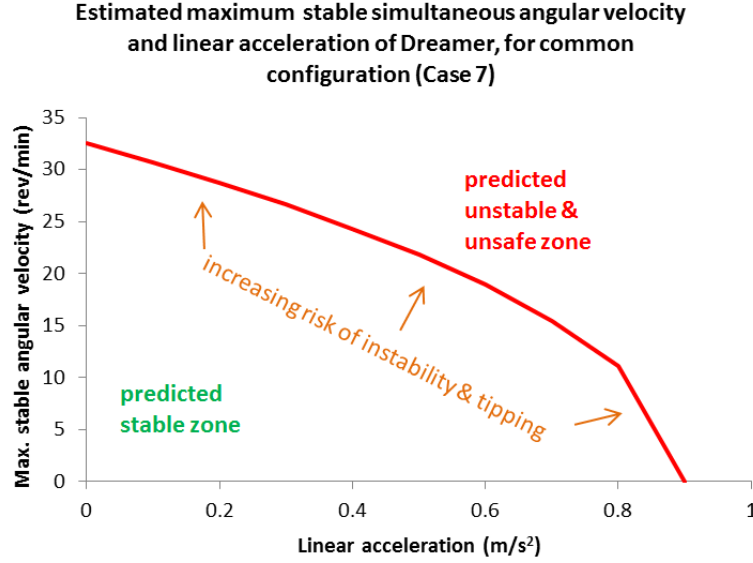


Figure 4.12: Simultaneous limits to safe linear acceleration a and angular velocity ω for the Dreamer robot in Case 7 (Table 4.2, Fig. 4.11).

certain linear acceleration then can be calculated as:

$$\omega = \sqrt{\frac{\frac{gd}{Y} - a}{r \sin(\alpha + \beta)}} = \sqrt{\frac{gd - aY}{Yr \sin(\alpha + \beta)}} \quad (4.28)$$

A curve can be obtained of the limit of ω versus a given a . An example is given for Dreamer Case 7 in Fig. 4.12. The graph indicates recommended kinematic limits in order to prevent tipping over.

Note that this graph is still a “worst-case” graph, meaning it applies when linear acceleration is in the worst-case direction, or perpendicular to the wheel contact axis closest to the center of mass. The graph is only a guideline for safe Dreamer/Trikey operation.

4.4 Generalized Safe Kinematic Limits on Level Flat Terrain

Trikey/Dreamer can safely accelerate its whole body up to certain limits before risking tipping over, depending on the position of its center of mass (CoM). Here, the analysis of safe kinematic limits to prevent tipping is extended beyond extreme cases (see Section 4.3) and uses the coordinate system defined in the kinematic and dynamic models (see Sections 4.1-4.2). The resulting generalized kinematic limit model can be implemented in the robot in real time, if necessary. *Note: The coordinate system here corresponds with the Kinematics Models and Dynamics Models (Sections 4.1-4.2), not the previous Worst-Case Analysis section. This is the more generalized coordinate system.*

4.4.1 Linear Acceleration Limit

The acceleration limit a on level ground is found when the wheel at the front of the direction of acceleration starts to lift off from the ground (Fig. 4.13). These limits can be estimated analytically for different robot designs and configurations, before physical experiments, to help avoid safety hazards. For a given CoM position $x\hat{\mathbf{i}} + y\hat{\mathbf{j}} + z\hat{\mathbf{k}}$ of Dreamer in the local frame of the robot, the maximum safe a for the CoM in any horizontal direction δ on flat ground from 0-360° (Fig. 4.14) can be calculated as follows.

First the most likely “tipping edge” \vec{E}_{PQ} corresponding to acceleration direction δ is identified. This edge is the line joining the ground-contact points of the two wheels in the rear of the direction of acceleration (Fig. 4.14). For Dreamer it

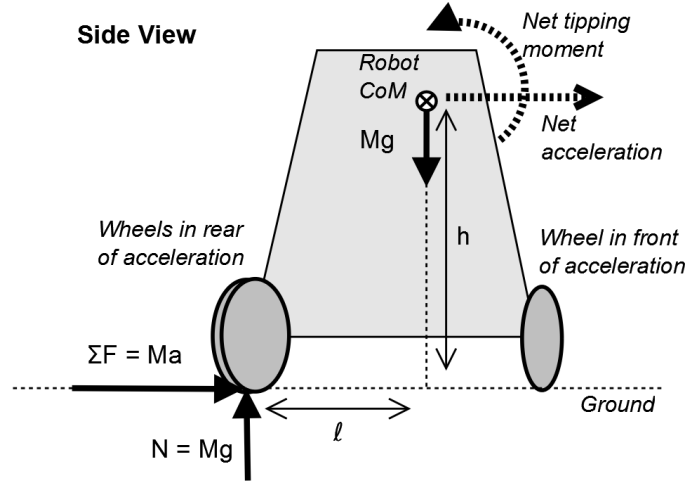


Figure 4.13: Free-body diagram of example case of robot instability. If net body acceleration is large enough, the wheel in front of the acceleration direction sees no normal forces from the ground. A tipping moment may occur around the center of mass that causes robot liftoff from the ground.

can be either \vec{E}_{12} , \vec{E}_{23} , or \vec{E}_{31} , defined as the vector:

$$\vec{E}_{pq} = \vec{w}_p - \vec{w}_q \quad (4.29)$$

where \vec{w}_p and \vec{w}_q are the position vectors of the p th and q th wheel contact points. On flat ground, vector $\vec{w}_i = R(\cos \alpha_i \hat{\mathbf{i}} + \sin \alpha_i \hat{\mathbf{j}})$, where wheel distance R and angle offsets α_i again are the same as in Eq. 4.1. For any given acceleration direction δ in the xy -plane, the corresponding tipping edge \vec{E}_{pq} is identified by first finding the critical acceleration directions δ_i of the robot. At critical directions δ_i , the robot could likely tip over two edges instead of one (Fig. 4.14). The three δ_i s in Dreamer correspond to the three wheel positions \vec{w}_i . Critical angles δ_1 , δ_2 , and δ_3 are calculated with the $\arctan2$ function to eliminate angle ambiguity:

$$\delta_i = \arctan2[\vec{c} - \vec{w}_i] \quad (4.30)$$

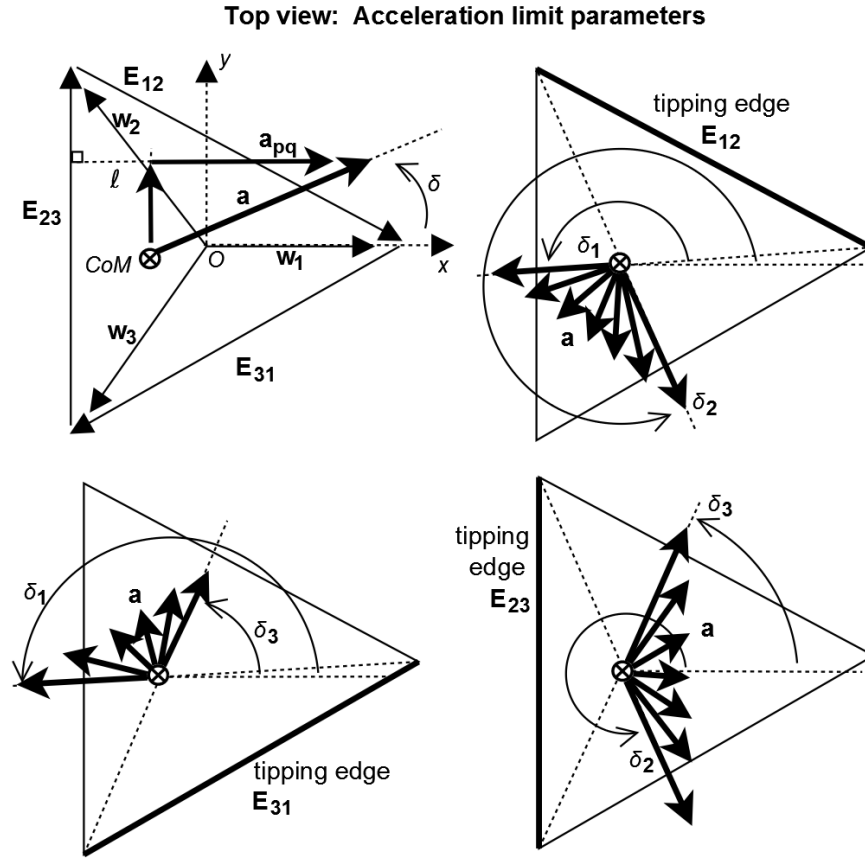


Figure 4.14: Parameters for estimating safe accelerations of the robot center of mass. Top-right and bottom diagrams show directions of accelerations \vec{a} that are most likely to cause tipping over each ground-contact edge \vec{E}_{pq} .

where $\vec{c} = x\hat{i} + y\hat{j}$ is the projection of the CoM position onto the ground. If $\delta_i < 0$ or $\delta_i \geq 360^\circ$, then they are converted to equivalent angles in the range $[0^\circ, 360^\circ)$ appropriately. If $\delta_1 < \delta < \delta_2$, then the tipping edge $E_{pq} = E_{12}$. If $\delta_2 < \delta < 360^\circ$, or $0^\circ \leq \delta < \delta_3$, then $E_{pq} = E_{23}$. If $\delta_3 < \delta < \delta_1$, then $E_{pq} = E_{31}$. Note that these logical statements apply when the CoM is within the triangular footprint of the robot. The logical statements may change if the CoM position lies outside the

triangular footprint; however, that position is nearly always an undesired or unstable case and hence is not examined here.

Next, the length ℓ of the tipping moment arm is determined, where ℓ is defined as the distance from the CoM xy -coordinate to the tipping edge E_{pq} (Figs. 4.13-4.14). On flat ground, ℓ is the vector dot product:

$$\ell = (\vec{w}_p - \vec{c}) \cdot \hat{n}_{pq} \quad (4.31)$$

where CoM position $\vec{c} = x\hat{\mathbf{i}} + y\hat{\mathbf{j}}$, vector \vec{w}_p is the same as in Eq. 4.29, and \hat{n}_{pq} is the outward unit normal to \vec{E}_{pq} :

$$\hat{n}_{pq} = \hat{\mathbf{k}} \times \vec{E}_{pq} / |\vec{E}_{pq}| \quad (4.32)$$

Let a_{pq} be the component of the acceleration that contributes to tipping instability over edge \vec{E}_{pq} . Then from Fig. 4.13, the safe limit to a_{pq} is:

$$a_{pq} = \frac{g\ell}{h} \quad (4.33)$$

where g is gravitational acceleration, h is the known height or z -coordinate of the CoM, and ℓ is calculated from Eq. 4.31. Since a_{pq} is also the projection of acceleration a at angle δ onto $-\hat{n}_{pq}$ (top-left of Fig. 4.14), the safe limit to a lastly can be found from:

$$a_{pq} = a(\cos \delta \hat{\mathbf{i}} + \sin \delta \hat{\mathbf{j}}) \cdot -\hat{n}_{pq}$$

or:

$$a = \frac{a_{pq}}{(\cos \delta \hat{\mathbf{i}} + \sin \delta \hat{\mathbf{j}}) \cdot -\hat{n}_{pq}} \quad (4.34)$$

If δ approaches a critical direction δ_i , then both tipping edges associated with i are considered separately in Eqs. 4.29-4.34, and the minimum allowable a is taken.

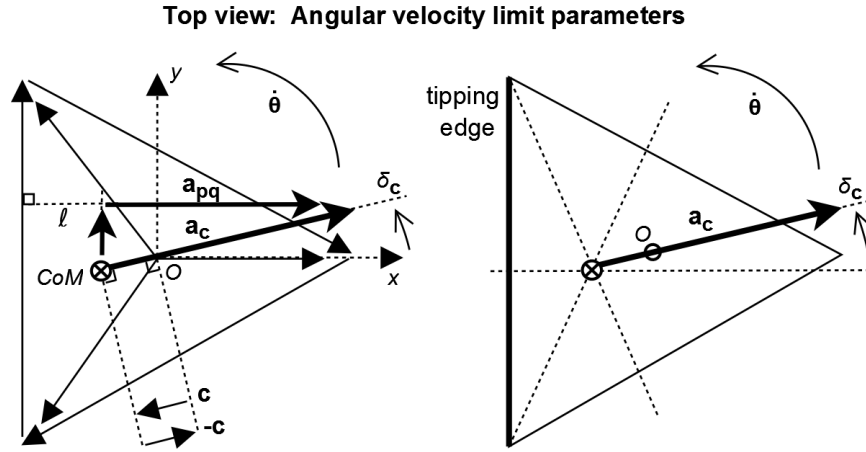


Figure 4.15: Parameters used for calculating safe angular velocity limits, when the base rotates about its geometric center O on flat ground. These are in addition to the parameters shown in Figs. 4.13-4.14.

4.4.2 Angular Velocity Limit

The method in Section 4.4.1 also was applied to estimate safe whole-body centripetal acceleration a_c , and thereby safe angular velocities $\dot{\theta}$ about the geometric center of the base O . Instead of checking all CoM acceleration directions 0° to 360° , the single centripetal acceleration direction δ_c always equals the angle formed by the CoM and the spin center O (Fig. 4.15). This fact gives a definition for direction δ as:

$$\delta_c = \arctan 2 [-\vec{c}] \quad (4.35)$$

Then the tipping edge and centripetal acceleration limit a_c at this direction are determined using Eqs. 4.30-4.34. Here a_c replaces a in Eq. 4.34. This is acceptable since a_c is still a linear acceleration, just corresponding to body angular velocity.

If we assume the standard no-slip relation that centripetal acceleration about

an axis equals the spin radius times angular velocity squared, then the angular velocity limit $\dot{\theta}$ is calculated from:

$$\dot{\theta} = \sqrt{a_c/|\vec{c}|} \quad (4.36)$$

where $|\vec{c}|$ is the CoM rotation radius or magnitude of vector \vec{c} , and a_c is the centripetal (linear) acceleration limit corresponding to Eq. 4.35 and its related calculations. This also assumes pure angular velocity, without concurrent angular acceleration, nor additional translational linear acceleration of the whole body at O .

4.4.3 Simulation of Safety Limits

In order to demonstrate the implementation of the algorithms in Sections 4.4.1-4.4.2, the general stable operating limits for Dreamer were found using a basic Matlab simulation (see Appendix C). As one example, the prototypical extreme pose CoM denoted in the first case of Table 4.1 was analyzed. Safe acceleration limits in this case were found in all acceleration directions, not just in the most unstable direction. Safe angular velocity also was calculated. The results for safe acceleration limits are graphed in Fig. 4.16.

Fig. 4.16 shows how the safe acceleration limit changes drastically with acceleration direction. The peaks correspond with accelerations directly away from a wheel, while the troughs correspond with accelerations directly away from and perpendicular to a ground-contact edge. Fig. 4.16 also agrees with earlier calculations (see Section 4.3) that the latest design is stable when seeing pure linear accelerations up to 0.10 m/s^2 in any direction from 0° to 360° , even in extremely off-center

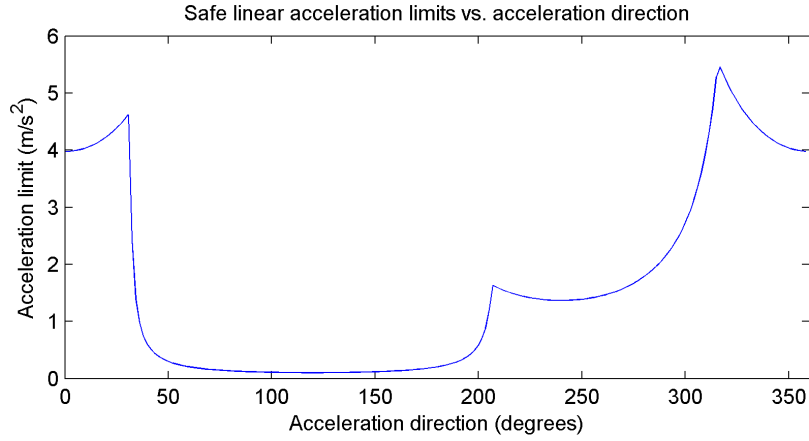


Figure 4.16: Safe linear acceleration limits versus acceleration direction, when Trikey/Dreamer center of mass is in an extreme position (Fig. 4.7). Acceleration direction refers to degrees counterclockwise from the front direction, when viewed overhead, as in Figs. 4.14-4.15.

poses with the arm fully outstretched carrying a 3.2 kg (7.0 lb) weight (Fig. 4.7). The model also confirmed that it is stable when seeing pure angular velocities up to $50^\circ/\text{s}$ (0.14 rps) in this extreme case.

In less extreme poses, with the arm close to the body and without a payload (Fig. 4.11), the robot is stable seeing pure linear accelerations up to $0.9\text{--}5.0\text{ m/s}^2$ depending on the acceleration direction, and pure angular velocity up to $190^\circ/\text{s}$ (0.53 rps). The corresponding linear acceleration limit graph is shown in Fig. 4.17.

Future implementation of an artificial vestibular system in the Dreamer robot can make use of these insights. For example, on flat ground it can quickly estimate CoM position of its body. Then instead of merely listening to hard limits initially programmed based on worst-case calculations, it can set more sophisticated limits. It could compare its intended acceleration vector with its corresponding pre-

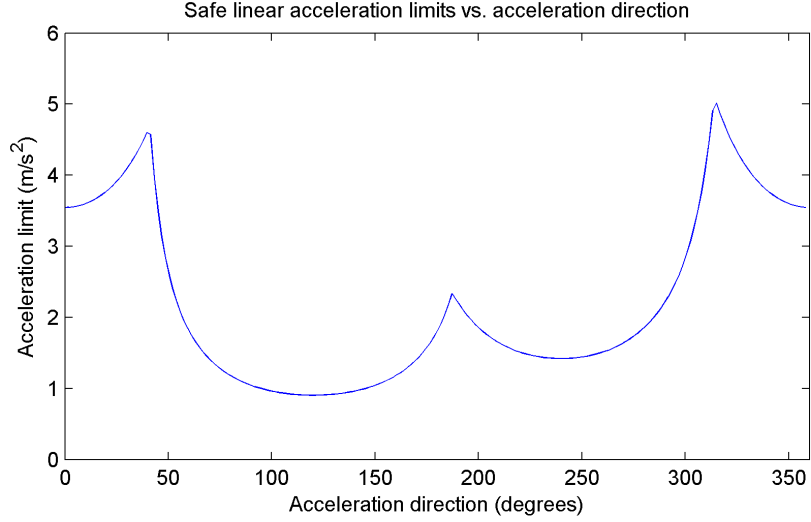


Figure 4.17: Safe linear acceleration limits versus acceleration direction, when Trikey/Dreamer center of mass is in a more common position (Fig. 4.11). Acceleration direction refers to degrees counterclockwise from the front direction, when viewed overhead, as in Figs. 4.14-4.15.

cise kinematic limits, and make sure never to exceed those limits. Further steps would be to implement this in the whole-body compliant control framework in three dimensions and on inclined terrain, which was not explored in this thesis.

4.5 Mechanical Strength & Failure Analysis

Previous strength analysis of the Trikey baseplate in Version 1 (see Section 2.1) was documented by Gupta [15], consisting of FEA that applied 500 N downward on each wheel-motor module slot, totaling 1.5 kN. The plate neither failed nor showed any deflections greater than 0.01 mm. The tested load is much greater than the actual load on Trikey currently in the Dreamer setup (<1 kN), so the baseplate is sufficiently strong.

The main additional part in Trikey Version 5 (see Chapter 3) requiring worst-case strength analysis was the upper vertical plate in the wheel-motor module (part B17, Fig. 3.10). It had to be large enough to be strong but also small enough to minimize weight. The final design strength was verified with FEA (SolidWorks 2011) assuming an extreme Dreamer configuration as in Case 1 (see Section 4.3.1). The lower-most fixation holes were held fixed. Then the plate was conservatively assumed to support all of the mass of the upper body and grasped weight, corresponding to a 445 N downward load on the upper fixation hole faces (Fig. 4.18).

To define the applied side loads on the upper fixation holes of the plate, the robot tipping forces were considered. As described in Sections 4.3-4.4, in the most extreme case, the maximum robot linear acceleration before risking tipping was estimated as 0.102 m/s^2 . Also the tipping angular velocity was $49.6^\circ/\text{s}$. These correspond to linear and centripetal forces on the robot center of mass of 4.5 N and 9.6 N, respectively, although in different directions, skew to the plate faces. As a reasonable estimate, it was assumed any forces on the plate greater than these values are likely to tip the Dreamer robot over. Much higher values of 50 N forces were applied to the upper bolt hole faces, perpendicular to the external plate faces (Fig. 4.18). This tests an extreme case where falling may be a bigger concern than mechanical failure.

FEA showed that this plate was sufficiently strong for these extreme boundary conditions (Fig. 4.18). Maximum material stresses of 31 MPa existed at the second and third rows of holes from the bottom face, but this is 44% less than the yield strength of the 6061 aluminum material (55 MPa). Given that loads are actu-

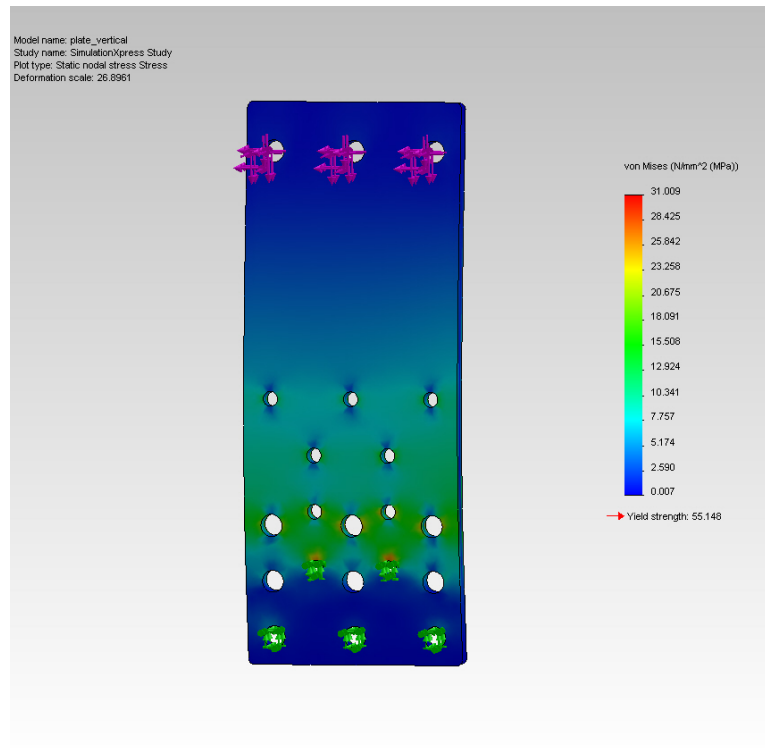


Figure 4.18: FEA result for extreme loading on upper vertical plate (part B17). Maximum von Mises stresses were less than the yield strength for the 6061 aluminum material of 55 MPa.

ality shared among three plates, not just one, and given the additional supporting struts and plates around this plate, this part is sufficiently strong enough for typical loads and configurations for Dreamer.

Additionally, the shear forces on the bolts through this plate were estimated to have sufficient strength. The bolts through the upper part of the plate are more susceptible to shear failure than the lower bolts, since they have less total cross-sectional area in comparison. Each of the three upper 3/8-16 bolts is rated by the manufacturer to have tensile strength at minimum 180 kpsi, with greater shear

Table 4.3: Recommended safe operating limits for Trikey or Dreamer robot in standard body poses and no extra payload.

Maximum body linear velocity:	1 m/s
Maximum body angular velocity (no load):	10 rpm (Safety factor >2)
Maximum body linear acceleration (no load):	0.32 m/s ² (Safety factor >2)
Torque limiter setting:	25 Nm

strength. Since the total bolt area would be 0.331 in², all together they can hold approximately 59.6e3 lbs shear load without failure. This is much greater than any loads expected on Dreamer.

4.6 Recommended Safe Operating Zones

Based on the previous sections, the recommended operating limits for the Dreamer robot in its current state (shortest height, 2.8 in forward waist offset) are given below. It is strongly recommended not to reach these various limits simultaneously, because combined extreme conditions are more likely to cause failure or operation complications. These numbers can only serve as a guideline since every situation is not testable.

Other parameters, such as maximum allowable Dreamer payloads, will most likely be determined by power and friction parameters for the various motors in the system. This can be observed experimentally.

Chapter 5

Integrated *Dreamer* Humanoid Robot

5.1 Design

Dreamer (Fig. 5.1) is a 91 kg, 31-degree-of-freedom (DOF), compliantly controlled robotic system consisting of a humanoid upper body atop an omnidirectional holonomic mobile base (see Chapter 3). It presently has one arm which can manipulate objects during locomotion, and which can sense external forces to guide locomotion. Table 7.1 in Chapter 7 gives technical specifications of Dreamer relative to similar human-centered robots already mentioned in Chapter 1, as well as the robots LOLA [22], ASIMO[26], and DLR-Biped [23]. Its size was chosen to resemble that of an adult human, so that it can fit through a standard 30 in wide US doorway (more conservative than the 32 in standard from the American Disabilities Act [35]) and reach items on a tabletop. Its cartoon-like head has actuated eyes with color cameras inside, as well as actuated ears with controllable color LEDs. This allows future experiments in visual servoing and human-robot emotional communication. The full capabilities of the sociable head are not within the scope of this paper. The upper and lower body hardware were developed separately but then integrated using one centralized communication protocol and whole-body control software.

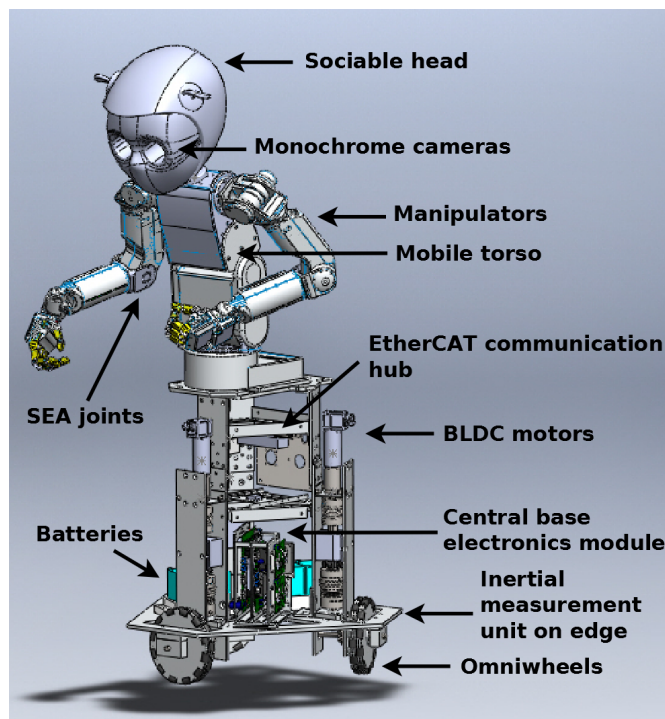


Figure 5.1: Features of Dreamer robot.

5.1.1 Upper Body Summary

The 41 kg upper body consists of a 2-DOF torso (internal-external rotation and flexion-extension), one 12-DOF arm (3-DOF shoulder, 2-DOF elbow, 2-DOF wrist, 5-DOF hands), and a 14-DOF head (4-DOF neck, two 2-DOF eyes, two 2-DOF eyelids, two 1-DOF ears). All DOFs are separately actuated, with load-bearing joints using series-elastic direct drive brushless DC motors combined with torque sensors for compliant control. An aluminum shell around all links protects internal electronics. The arm performs manipulation via the thumb and three fingers, whose surfaces are made of compliant polyurethane for increased grip.

The upper body was built by Meka Robotics (San Francisco, CA, USA) in consultation with our lab originally as a standalone robot platform for users to test their own control software. Philippsen [25] already implemented compliant manipulation in the stationary upper body, based on prioritized motion tasks. Another arm could be added in the future to investigate more complicated multi-contact manipulation with two hands.

5.1.2 Mobile Base Summary

The 50 kg base was designed to hold the upper body, allow compliantly controlled locomotion, and still remain simple enough for new users to understand and modify (see Chapters 1-4). Consequently a low-cost 3-wheeled holonomic design was chosen over any legged, caster wheel, or nonholonomic option, since it is easiest to both fabricate and control. Each of the three wheel modules were driven by a back-driveable brushless DC motor and gearbox (Maxon, Fall River, MA, USA) with 43:1

gearbox ratio, capable of an estimated 9.6 Nm of wheel torque each. In-line torque cells (Sensor Developments, Lake Orion, MI, USA) allow direct feedback control of the wheels, in conjunction with indirect feedback from driver current sensing. A clutch (R+W, Bensenville, IL, USA) protects the rotary hardware from excessive torques greater than 25 Nm. Wheel angular velocities are measured directly via 2500 ppr encoder (US Digital, Vancouver, WA, USA). The wheel modules were designed such that they could be replaced by more robust, optimized omniwheel designs [8] in the future. Other design considerations encourage future changes, including fixtures that allow adjusting the height and horizontal position of the upper body relative to the base, and extra space within the system for additional electronics.

Mechanical design accounted for predicted extreme loading conditions for Dreamer, assuming 10 kg payloads in the upper body hands and whole-body accelerations up to 1 m/s^2 . Critical parts were iteratively designed and modeled with finite element analysis to have sufficient strength. Most frame materials are 6061 aluminum alloy for its strength-to-weight ratio and machineability. An Attitude Heading Reference System (AHRS, MicroStrain, Williston, VT, USA) connected to the frame measures robot inclination, orientation, and acceleration. Internal electronics can be shielded with plastic covers.

5.1.3 Power & Communication

The Dreamer electrical system is composed of two parallel systems joined by a central communications hub (Fig. 5.2). It can be powered either tethered

(120 VAC) by plugging in the relevant AC/DC converters, or by battery power (24 VDC) housed in the lower base, if disconnected from AC power. Plugging in to AC power will also recharge the lead-acid batteries. DC/DC power distribution boards operate in both the lower and upper body, smoothing voltages coming from the battery and AC/DC converters and switching power modes as needed. Two emergency stops can cut off power at this level for the lower body, and one can do so for the upper body.

The base and upper body each have smaller power boards that further distribute different levels of DC power and send and receive communication signals. An EtherCAT hub (Beckhoff, Verl, Westphalia, Germany) connects to a real-time PC and communicates between the PC and the upper and lower body hardware. EtherCAT (Ethernet for Control Automation Technology) is a high-speed fieldbus system based on Ethernet physical infrastructure but optimized for faster communications [18]. Human-centered robotic systems are moving toward more EtherCAT communication protocols (Tables 1.1, 7.1).

The real-time PC (2.67 GHz Quadcore i5, 6GB RAM) runs Ubuntu with Real Time Application Interface (RTAI) for Linux. RTAI is an open-source interface that patches a standard Linux kernel and adds real-time capabilities. Other recent robots have used this operating system (Tables 1.1, 7.1). Commercial control software (M3, Meka Robotics, San Francisco, CA) runs in Ubuntu-RTAI and uses shared memory to send and receive joint-torque signals between higher level WBC software on the PC and the Dreamer motor controllers. Various sensor data also is sent to the PC through the the M3 software via EtherCAT.

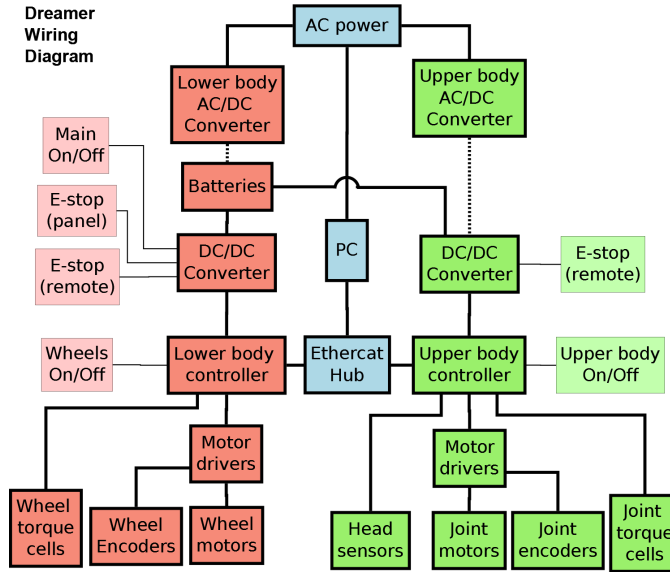


Figure 5.2: Block diagram of Dreamer system wiring and electrical connections.

5.2 Whole-Body Compliant Control (WBC)

Modified WBC software [25] was built into Dreamer, integrated onto the lower-level M3 motor controller already built into the Meka Robotics hardware. The WBC software architecture operates the robot dynamics in three decreasing tiers of priority: first the body center of mass (CoM), then the hand (end effector), and then the torso posture. Control of the CoM constrains control of the hand, and both CoM and hand constrain control of posture.

The mathematical foundation of WBC for humanoids was detailed previously [28]. Briefly, if link and motor mass-inertia and sensor data are accurate, they determine the Jacobians that transform joint torques to whole-body dynamics. The

general control equation for the system is:

$$\tau = \mathbf{J}_{com}^{*T} \mathbf{F}_{com} + \mathbf{J}_{hand}^{*T} \mathbf{F}_{hand} + \mathbf{J}_{posture}^{*T} \mathbf{F}_{posture} \quad (5.1)$$

where τ is the output joint torque matrix, and the \mathbf{J}^* matrices are the prioritized constraint-consistent Jacobians of the CoM, hand, and posture, respectively. The Jacobians must be found recursively, CoM first and posture last. The matrix sizes reflect the degrees of freedom in the robot.

The controller uses joint torque feedback to determine joint positions and guide the CoM, hand, and posture to desired configurations, while minimizing joint accelerations (and torques) if desired. The closed-loop dynamics follow linear control equations (Fig. 5.3). More information on accessing the open-source WBC code is in Appendix C.

5.3 Automatic Balancing

Most humanoid robots previously described in the literature are only meant to move in flat, level surfaces. However, human-centered robots should foreseeably be able to traverse sidewalks, city streets, and other non-flat or non-level terrains that people use. For these reasons basic behaviors were implemented to help keep Dreamer balanced and stable on sharp inclines, similar to a person.

The incline of the robot base is measured directly via the Attitude Heading Reference system (AHRS), which contains an inertial measurement unit sensitive to gravity. The posture can then automatically adjust to compensate for measured sagittal tilt.

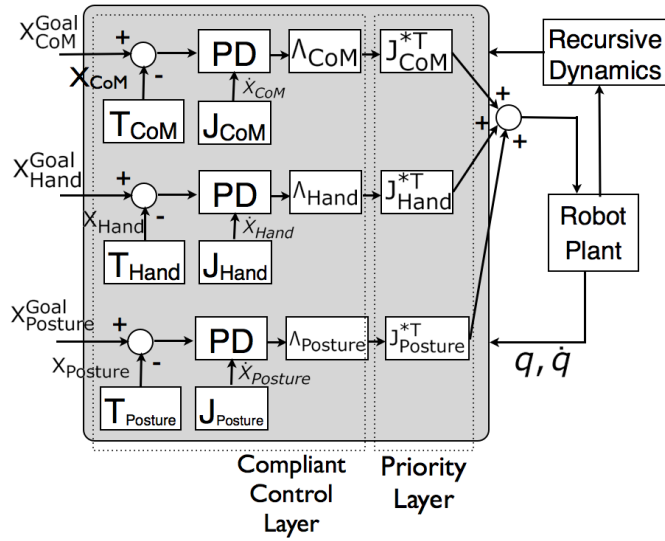


Figure 5.3: Block diagram of prioritized, closed-loop, whole-body compliant controller for Dreamer. Joint torque outputs are adjusted based on desired and actual CoM, hand, and posture positions, prioritized Jacobians, and controller gains, following the general linear control equation $\ddot{x} + K_p e + K_d \dot{x} = 0$. *Image courtesy of Kwan Suk Kim.*

More advanced balance techniques have not yet been implemented but can use the CoM position. The CoM coordinate can be estimated in real-time and adjusted to stay over the triangular base along the line of gravity. Furthermore, algorithms similar to those described in Section 4.4 should also be implemented in the future, in order to update safe robot operating limits in real-time. These more complex algorithms on center of pressure are not detailed here.

Chapter 6

Test Results

6.1 Component Calibration

6.1.1 Torque Limiters

During the design of Trikey Versions 2 and 3 (see Chapter 2), the torque limiter slipping torques were tested using a basic setup of custom fixtures (Figs. 6.1-6.2). The test consisted of systematically applying greater torque load to the device until it slipped. Hanging weights were successively added to a moment arm fixed to a central rod that was rigidly attached to the torque limiter on one end. The torque limiter was rigidly clamped to a table to prevent it from turning. Slippage was observed when the torque limiter rotated from the starting static position. All three torque limiters were shown to slip at the desired 60 Nm threshold during the design of Trikey 2, and then at the desired 25 Nm threshold during the design of Trikey 3.

6.1.2 Torque Cells

The torque cells were calibrated (Fig. 6.3) similarly to the torque limiters (see Section 6.1.1) so they could be properly integrated with the BLDCMCs (Fig. 2.5). For this test, though, loads were both successively increased and decreased in both positive and negative moment directions, in order to find any complicating hysteresis behaviors. The expected linear relationships were confirmed between

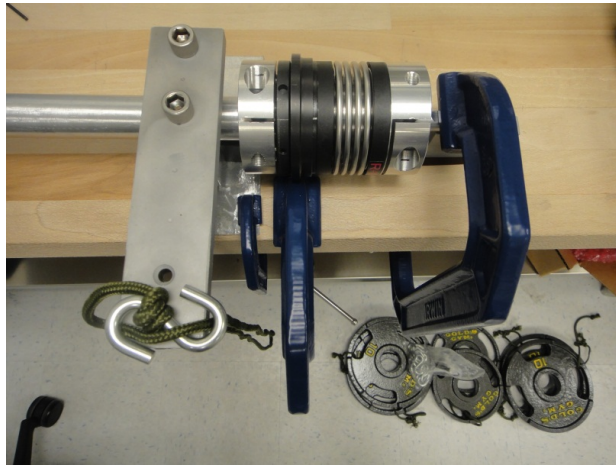


Figure 6.1: Torque limiter limit test setup (top view).



Figure 6.2: Torque limiter limit test setup (side view).



Figure 6.3: Torque cell basic calibration test setup. The setup required a multimeter, a 5 VDC power source (or the HCRL motor controllers, supplied with 24 VDC), custom test fixtures (see Appendix), the torque sensor and connector, 0.5 in square keys, rope, weights, S-hooks, 6 in C-clamps, and shim. An alternate, more robust calibration method would use a materials testing frame but would require more elaborate fixtures.

torque and output voltage, with very minimal offset and hysteresis, as shown in the following results.

The nominal sensitivity of each sensor was 2 mV/V at a 500 in-lbs load - i.e. 2 mV per excitation volt, per 500 in-lbs. Approximately 5 V excitation was supplied to the sensors via the HCRL-BLDCMCs, implying an expected linear voltage-to-load relationship of 0.02 mV/in-lb for each sensor. The actual voltage-to-load relationship was measured (Fig. 6.4) and compared with the expected relationship (Table 6.1.2).

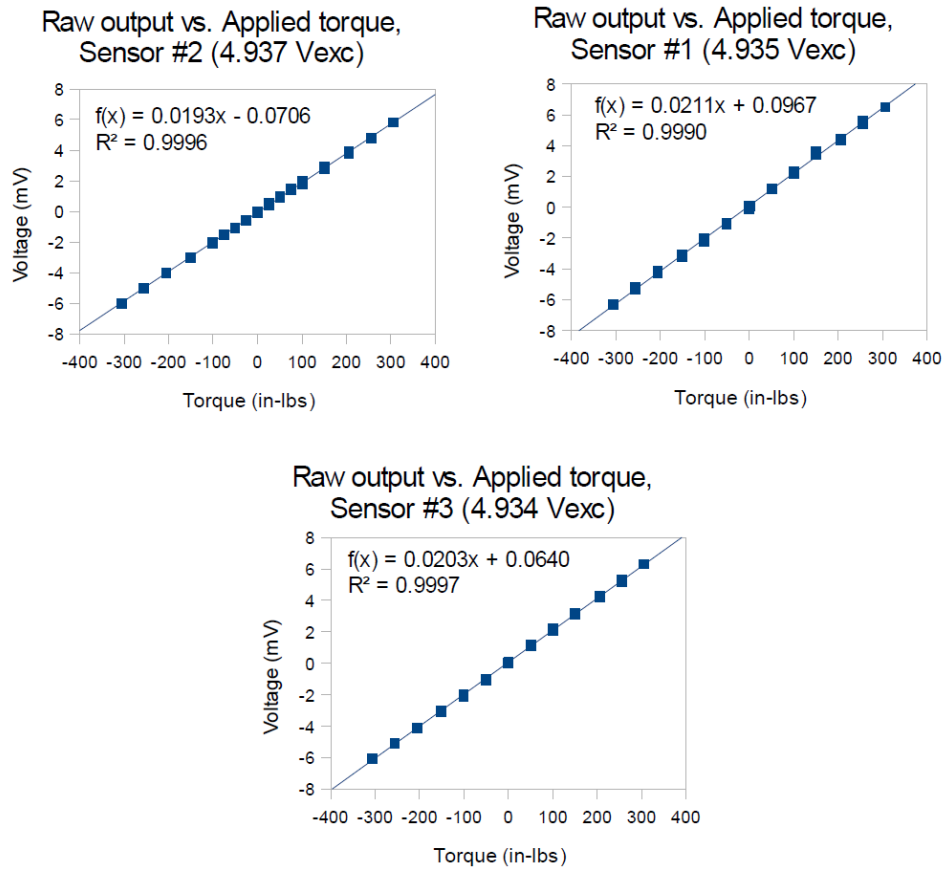


Figure 6.4: In-house raw calibration data for the three Trikey torque cells in March 2011, matching well with manufacturer data supplied in Summer 2010.

Table 6.1: Calibration data for the three Trikey torque cells in March 2011, matching well with manufacturer data supplied in Summer 2010.

Torque sensor	Excitation voltage (V)	Nominal mV/in-lb	Measured mV/in-lb	% Difference
1	4.935	0.01974	0.0211	7.08%
2	4.937	0.01975	0.0193	-2.49%
3	4.934	0.01974	0.0203	3.01%

The measured calibration curves matched well with the manufacturer’s supplied calibration data, with differences of <10%. This may be reasonable, because errors are likely also due to the nature of the testing fixtures, which had to be set up completely by hand each time. These relationships could be used in determining proper sensor gains later in the system design.

Additional data were measured after signal conditioning via the HCRL-BLDCMCs in both March and December 2011, but not shown here, since they indicated similar healthy results.

The Meka signal conditioners were eventually used in the Trikey Version 5 design (see Chapter 3). Initial indications suggest that the torque sensors continue to function properly, but that the Meka signal conditioners may have too small a gain or an ineffective filter. Currently work is being done to solve this problem and quantitatively confirm the calibration curves again with the new electronics.

6.2 Investigation of Original Gearbox Failures

Observations and testing showed that the original motor-gearbox assembly that was used up to Trikey Version 2 (see Section 2.2) showed inferior performance



Figure 6.5: Original motor-gearbox assembly from Trikey 2 that exhibited poor mechanical performance.

and had to be replaced. It consisted of the MOOG motor and gearbox described previously [15] and transmitted rotation downstream to the torque sensor and wheels through a rigid monoblock aluminum coupler (Fig. 6.5). Qualitatively, the assembly was very noisy and felt mechanically erratic to the touch. Specifically it exhibited high backlash when changing rotary direction, and it gave nonconstant torque, current, and speed readings even when given a constant driving signal.

The root causes of this inadequate performance were unknown at first. Hypotheses of the causes were presented and ruled out one by one via reasoning, more observations, and tests. The HCRL-BLDCMCs and wiring were deemed not a main cause because they ran other types of motor-gearbox assemblies smoothly and mea-

sured smooth signals. The clutch and torque cell were ruled as unlikely causes, since they were OEM parts, and upon isolation from the wheel-motor assembly, they moved smoothly without problems.

When the wheels were isolated from the motor-gearbox and tested manually, laxity in the keyways of the wheels, axles, and miter gears were found to be one significant contributor to backlash and inconsistent torque. Attempts to tighten the laxity by filling gaps with shim appeared to mitigate the problem for the wheels, at least temporarily, suggesting a partial mechanical solution. However, when isolating the motor-gearbox from the rest of the assembly, some complications arose.

When isolated from everything else, the motor-gearbox was observed to move mostly smoothly and with much less noise. This suggested lower internal friction and good operation for these two components. When they were connected to the rest of the assembly, however, they appeared to be much noisier and again showed inconsistent current from the HCRL-BLDCMC readings, even when the lower axles and wheels were disconnected.

Following this evidence, it was hypothesized that the motor-gearbox housing was becoming misaligned only upon fixation in the assembly, and that the misalignment was exerting undesired forces on the planetary gears of the gearbox and increasing friction. Opening the gearbox (Fig. 6.6) gave evidence supporting this hypothesis. The gears were found to bind more when the central rotor saw side loads, especially at particular angular positions where gears would “catch” the side more. Greasing the gearbox did not solve the problem. It also was hypothesized that further operation while misaligned would cause more wear over time and higher



Figure 6.6: Original planetary gearbox from Trikey Version 2, open and greased.

friction.

The misalignment could have been caused by loose tolerances in the original aluminum plates and coupler; the aluminum fixtures were likely not square enough. An aggravating factor was that the gearbox housing was not robust, as it was shown to be relatively easily detachable from the front face, even by hand. Given all these observations, the decision was made to replace the motor-gearbox components. Additionally the monoblock coupler was to be changed to a more robust OEM coupler that would allow some shaft misalignment between the gearbox and the torque cell, to help avoid unwanted stresses in components that could cause misalignment. The changes were detailed by Gupta [15] and implemented in Trikey Version 3 (see Section 2.3). Tests at that point showed much smoother operation, less backlash, and

less noise than the old motor-gearbox assembly, and the project could proceed with the new designs.

6.3 Whole-Body Compliant Control (WBC)

We conducted physical experiments on Dreamer to test the performance and safety of the control algorithm and overall robot design. The most sophisticated example of demonstrated successful WBC thus far was a human-robot interaction task where the experimenter guided the robot up a small incline (Fig. 6.7). The CoM and posture positions were set to low impedance, while the relative hand position was set to high impedance. An experimenter could move the whole robot with minimal force by dragging the hand only, while the hand remained stable in the local robot coordinate frame. Similar experiments showed the ability to have “soft” control of various joints. These tests are detailed in other upcoming publications of the HCRL.

6.4 Auto-Balancing on Inclined Terrain

Use of the AHRS sensor to aid in automatic posture adjustment for balance was successfully demonstrated over multiple trials (Fig. 6.8). This behavior is a proof-of-concept that encourages further software development. Currently the feature was only practical up to inclines of 10° , even on the high-friction test surface of wood with sandpaper (Fig. 6.9). The robot wheels could not function properly at greater inclines under force-guided motion. This suggests that the act of adjusting the CoM position may be overloading a wheel, which can prevent normal spinning.

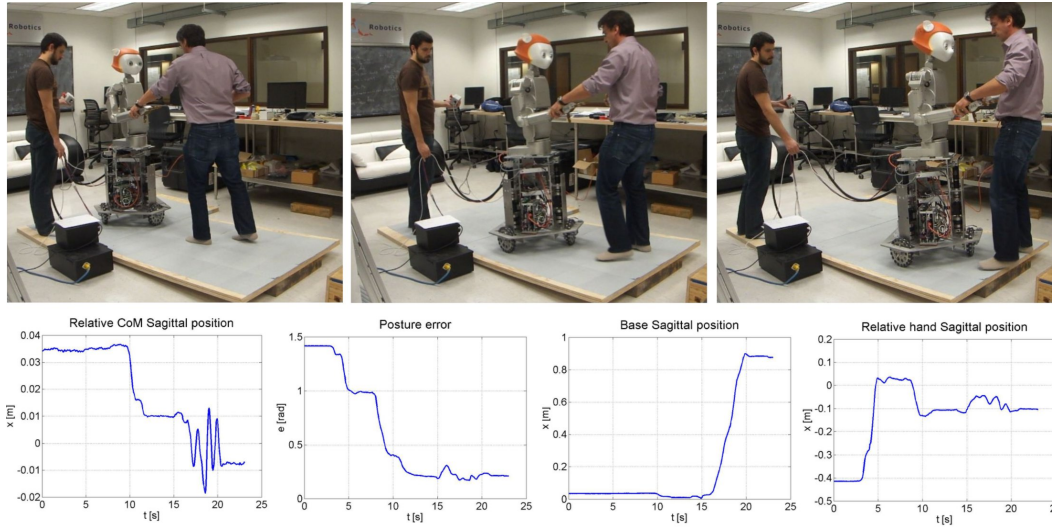


Figure 6.7: Demonstration of whole-body compliant control experiment. Dreamer body and posture position could be altered by a human (center) without altering the relative hand position (right). *Image courtesy of Luis Sentis and Josh Petersen.*

Future designs should consider the overload case, especially if the robot is intended to cross inclined terrains.

6.5 User Experience

An additional qualitative result from these tests was that people could reasonably safely and comfortably handle the robot under compliant control. The effort required to displace the robot hand in Figs. 6.7 and 6.9, for example, were minimal, since the control algorithm modulated all the joint torques to aid robot movement along a path. Future work should address the issue of unexpected forces or displacements on the heavy main body or base, since the compliant control algorithm may have limited safety benefits in those crash cases. Tests showed that the wheel

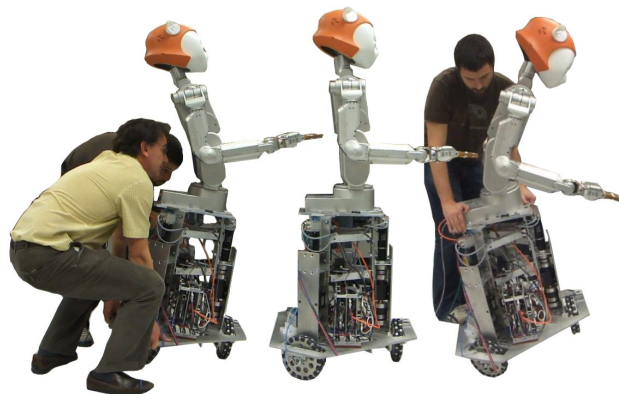


Figure 6.8: Example demonstration of automatic balancing. The torso adjusts to account for base tilting measured by an inertial measurement unit. *Image courtesy of Luis Sentis and Josh Petersen.*

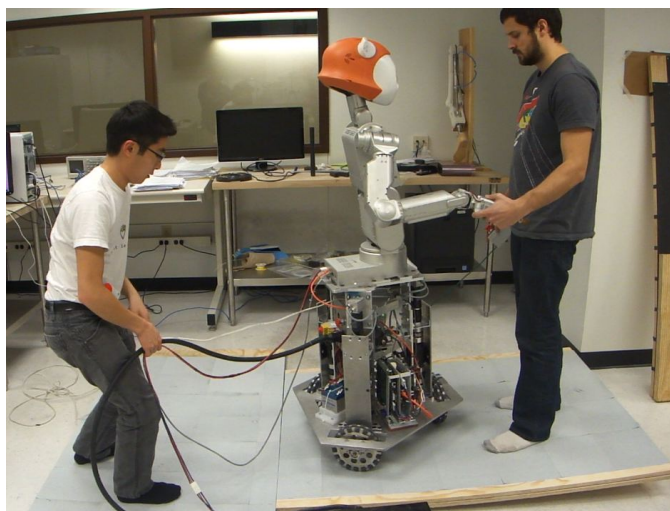


Figure 6.9: Example demonstration of force-guided motion up a ramp, where Dreamer is led by a human. Tests were run tethered to AC power here.

actuators can function well in force-control mode, too; however, having a “floating” heavy, high-momentum base that can be bumped around a room easily may not be safe. To address that concern, other behaviors must be developed. Also, additional soft and smart electromechanical structures could be attached to the outer frame.

Chapter 7

Design Evaluation & Method Recommendations

7.1 General *Dreamer* Evaluation

According to the literature (Table 7.1), recently developed robots similar to Dreamer have much potential to improve their human-centeredness. The AZIMUT-3 [12], Walbot [32], and DLR-Biped [23] robots are or have the capability to be compliantly controlled, but they do not have a humanoid upper body nor multi-link manipulators. This lack of human-centered characteristics (see Section 1.2) can be disadvantageous for working among people. The Justin robot [37] has a humanoid upper body and may have the potential for WBC, but this has not yet been published. It also has a complex system of reconfigurable actuators that add functionality at the cost of much greater mass than an average human. The humanoids LOLA [22] and ASIMO [26] are lightweight, but they demonstrate position control instead of compliant control.

The Dreamer system was designed mainly for implementing safe whole-body compliant control (WBC) in a humanoid mobile robot for the first time, and experiments have demonstrated this capability (see Chapter 6). In comparison to the published specifications of other human-centered robots (HCRs), Dreamer is novel mainly for its WBC capability, as shown in Table 7.1, which compares Dreamer to related precursor HCRs across a range of characteristics. The robots were chosen

for comparison because they all have similar structures or goals of working among people, are mobile, and appear in recent research publications. Dreamer uniquely implements control code that was only previously simulated, and it is open for future hardware and software upgrades for continually improved performance.

Table 7.1 also indicates several design directions for HCRs. Basic traits show that they should be lighter, have more DOFs, and use less power for a longer battery life. Other desired human-friendly characteristics include WBC, configurable limbs or terrain adaptability, and an as-yet undefined set of increasingly complex senses and behaviors. No single robot thus far excels in all these criteria. Robotics is moving toward better human-centeredness with increasing integration of approaches, but ideally all approaches would be taken. In the future, these criteria could be a checklist or metric for human-centeredness.

Future redesign avenues for Dreamer, and for HCRs generally, should aim to improve each of the criteria in Table 7.1 and ultimately expand the criteria list. In the short term, more complex WBC tasks will be programmed into Dreamer given the existing hardware, including picking up and placing objects, writing on a chalkboard, and navigating. In the longer term, future work will encompass advanced perception and sociability, making use of the head DOFs and sensors for object recognition and facial communication. Mechanical redesigns should include replacing the wheels to accommodate larger obstacles, and replacing structures with lighter plastics or composites to approach the masses of LOLA or ASIMO.

Other redesigns should only be made conditionally, depending on practical considerations. For example the wheel control algorithm could potentially improve

if it incorporates wheel-floor slip. However, this may only be effective for a more robust, dirt-resistant wheel design; the current design will not tolerate dirty outdoor surfaces in the first place, where slip is present. As an educational tool Dreamer will see multiple users and redesigners, and these design forks that the users may address must be monitored for efficient development.

In the long term, design advancements will come from resolving the many conflicts in HCR design criteria. Example conflicts include the tradeoff between increasing the number of DOFs and increasing mass and control complexity. Efficiency and battery life also tend to decrease when other capabilities are added. These conflicts offer numerous opportunities to mine creative design methodologies [24] for solutions.

Table 7.1: Published specifications and abilities of *Dreamer* robot versus similar recent human-centered robots. N/A = not applicable, N/I = not indicated in citation.

Trait	Robot						
	Dreamer	Rollin' Justin	ARMAR-III	AZIMUT-3	Walbot	LOLA	ASIMO DLR-Biped
General							
Humanoid lower body	-	-	-	-	-	✓	✓
Humanoid upper body	✓	✓	✓	-	-	✓	-
Mass	91 kg	199 kg	N/I	N/I	N/I	55 kg	49 kg
Height	1.65 m	N/I	N/I	N/I	N/I	1.80 m	1.1 m
Degrees of freedom (DOFs)	31	51	43	8	4	25	12
DOFs, lower body	3	8	3	8	4	14	12
DOFs, upper body	28	43	40	0	0	11	0
Whole-body compliant control	✓	N/I (in progress)	N/I	N/A	N/A	N/I	N/A
Self-reconfigurable	-	✓	✓	-	-	-	-
Power							
Supply	internal	internal	internal	internal	N/I	external	internal
Input voltage	24VDC	48VDC	24VDC	N/I	N/I	N/I	48VDC
Rated power	1kW	0.5-1kW	N/I	N/I	N/I	N/I	N/I
Battery type	Lead acid	Li-polymer	N/I	Ni-hybrid	N/I	N/A	LiFePO ₄
Rated battery run-time	>15 min	3 hrs	8 hrs (25% drive)	2-3 hrs	N/I	N/A	5 hrs
Communication and Computation							
Communication protocol	EtherCAT	EtherCAT	Gigabit Ethernet	CAN bus	N/I	Sercos-III	Sercos-II
Processor	Quadcore i3 PC	4 MiniITX	PC, PC/104	MiniITX	N/I	PC	MiniITX

Continued on next page...

Table 7.1 ...continued from previous page

Trait	Dreamer	Rollin' Justin	ARMAR-III	AZIMUT-3	Walbot	LOLA	ASIMO	DLR-Biped
Operating System	Linux Ubuntu RTAI	Linux	Linux RTAI	RealTime Linux	N/I	QNX Re- alTime	multiple	VxWorks
Locomotion								
Footprint	3 wheels (omni)	4 wheels (caster)	3 wheels (omni)	4 wheels (caster)	4 wheels (omni)	2 feet	2 feet	2 feet
Rated maximum speed	1 m/s	1.5 m/s	1 m/s	1.47 m/s	N/I	1.4 m/s	0.44 m/s	1.35 m/s
Lower body compliant control	✓	-	N/I	✓	✓	proposed	N/I	proposed
Maximum passable incline	10°	17°	N/I	N/I	N/I	N/I	N/I	N/I
Manipulators and Arms								
No. of arms	1	2	2	0	0	2	2	0
DOFs per arm (minus hand)	7	7	7	N/A	N/A	3	5	N/A
DOFs per hand	5	12	8	N/A	N/A	N/A	1	N/A
Upper body compliant control	✓	✓	N/I	N/A	N/A	proposed	N/I	N/A
Sociability & Human Interaction								
Expressive head	yes (eyes, ears)	N/I	possible	-	-	-	-	-
DOFs, head and face	14	2	7	N/A	N/A	3	2	N/A
Speech recognition	no	yes (Sphinx)	N/I	no	no	N/I	yes	N/I
Sensing & Perception								
Direct torque sense	✓	✓	✓	✓	✓	✓	✓	✓
Inertial measurement unit	✓	N/I	N/I	-	-	✓	N/I	✓
Vision and cameras	✓ (stereo, monochrome)	✓ (stereo)	✓ (stereo, color)	-	-	can connect	✓ (stereo)	N/I
Artificial skin	-	-	✓	-	-	-	-	-
Obstacle sense	-	✓ (vision)	-	✓ (laser)	✓ (laser)	N/I	✓ (vision)	N/I

Continued on next page...

Table 7.1 ...continued from previous page

Trait	Dreamer	Rollin' Justin	ARMAR-III	AZIMUT-3	Walbot	LOLA	ASIMO	DLR-Biped
Facial recognition	-	N/I	N/I	-	-	N/I	✓	N/I
Documented Behaviors & Skills								
Automatic balancing	✓	N/I	-	-	-	N/I	N/I	N/I
Force-cooperative guidance	✓	N/I	-	✓	✓	N/I	N/I	N/I
Navigation	-	✓	-	-	✓	N/I	✓	N/I
Manipulation tasks	✓	✓	✓	-	-	N/I	✓	N/I
Data Sources								
Publication dates	2012, 2011	2009	2006	2010	2011	2009	2002	2010
Sources	Wong (present work), Gupta [15]	Fuchs [13], Wimbock [37]	Asfour [3]	Freny [12]	Song [32]	Lohmeier [22]	Sakagami [26]	Ott [23]

7.2 Proposed *Dreamer* and *Trikey* Applications

Another metric of robot human-centeredness besides objective specifications (Table 7.1) is the amount of realistic applications there are for a robot. Given the current states of the Trikey and Dreamer robots, real-world applications will require more development work, particularly in software. However, several achievable applications are proposed here for future testing.

To date, the Dreamer robot has demonstrated a set of basic abilities that theoretically can be used in everyday environments. These include compliant control at all its actuated joints, the ability to adjust center of mass according to inclines, the ability to calculate joint and end-effector loads in real-time, the ability to grasp lightweight objects, and the ability to use facial actuators for potentially emotive expression. This set of skills can be expanded with further programming. Even with these limited and minimally robust abilities, however, it potentially could perform many human tasks: wipe tables and windows by hand, deliver papers and objects, inspect the masses of objects on an assembly line, give facial “expressions” in response to sensed forces, assist and support elderly or disabled persons walking through a building, and walk a dog, for example. In the broader scope, these tasks suggest potential niches for Dreamer-like robots in service industries, or perhaps entertainment industries. A more expansive set of skills will lead to even more applications in other industries.

The Trikey robot, even detached from the Meka upper body, also has many potential applications. It can be controlled compliantly as well. If additional sensors were added, it could perform tasks like couriering payloads of at least 41 kg, leading

or following moving objects, or crashing into obstacles with controlled energies. Such skills could be useful for service industries, or in rescue or demolition activities where obstacles must be cleared.

The most obvious and immediate application of both Trikey and Dreamer is in research and education. The robots have already been used to develop and refine new control software, as well as educate many students. If the user interface of the robot can be improved, then more people may be able to access the robot for experimentation. The open structure of the Trikey base allows further sensor additions, and the open documentation of its systems here and in Gupta [15] allow others to critique, duplicate, and branch from previous work.

7.3 *Trikey* Design Evaluation

Construction and experimentation revealed a set of design advantages and disadvantages to the Trikey robot, which is the foundation of this work. The advantages mainly relate to speed of fabrication, implementation of compliant control, safety controls, flexible and modifiable design, and simplified design for educational purposes. The disadvantages mainly relate to wheel and transmission robustness, weight or mass, user-friendliness of assembly and disassembly, suboptimal electronics placement, and suboptimal geometry for integration with the Meka upper body.

The speed of fabrication was greatly improved by designing for fabrication (or manufacturability). Choosing more easily purchasable and machinable materials, designing smaller parts with simpler geometries, and using OEM parts when possible all contributed to the ease of construction. These design decisions also carried some

disadvantages, such as decreased robustness and looser tolerances for several custom parts. Nevertheless, if the design accommodated these looser tolerances, this was acceptable, such as when the shaft couplers were used in Trikey Version 3 onward (see Chapter 2). A second related disadvantage is that the robot is still heavy, and the materials could be further optimized for higher strength-to-weight ratios. However these lighter composite or smart materials are more difficult to fabricate and machine and are more appropriate for future redesigns. Finally the overall form of the base challenged modular design, because many alignment angles between parts were 60° . A four-wheel design would allow more 90° connections, which would likely allow more OEM parts.

The base accounts for safety in a few different ways. Its mechatronics were successfully controlled compliantly, both when Trikey was alone and when it was integrated into Dreamer. As noted in Chapter 1, only a few mobile robots meant to interact with people have been shown to be compliantly controlled. Currently this is an advantage for the base, although in the future such control methods are expected to be more commonplace. Besides the control algorithm, the two emergency stops add another physical layer of safety for the system, since it can be shut off up close or remotely (Section 5.1.3). Finally the potential to program kinematic limits in software based on models adds a third layer of safety (Section 4.4). The only clear disadvantage thus far for safety is that its mechanical design is not soft nor light and could cause damage upon impact if the compliance algorithm fails.

As predicted, another main advantage of Trikey is its simplified three-wheeled, omnidirectional structure. Being holonomic, Trikey does not have to account for re-

dundant actuators, and under ideal conditions there is only one set of wheel inputs to obtain a whole-body output. This was demonstrated in motion tests of the base and Dreamer. Persons with a general engineering background can refer to the design models of Chapter 4 to get an idea of its equations of motion. It is a good initial platform for testing compliant control algorithms before testing them in more complex nonholonomic or redundantly actuated systems.

Regarding design modularity, Trikey succeeded in some components more than others. The electronics module is the most easily removable module of the entire design, even when considering the electrical connections. It requires the least amount of tooling and complex steps to remove and replace as an independent unit, compared to the other modules, other than perhaps the EtherCAT module. However, the other parts of Trikey are not as modular and generally cannot be modified independently of the rest of the design.

One of the reasons for the lack of modularity in some parts of the design was a lack of an integrated design plan at the start of the project, which is not uncommon for open-ended projects. In other words, the Trikey base and Meka upper body were conceived separately, and the Trikey base had to be retrofit for the upper body beginning in Trikey Version 4. Consequently the basic frame of the base turned out too small to easily fit to the waist of the Meka upper body. The wheel modules specifically obstructed potential fixation holes and also blocked the upper body from easily being fixed to lower heights. This reduced design choices, leading to reduced modularity. These problems attest to the value of defining design specifications and early project planning whenever possible.

A final observed disadvantage is that the electronics module is currently placed in a vulnerable position on the outer edge of the baseplate. If the base crashed into a low ledge, such as a coffee table in a home, the electronics module could take direct damage before the wheels have time to react. The module was placed there to make room for all four planned batteries, but better layouts on the base might be possible in the future.

7.4 *Trikey* Redesign Avenues

Based on the observations, tests, and literature presented in previous chapters, several possible redesign avenues are compiled below, categorized approximately by overall purpose. The most recommended functional redesigns are listed first in each category, ranked subjectively by decreasing importance and ease of implementation. Possible features that can execute the functions are given for each.

7.4.1 Safety Improvements

1. **Decrease damage caused by collisions with the robot.** Although whole-body compliant control greatly aids collision safety, the current design has many hard surfaces and corners on the outside that can still cause damage.

How to implement: Attach a bumper along the entire lower base edge made of rubber or another compressible material. Cover other protrusions. Attachment holes do not currently exist along the outside, so the easiest attachment solutions may be to connect bumpers with Velcro, or to ma-

chine an undersized pocket or detent in the bumper that snaps over the baseplate edge.

Challenges: If drilling new holes in the baseplate, the electronics must be protected from debris. Bumpers must also avoid interfering with the ADHR inertial sensor.

2. **Increase the mechanical security of emergency stops.** The current push-button e-stops (nominally/normally open) can sometimes unexpectedly pop up and turn the machine on, if the button sees an impact.

How to implement: Replace the push-button e-stops with twist-button e-stops, which require a twist and a pull to reset. The extra twist step decreases the likelihood of popping open on its own. The remote e-stop particularly should be replaced.

Challenges: Some work is required to connect the new e-stop to the EtherCAT connection.

3. **Implement real-time knowledge of safe acceleration limits in software.**

Currently control software places hard global limits on robot acceleration. Smarter limits can be implemented that change according to intended motion direction, so as not to sacrifice as much performance. Especially unstable acceleration directions can be avoided entirely.

How to implement: One option is to program behavior into the robot similar to the algorithm described in Section 4.4. Another option is to continue using the existing WBC algorithm to calculate the contact forces at the wheels, which are then used to calculate the real-time center of pres-

sure or zero-moment point [27] of the robot. The point can be controlled to remain within the footprint of the base.

Challenges: This requires good knowledge of the current WBC code to properly integrate new code.

4. **Protect the electronics better.** The electronics module is somewhat exposed (Section 7.3). It also may be susceptible to vibration.

How to implement: Attach a shield around the outside of the base, or just around the electronics module with room for cable connections. Move the electronics module inward on the baseplate, and stack the batteries on top of each other to make room for this. Add a suspension system between the wheels and the electronics, or suspend the electronics module itself in a padded or compliant holder.

Challenges: A suspension or compliant case for the electronics requires significant redesign and testing.

5. **Decrease mass while retaining strength.** A smaller robot mass would decrease the energy stored in the moving system, making it safer upon accidental impact.

How to implement: Replace aluminum parts with lower-density and higher-strength materials, such as titanium or carbon-fiber-reinforced composites. Replacing some plates with beams or more open structures might also help. The wheel-motor modules take up the most weight (Table 3.2) and could be lightened by changing the motor-gearbox assembly.

Challenges: Better materials will cost more and may be more difficult to machine. Lighter actuators with the same performance are currently difficult to find, based on the original search of OEM products. A custom actuator may be ideal.

6. **Decrease the chance of tipping.** The center of mass of the Trikey base is positioned approximately halfway up its height, but a lower center of mass would help balance even more, especially when it carries a payload. A moveable center of mass also could counter instability caused by high accelerations.

How to implement: Upper structures can be selectively made lighter. Additional batteries or counterweights may be added to the lower structures. A new internal system could be added that actively moves a counterweight in response to sensed loads. Sensors added in line with the wheel contact points can help indicate load imbalance, or when the robot is close to lifting off from the ground, and trigger the counterweight to move.

Challenges: Adding weight, even if only on the lower structures, counteracts the alternate goal of decreasing the system weight. Ideally existing structures can be shifted lower to the ground, such as electrical components.

7. **Inform surrounding people of robot presence and status.** Currently the status of the robot is only known to the user at the controlling computer workstation. If all people around the robot know the states of the robot, people can more safely react to it.

How to implement: A screen or set of LED signals can be added to the structure. It should communicate the robot on/off status, load conditions, battery or power usage status, inertial measurements, current objective, and other information that may be useful to onlookers. A basic highly visible error light should be added to warn people when the robot is experience a problem, so that they can alert others or clear away if necessary. Some audible chimes could be added to the robot to make people aware of its presence as it moves.

Challenges: Requires hardware and software development.

7.4.2 Performance Improvements

1. **Improve the transmission between gearbox and wheel.** Although several transmission issues were already improved between Trikey Versions 2 and 3 (Chapter 2), the miter gears between the torque limiters and wheels too easily become misaligned after use, increasing backlash and friction.

How to implement: Replace the miter gears with a pre-aligned, pre-assembled component. Replace the wheels with a more robust design without keyway laxity. This may also aid user-friendliness of assembly and disassembly procedures.

Challenges: Increased cost and potential mechanical redesign necessary. Choosing an appropriate OEM 90° geartrain may be difficult.

2. **Improve wheel performance and robustness.** Relatively small obstacles

can obstruct the wheel, if the obstacle approaches perpendicular to the wheel face. Rotational backlash results from laxity in the wheel keyway. The soft aluminum wheel hub is susceptible to deformation and wear over time at the keyway, which mates with a steel key and axle. The design exhibits vibration and noise. The bolts holding together wheels are prone to vibrating loose when attached without locking washers.

How to implement: Redesign the wheel to address all issues. If keeping the omniwheel concept, then increase the minimum radius on the omniwheel, replace the hub-axle interface material with steel to match the axle and key, and improve the amount of continuous contact between the wheel and ground. Consider the optimized omniwheel design previously described by Byun [8]. Choose a roller material with better ground-friction properties for increased traction.

Challenges: A new wheel redesign requires weeks of design, construction, and testing steps.

3. **Resist instability and vibration from rough terrain.** The internal electronics are currently not isolated well from ground irregularities. Trikey functions best on smooth ground. Also since it has three wheels, it must keep contact with the ground at all wheels at all times to remain stable. Other bases with comparable mass already have suspension systems to address this issue (Table 1.1).

How to implement: Redesign the lower structures to leave room for a spring and damper system between the motor-wheel module and the rest of the

base. Alternately the spring-damper system can be incorporated between the wheel axle and gearbox, within the wheel-motor module, itself. These two cases are very different, both in terms of mechanical design and in terms of frequency response. The ratio of the sprung-to-unsprung mass may be different enough to affect the amount of vibration seen in the main body [38].

Challenges: Requires major hardware development and testing, and possibly vibration modeling of the system. A suspension may not fit in the current Trikey setup.

7.4.3 User-Friendliness Improvements

1. **Improve ease of assembly/disassembly.** The assembly/disassembly steps for Trikey and Dreamer (Section 3.7), though improved, are still tedious. Wheel-motor module assembly steps are particularly difficult and require a fair amount of practice and time to perform well. The wheel-motor module cannot be assembled completely before attaching to the baseplate.

How to implement: Completely redesign the original frame parts from Trikey Version 1, including the baseplate and wheel-motor module support plates. Make it possible to completely assemble one wheel-module independently and then attach it to the base. If possible, expand the space available for the Meka upper body waist by moving the motors outward. Parts B14 and B17 (Fig. 3.10) should be one single part. Replacing the miter gears

with one part as described above will diminish alignment difficulties.

Challenges: Redesign for further modularity is a large, adaptive overhaul that can affect many other components. If this is performed, other redesigns should be considered simultaneously. Care must be taken not to expand the size of the robot too much.

2. **Add teleoperation capabilities.** All control currently is performed via typed commands at the main workstation computer. Kemp [19] notes that the ability to be operated easily by a human is a growing trend in robotics. Teleoperation, preferably wirelessly, could greatly simplify user experience..

How to implement: Incorporate mouse control, joystick or gamepad control, or control with an inertial controller such as a Wii controller or smartphone. Develop a display or user-interface that helps a human understand and control the robot.

Challenges: Many design directions are possible, so difficulties depend on expertise of the developer.

3. **Improve aesthetics to make the robot more likeable.** The industrial design of the base does not match the quality of household products and may make people uncomfortable. Market research on consumer robotics [39] shows that everyday users, particularly children, base their perception of a robot on its looks. Also users have a desire to personalize or customize robots.

How to implement: A screen or display could be added that shows a face or other anthropomorphizing trait. A mechanism for attaching different skins or anthropomorphizing decals could be added to make the robot more personalizable and likeable. Square geometries could be replaced with curves, or the outside could be covered in a plastic shell to reduce the industrial look. Add color to the shell.

Challenges: Requires mechanical design and possibly new electrical parts and software.

7.4.4 Feature Additions

1. **Develop machine vision and object sensors.** Currently Trikey has no long-range or visual perception capabilities. Even as part of Dreamer, machine vision and object avoidance has not yet been integrated.

How to implement: In Dreamer, use the monochrome cameras in the eyes for perception. In Trikey alone, add laser scanners similarly to other robots (Table 7.1). Alternately, other sensors can be added, such as a camera, capacitance sensors, or microphones.

Challenges: Requires major hardware and software development.

2. **Continuous external sensing (artificial skin).** Continuous sensation across the whole robot gives the potential for reflex behaviors, self-preservation behaviors, and increased intelligence.

How to implement: Smart materials or another custom device can be laid over all external surfaces to detect pressure, light, temperature, humidity,

electromagnetic fields, strains, or other environment data. The data can trigger intelligent responses, such as stopping when detecting unexpected touches or impacts.

Challenges: Requires major hardware and software development.

3. **Add self-reconfigurability.** Trikey remains the same shape, height, and form at all times unless manually adjusted, which takes significant time.

How to implement: Add actuators to allow height or wheel configuration adjustment, or the ability to cross obstacles and climb or descend stairs.

Challenges: Requires major hardware and software development, and likely a complete rebuild.

7.5 Method for Prioritizing Potential Redesigns

For this robot, and likely for any complex human-centered robot, a very large number of redesigns are possible, but it may not be practical to implement them all. In these cases it can be difficult to choose which redesign to address first. A systematic method for organizing, ranking, and grouping the specific redesign options may be needed. One suggested method is given below.

To sort the possible feature additions or changes, each feature can be given a score that says approximately how many different functions it can achieve, and how well. First all the desired *functions* of the new system are listed, and then all the possible *features* to achieve these functions are listed. Then a simple matrix inspired by, but different from, the House of Quality method [24] can be made to score potential redesign projects. An example is given below (Fig. 7.1) based on

the redesigns in Section 7.4.

In the top row, all the desired high-level functional improvements or changes are listed. This row can also include desired system constraints, such as low cost or mass, or development time. On the left column, all the possible feature additions that could cause the functional improvements are listed. In each cell, a score is given for how well the feature is predicted to address each functional improvement. Larger positive scores mean they promote the function, while larger negative scores mean they undermine the function. A priority score is given for each feature by summing the entire row. Each column or function can be weighted differently to emphasize the importance of some functions more than others. The end result is a priority score for each feature, where higher scores mean that the feature will address the most desired functions. These high-scoring features are recommended for initial implementation projects. Features that can be implemented relatively easily, requiring minimal time and costs, are also recommended for initial implementation.

Features then should be grouped together appropriately, if they are similar in structure. For example, in Fig. 7.1, if the desired function of “informing people of robot presence and status” were weighted very highly, then the additional screen or display feature might be the highest-priority feature. When implementing this, other similar features can be combined into the same project, such as warning or error signals, a user-interface to aid human control, and anthropomorphic decals, since all of these features could potentially be integrated into one display.

Example Ranking of Redesign Options

Possible feature additions	Desired functional improvements/changes															
	Decrease damage caused by collisions	Increase mechanical security of e-stops	Real-time knowledge of safe acceleration	Protect the electronics better	Decrease mass; maintain strength	Decrease chance of tipping	Inform people of robot presence/status	Improve transmission to wheel	Improve wheel performance, robustness	Resist instability, vibration from terrain	Easy assembly/disassembly	Teleoperation capabilities	Improved aesthetics for likeability	PRIORITY SCORE (unweighted)	PRIORITY SCORE (weighted)	Estimated cost
	3	3	3	3	3	3	3	2	2	2	2	1	1			
Rubber bumpers	2			1	-1						-1			1	4	lo
Cover protrusions	2											1		3	7	lo
Replace e-stops		2												2	6	lo
Program simplified safety limit algorithm			2	1	1									4	12	
Program center-of-pressure algorithm			2	1	1									4	12	
Shield around base	1			2	-1						-1	1		2	5	lo
Move electronics inward, stack batteries	1			2	1							1		5	13	lo
Add suspension, outside wheel module				1	-2	1				2	-1			1	2	hi
Add suspension, inside wheel module				1	-2	1				2	-1			1	2	hi
Suspend electronics in compliant case				2	-1					1	-1			1	3	hi
Replace parts with lighter materials	2			2	-1			1	-1	1				4	11	hi
Replace motor-gearbox with lighter one	1			2	-1			1	-1					2	6	hi
Lighten upper structures selectively	1			2	2			1						6	17	hi
Active counterweight at base	-1			-2	2					1	-1			-1	-3	hi
Vertical load sensors in wheel modules			1			2					-1			2	7	hi
Screen/display for information, face							2				-1	1	2	4	7	hi
Warning/error lights, chimes	1						2					1	1	5	11	lo
Replace miter gears with prealigned part								2			2			4	8	hi
Larger wheels, steel, higher quality					-1			1	2	2				4	7	hi
Independent wheel-motor modules								1	1		2			4	8	hi
Move motors outward, increasing space											1			1	2	
Integrate joystick, mouse, smartphone												2		2	2	hi
User-interface for aiding human control							1					2	1	4	6	hi
Anthropomorphizing decals											-1		2	1	0	lo
More curved geometries	1												1	2	4	lo
Colored non-metallic outer shell	1				-1		1				-1		2	2	3	lo

Figure 7.1: Example design feature priority matrix. Feature ideas are on the left. Desired functions are at the top. Each cell scores how well a feature can achieve a function. For example adding rubber bumpers (1st row) can decrease damage in collisions (+2 score) but also increase robot mass (-1 score). The final score for each feature is the weighted sum of row scores. High-priority features are highlighted in yellow. Low-cost and low-development time features are highlighted in green.

7.6 Method for Measuring Quality of Redesigns

Any future redesign project should objectively compare the old system to the new system, to confirm and quantify functional improvements. If several redesigns are concurrent, one method of organizing the improvement metrics was previously described by Otto [24] as the House of Quality matrix. An example is shown in Fig. 7.2 for evaluation of safety improvements. On the left side are all the desired new functions related to safety, detailed in Sections 7.4-7.5. On the top row are quantitative metrics that can be found for the new and old system, where each function corresponds with at least one metric. In each cell is an arbitrary weight for how well a function can be judged by a given metric. Higher scores mean that the metric measures that function better. At the top, the up- and down-arrows indicate the desired direction of values for the metric; for example system mass should be lower and has a down arrow. The triangular region at the top is an approximate correlation matrix, which shows which metrics are positively and negatively correlated. For example, better system mass likely means that the robot is smaller, which might make the robot less noticeable to people. The negative sign at the top indicates this negative correlation between better system mass and better noticeability. At the bottom is a set of desired values for each of the metrics. The philosophy behind the matrix is that the only relevant improvements of a system are the ones that can be measured.

If a safety redesign of the robot is implemented, this example matrix gives a set of tests that can be run to help evaluate quality of the redesign. The resulting metrics before and after the redesign can be ranked. Specific desired functions then

[illegible]

Decrease damage caused by collisions	3		9	9	9								
Increase mechanical security of e-stops	3				9								
Real-time knowledge of safe acceleration	3					9	9						
Protect the electronics better	3							9	9				
Decrease mass; maintain strength	3	9											
Decrease chance of tipping	3					3	9					9	
Inform people of robot presence/status	3												9
Technical Difficulty		2	1	4	2	3	4	3	1	2	3		
Measurement Units		kg	Gpa	kPa	%	%	%	m	#	#	#		
Object Target Values		70	0	0	0	0	100	0	0	0	TB		

Figure 7.2: Example “House of Quality” matrix for desired functional improvements in robot safety. Desired functions are on the left. Metrics of quality for these functions are at the top. The first function (1st row) of “decreasing damage caused by collisions” corresponds well with lower system mass, lower elastic moduli at the exterior, and lower stresses in crash tests, and hence scores 9 for those metrics.

can be compared before and after using weighted averages of the relevant rankings. Ideally other robots in the literature could be compared as well, but oftentimes such data is not published, as implied by Tables 1.1 and 7.1.

7.7 Metrics of Human-Centeredness

Based on the review of literature, design process, analysis, testing, and evaluations performed in this work, below is a set of recommended functions to incorporate into an ideal, all-purpose human-centered robot (HCR). For each function, suggested metrics are given, based on the principle of measurable quality in Section 7.6. One main goal of this list is to provide more comprehensive design guidance for robot developers, especially students. It details and adds to the suggestions of Kemp [19], which already outlines many desired functions for new manipulator robots.

The second goal of the list is to suggest common measurements for all HCR developers to make, across different institutions, so that robots can be better compared in the future. This is analogous to how biologists compare organisms according to lifespans, bone stiffness, running speed, and other quantifiable traits. The features that produce these functions will probably be varied and numerous, just as genetic markers, bone structures, and muscle physiology all differ in organisms to produce different performance.

The metrics of robot function below can give an overall idea of the human-centeredness of a robot, and additional ones are possible. Each function and metric can address multiple issues of safety, performance, user-friendliness, and intelligent behavior. The following is the list of desired general *functions* and associated *metrics*

for an ideal human-centered robot:

Minimal damage in unexpected collisions: System mass (kg), average elastic moduli of exterior materials (GPa), highest stresses resulting from crash tests and simulations (kPa), head-injury criterion [40] and/or manipulator safety index [30] associated with maximum manipulator and robot velocities and impact accelerations.

Ability for safe, fast system shutdown: Longest time necessary to trigger the emergency stop and for the robot to stop all motion (ms), braking time to stop from 1 m/s to 0 m/s and remain stable, chance that an emergency stop button will unintentionally reset upon impact (%).

Real-time knowledge of safety limits: (Artificial vestibular system) Percent error between detected and actual accelerations (%).

Protected electronics: Number or area of exposed electronic circuit boards, amount of sprayed water that seeps through external protective housing (m^3).

Lower mass / human mass: System mass (kg), system density (kg/m^3).

Minimal loss of balance: Height of system center of mass in standard and extreme body configurations (m), horizontal distance of center of mass to closest tipping edge (m), chance that the robot falls over with sudden side and front loads resembling a human push (%).

Inform people of presence and status: Time needed for a person to recognize that robot is present or arriving for a standard task, such as cleaning or delivering items (s).

Energetic efficiency: Power usage (W), motor efficiencies for individual joints (%).

Long untethered operating time: Battery lifetime at rated power (min).

Protection from vibration: Root-mean-squared of vibration profile measured by an accelerometer internal to the robot near the electronics (m/s^2).

Easy assembly/disassembly: Assembly time (min), disassembly time (min), number of parts, number of required fasteners, number of independent modules.

Easy to maintain and clean. Number of parts, number of exposed parts, number of parts exposed to or interfacing with the ground, fatigue life of cyclically loaded parts.

Teleoperation capabilities. Lag time between controller and plant for straight motion, decelerating, and other standard motions (ms), maximum distance possible between user and robot during operation (m).

Ability to carry a payload. Maximum payload the robot can safely pick up, move, and set down (kg); maximum payload the robot can carry directly over its center of mass (kg); power consumption rating when carrying 1, 10, and 20 kg payloads.

Complex / human kinematics. Number of degrees of freedom in the system, individual limbs, the hands, and the head; number of limbs; number of fingers.

Mobility in home environments. Maximum linear and rotational velocity and acceleration ratings on flat, smooth or carpeted ground (m/s , rad/s , m/s^2 , rad/s^2), time needed to climb 10 stair steps (s).

Mobility in city environments. Maximum linear and rotational velocity and ac-

celeration ratings on flat and 10 ° inclined ground with street roughness (m/s, rad/s, m/s², rad/s²), maximum passable incline and decline (°), maximum passable obstacle height and width (m).

Aesthetics for likeability. Surveys on robot likeability for children, adults, and elderly, before, during, and after robot operation.

Acceptance by humans as a coworker. Survey results about acceptance of a robot as coworker; amount of time that a group of human workers are distracted by a robot from their own jobs, such as in a restaurant or cleaning situation (s).

Continuous exterior sensing. (Artificial skin) Area covered by external sensors (m²), number of types of data measurable by outer sensors (e.g. thermal, pressure, radioactivity, etc) and their ranges.

Continuous internal sensing. (Artificial proprioception system) Number of internal pressure, heat, and vibration sensors and their sensor ranges.

Chemical sensing. (Artificial nose) Number of chemicals or particle types that are detectable by the robot, sensitivity of robot nose to each.

Active visual perception. (Smart actuated eyes) Number of degrees of freedom for the eyes or cameras, time needed to focus on an object (s).

Visual object recognition. (Machine vision) Number of objects that a robot has learned or can categorize, time needed to recognize and object (ms).

Tactile perception. (Machine touch) Time needed for the robot to recognize the size, shape, weight, roughness, and type of an object on a table, based on tactile feedback (s).

Intelligent grasping. (Smart artificial hand) Number of different grasp configurations that the hand can take to manipulate different objects; time needed to safely grasp and pick up off a table a glass of water, a pen, an envelope, and an exercise weight (s).

Fast decision-making and reaction times. (Capability for reflexes and computation) Processor speed (Hz), control loop frequency (Hz), joint actuator frequency response (plot of actuator gain versus input control frequency).

Speech recognition and response. Number of verbal commands recognized, percent accuracy of word or phrase recognition (%), time needed to understand commands (s).

Desired functions near the end of the list approach more human-like behaviors. Methods from developmental psychology could be explored to quantify robot performance of these functions.

7.8 Method for Designing a Human-Centered Robot

Based on the experience of this thesis and background research, a high-level 12-step process for designing a human-centered robot is recommended as follows:

1. **Decide on a set of desired prioritized *functions* for the robot.** Identify the problems that the robot should address. Identify the desired environment, roles, and system constraints for the robot. Also decide whether a humanoid or non-humanoid structure is desired, which is discussed in Section 1.2. Safety, performance, user-friendliness, and capability for intelligent

behavior all should considered, as described in Section 7.7.

2. **Identify possible *metrics* for each desired function**, as described in Sections 7.6-7.7. This includes finding objective goals for each metric. The goals may come from analogous human or robot performance, as obtained from literature or biological experiments.
3. **Break down the robot functions into *possible modules*** to explore more independently. Translate system-level concerns into manageable module-level concerns. Examples include modules for head/perception, legs/mobility, power supply, etc; or as in Table 3.2. Each module to explore should have a defined, limited set of functions. Design teams could be allocated by module. Lay out plans and requirements for module integration.
4. **Generate a large number of *concepts for features* in each module.** Obtain ideas from observations of people and existing robots, literature and patent searches, consultation with experts and interested parties, group brainstorming, and other systematic concept generation techniques [24]. Examine the features and trends of existing robots with similar functions, as in Tables 1.1 and 7.1, and identify new candidate technologies. Identify necessary bodies of knowledge (electronics, mechanical engineering, biology, etc), resources, time, and people needed to fully explore each concept.
5. **Decide on a *limited list of features and modules to explore***, which can execute the desired functions. If the possible function and feature lists are very large for each module, which is likely for a human-centered robot, prioritize the features as in Section 7.5. Generate manageable combinations

of robot functions and features to include in initial prototype designs.

6. **For each module, generate and evaluate a few different *prototype designs*** with different features for achieving the functions. Evaluate and rank the features based on the metrics chosen in Step 2. At this stage, simpler metrics will be used, such as number of parts, degrees of freedom, number of sensors, or system mass, as well as modeling/simulation data as needed. Always evaluate the potential for manufacturing, assembly, and user-interface complications. If necessary, build simple prototypes and run physical tests.
7. **Iterate on the prototypes to focus on a *final set of modules and features*.** Rule out ideas and add or change functions and features as needed, depending on whether the metrics of human-centeredness are improving, or if they meet system constraints such as cost or development time.
8. ***Organize the development of the final robot, based on a final set of modules and features.*** Plan the design, modeling, construction, and testing tasks for each module, as well as for the integrated robot, as in Fig. 1.3. Define a final set of quality metrics for each function.
9. ***Design and construct the detailed modules.*** Record and/or update a bill of materials, maintenance suggestions, assembly and disassembly steps, and safety recommendations, as in Chapters 3 and 4.
10. **Run necessary detailed *tests and analyses* on modules** to evaluate the metrics of human-centeredness, i.e. if a module can perform desired functions. Draw design improvements from the results.
11. ***Integrate the detailed modules and perform additional testing on***

the integrated design. Draw more insights into design improvements.

12. **Iteratively *optimize and finalize* the detailed design** based on the previous tests and models. Build, test, and integrate the new detailed design until the metrics of human-centeredness meet target values.

The method above reflects a systematic implementation of the design process in this thesis. Software development will lie on top of this process and is not detailed here, since that is not the focus of this work. The core principles of the method above are organization of complex processes, quantifiable metrics of performance, iterative design and testing, design and modeling for safety, design for manufacturing, and design for assembly/disassembly. As technology expands what is possible in robotics, such systematic approaches to design will become more essential.

Chapter 8

New Design Concepts

Chapter 7 gives redesign ideas for the existing Trikey and Dreamer robots. Concepts for two of the possible redesigns were drawn in CAD and described below: one for a new omnidirectional wheel, and another for a suspension system. Both concepts intend to let a wheeled robot move into rougher and more irregular terrains. Although the designs are not final working models, they are novel ideas that have potential to work well. They also are meant to inspire future research and design projects.

8.1 Tracked Omniwheel Concept

After design evaluation, a new 10 in-diameter wheel idea was conceived that specifically addressed three main functions: omnidirectionality, the ability to traverse obstacles in multiple directions, and ease of assembly. To a lesser extent it addressed ease of fabrication. Areas of improvement are specifically needed for weight, cost, strength, vibration resistance, and cleanability, as these issues were not considered in this concept. This new wheel idea was not seen in any literature reviewed so far.

The design builds off previous omniwheel ideas that use rollers to allow lateral motion. The rollers alone are inherently restricted in how tall of a side

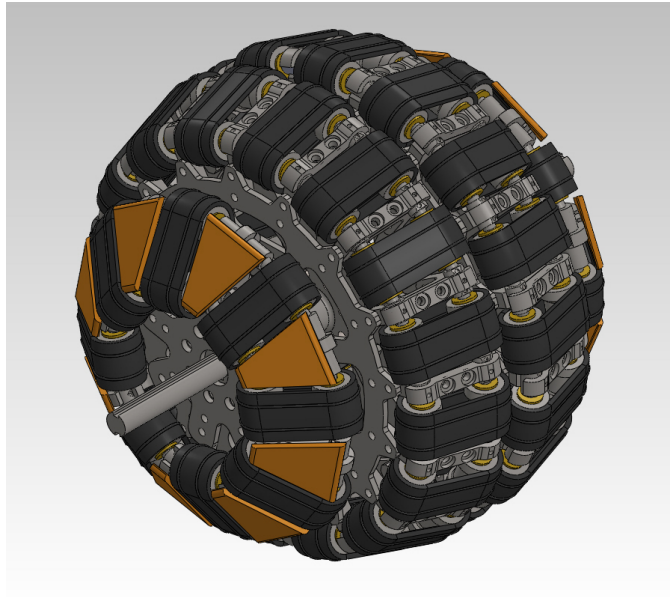


Figure 8.1: CAD of tracked omniwheel concept.

obstacle they can cross. However, this new concept uses rubber treaded tracks on rollers instead of rollers alone. The tracks turn the wheel into an almost spherical shape, allowing a much larger side radius than using rollers alone (Figs. 8.1-8.3). In effect the wheel is predicted to be able to cross 5 in high obstacles from the front and approximately 3 in high obstacles from the side. This translates to an ability to cross obstacles from the side that are 60% as tall as the main wheel radius, which is better performance than the currently used wheels, and theoretically better than the optimized roller omniwheel by Byun [8].

A tracked wheel concept could easily be unmanufacturable and rendered useless. One specific challenge to manufacturability was considering how to attach the roller-tracks into a supporting frame. Several designs were considered where

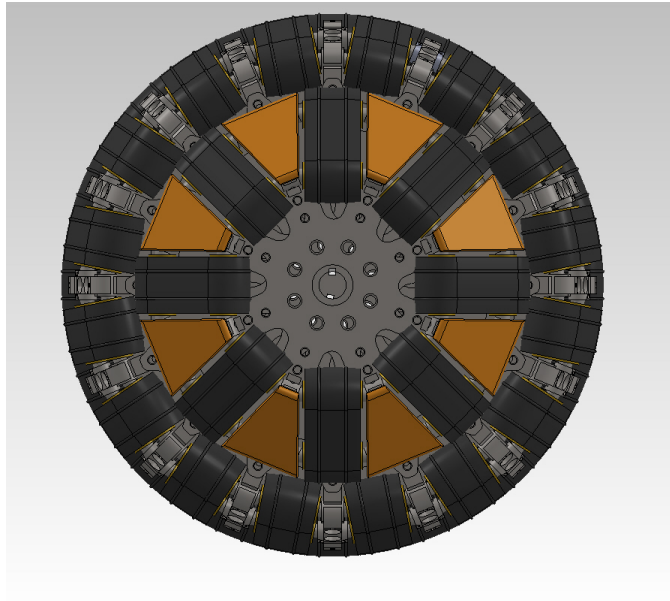


Figure 8.2: Side view of concept wheel.

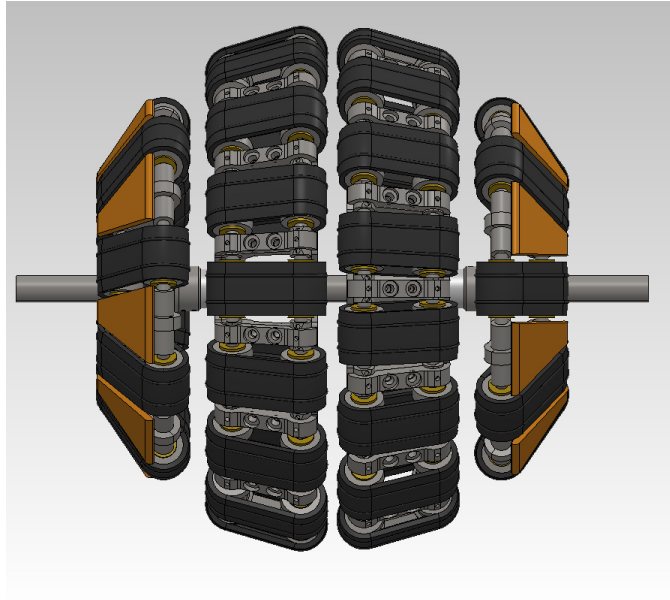


Figure 8.3: Front view of concept wheel.

assembly would be practically impossible without an all-in-one 3D printing solution. The design that had the best property of ease of assembly is described here.

Although the ease of assembly of this concept is not perfect, it addresses design for assembly by separating the wheel into four main layers around the axle (Figs. 8.3-8.4). The layers separate the roller-tracks into small components that prevent interference among different tracks, ultimately making the wheel easier to assembly. These layers are not independent modules, though, because they cannot be assembled as separate units. They must be assembled at the same time in order to properly access the spaces between layers, which require fasteners. This poses an area of improvement, since truly independent modular layers would aid ease of wheel assembly. Closer views of the inner and outer layers of the wheel show other design features to aid ease of construction, as shown in the next sections.

The design only minimally addresses reduction of vibration. The design should allow constant contact with flat ground in the forward-backward direction. The two inner layers are fixed onto the central axle with slight angular offsets, so that tracks from either side of the inner layer will alternately contact the ground. However, in the side directions, there would be gaps in ground contact. Presumably this is acceptable, since the side our outer layer rollers will only contact the ground some of the time in rough terrains.

8.1.1 Inner Layer

For the inner layer (Fig. 8.5), although there are many parts, they can be assembled systematically starting from the center hub to the outer roller-tracks

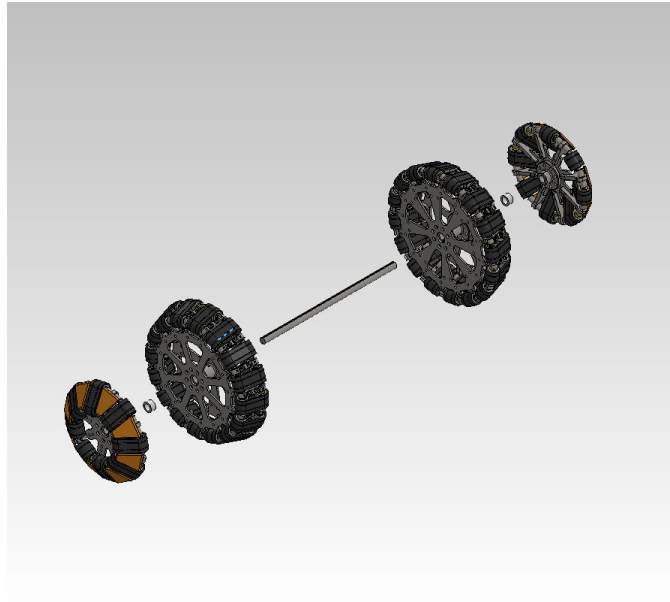


Figure 8.4: Exploded view of wheel concept modules.

(Fig. 8.6). The parts have clearance from the rollers to allow free movement (Figs. 8.7-8.8). The roller tracks are held in place by clamping fixtures, which have tapped holes to allow their own attachment to the supporting frames (Figs. 8.9-8.10). The clamps could be fabricated from a single sheet of metal using a water cutter, followed by some milling.

8.1.2 Outer Layer

The outer layer is the smaller, side-most layer of the wheel (Fig. 8.11). In this concept, the outer later tracks are the same dimensions as in the inner layer, and so fewer tracks fit in it. The exposed spaces between tracks are then covered with plastic material (shown in orange) that can help reduce friction if it slides against a surface. Removing these panels exposes a similar frame structure to the inner layer



Figure 8.5: Inner layer of the wheel concept.

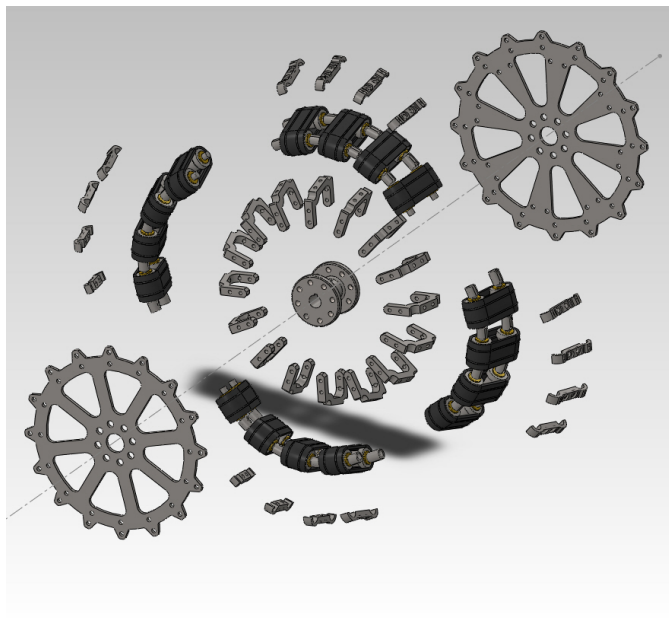


Figure 8.6: Exploded view of the inner layer of the wheel concept.



Figure 8.7: View of inner layer from the side, with the outer frame or "spokes" removed to reveal the clamping fixtures.



Figure 8.8: Zoomed view of the inner layer from the side, showing clearance from the roller-tracks.

(Fig. 8.12-8.13). Unlike the inner layer, the outer layer central hub only has a single flange and support frame (Fig. 8.14). Similar to the inner layer, the tracked rollers can be held in place using a set of clamping fixtures (Figs. 8.15-8.16).

8.1.3 Tracked Rollers

The same types of tracked-roller subassemblies are in both the inner and outer layers. A closer view of the tracked rollers shows their function (Fig. 8.17). A flexible rubber track about 1 in wide runs around two metal rollers (Fig. 8.18), which rotate about their own axes. An inner sleeve bearing lets the roller spin about a central steel rod. The shapes of the rollers and tracks should minimize the chance of the tracks slipping off the rollers. For this reason, a ditch in the roller shape is

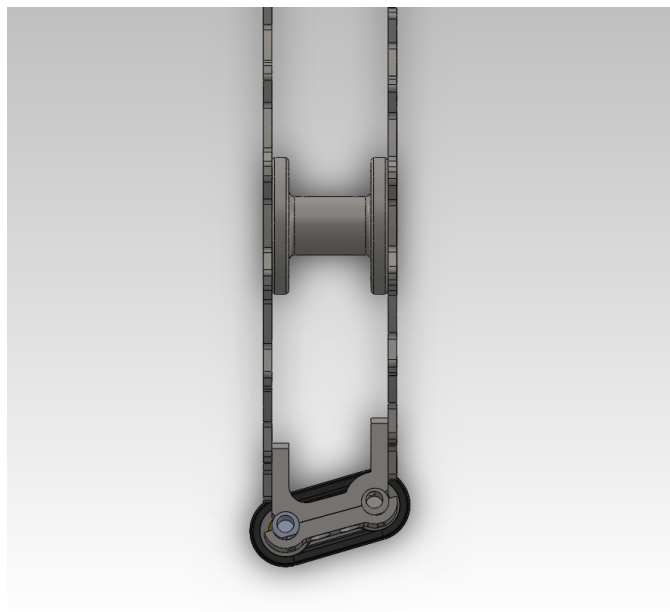


Figure 8.9: Front view of the inner layer frame and tracked-roller construct. The U-shaped upper part of the clamp connects the lower clamp and side frames together.

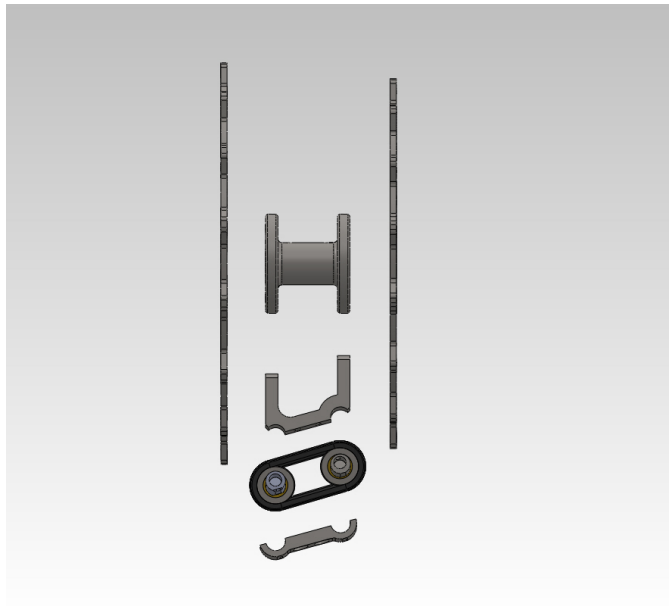


Figure 8.10: Exploded front view of the inner layer frame and tracked-roller construct.

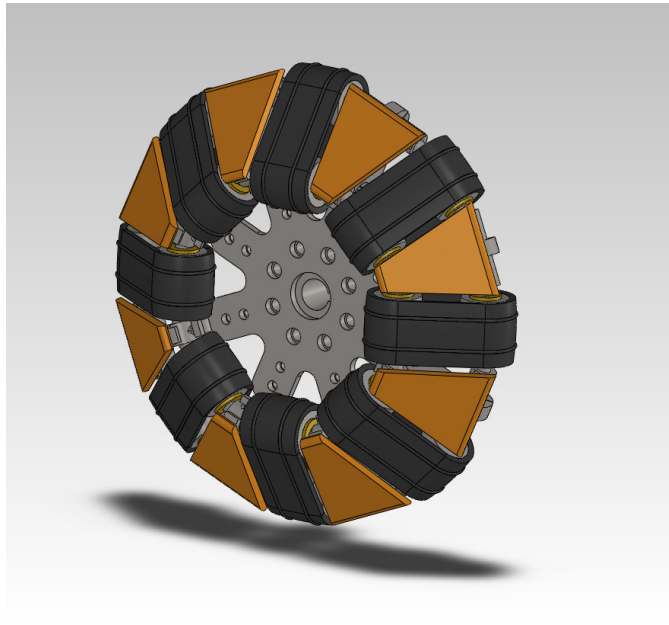


Figure 8.11: Outer layer of the wheel concept.

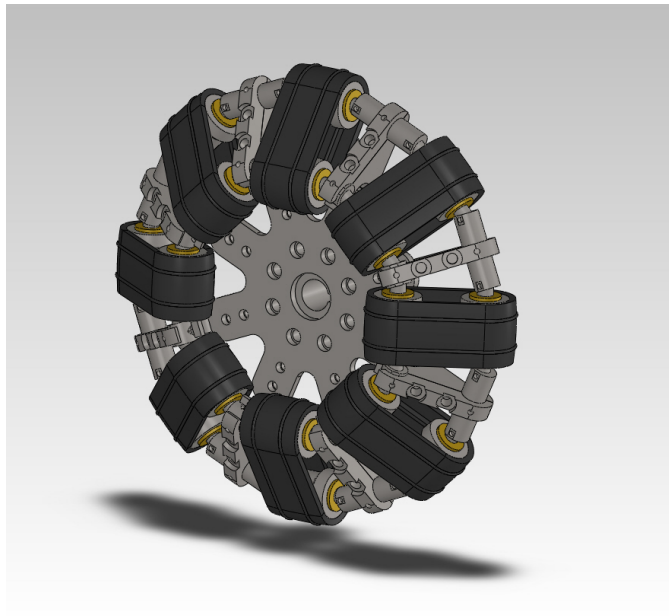


Figure 8.12: Outer layer of the wheel concept, with plastic panels removed.

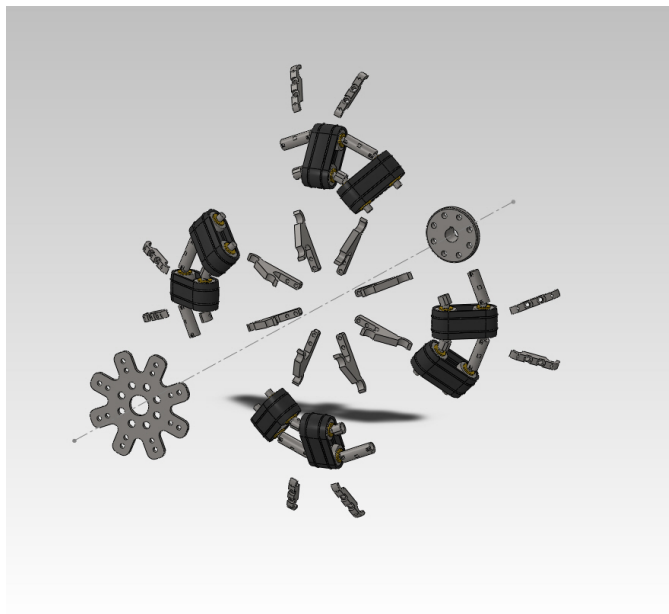


Figure 8.13: Exploded view of the outer layer of the wheel concept, with plastic panels removed.



Figure 8.14: View from the inner direction of the outer layer of the wheel concept, with plastic panels removed.

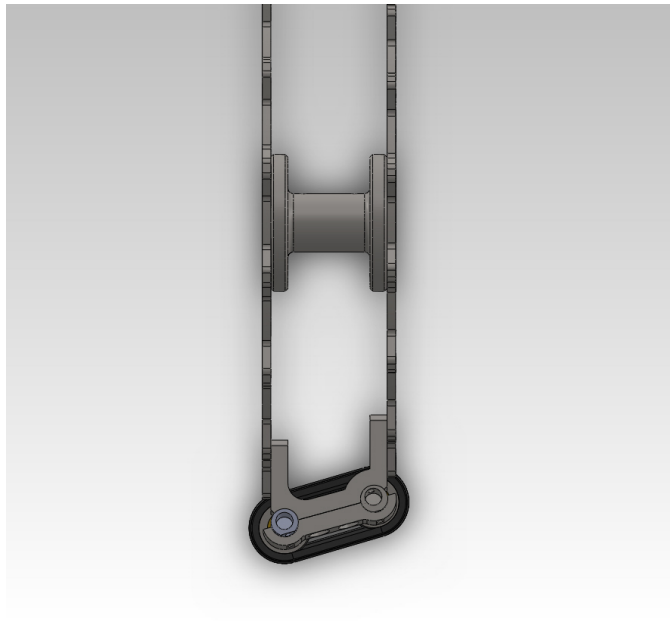


Figure 8.15: Front view of the outer layer frame and tracked-roller construct.

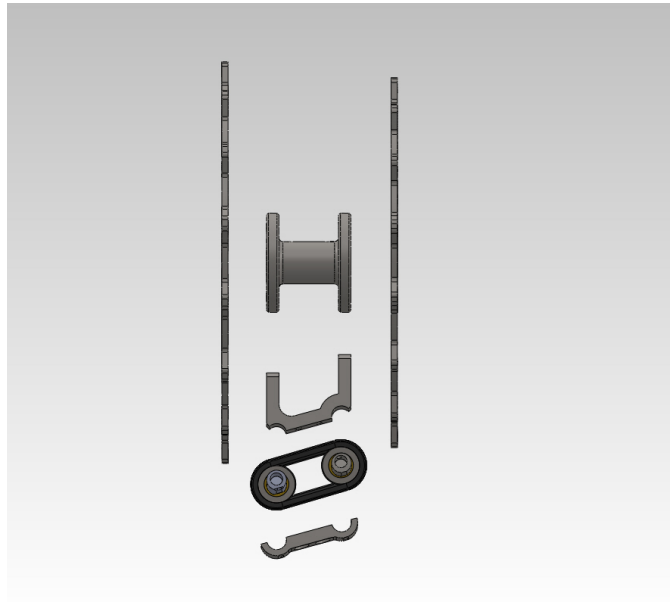


Figure 8.16: Exploded front view of the outer layer frame and tracked-roller construct.

meant to accept a thicker protrusion coming out the inside of the track, helping stabilize the track on the roller. This design calls for additional improvement and experimentation. Materials and geometries could be changed significantly for better function.

Multiple tracked rollers are fixed together in a ring shape in each layer. In this concept, the central rods of the rollers are joined via small cylindrical fixtures with obliquely milled pockets on both endfaces that accept the central rods of the rollers. Setscrews can help fix the rods into these cylinders. This fixation method also has room for improvement. One weakness of the current cylindrical fixture designs are that they may be difficult to align properly around the wheel. Secondly, the very last tracked roller assembly may be difficult to assemble around the wheel

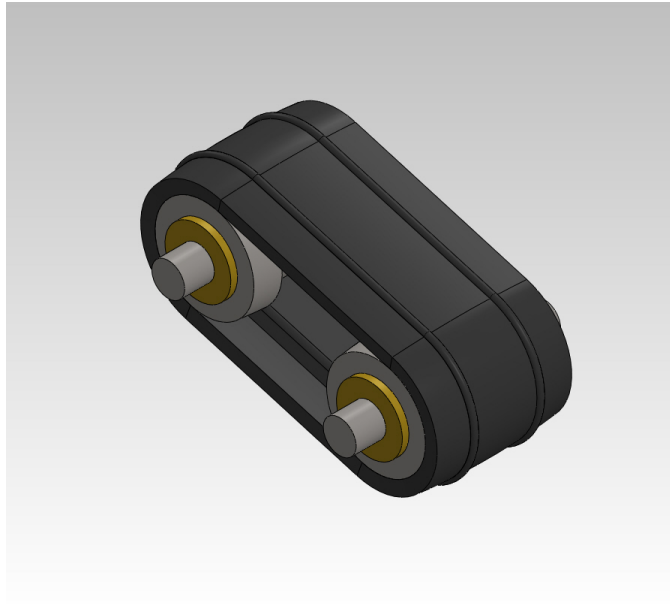


Figure 8.17: Exploded front view of the outer layer frame and tracked-roller construct.

circumference.

8.2 Suspension Concept

No matter what wheel is used, a suspension can also help a wheeled robot access rough terrains. A concept suspension is shown below including the novel wheel concept described previously. It features an independent-wheel design, meaning that it does not require any direct rigid coupling of more than one wheel. It also can be completely assembled separately and attached to other base frames or wheels.

Its basic structure is not novel, following a MacPherson strut linkage model [1]. The linkage allows the wheel to move up and down as it crosses an obstacle, while a shock absorber composed of a spring and damper smooths the transmission

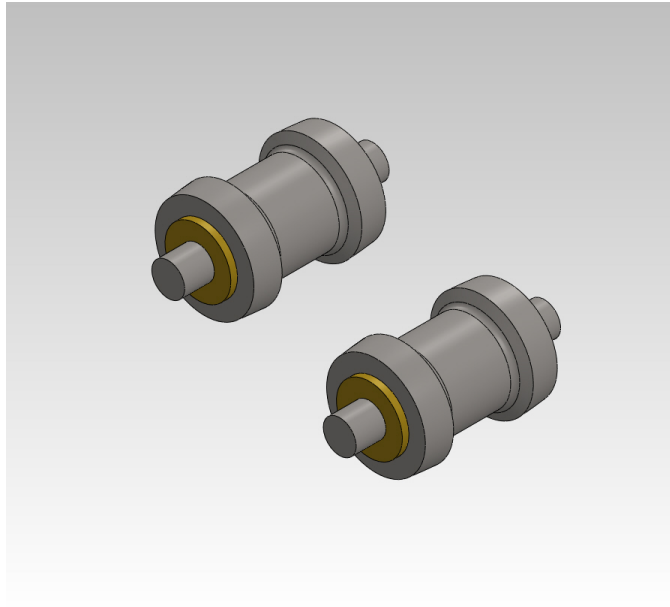


Figure 8.18: Exploded front view of the outer layer frame and tracked-roller construct.

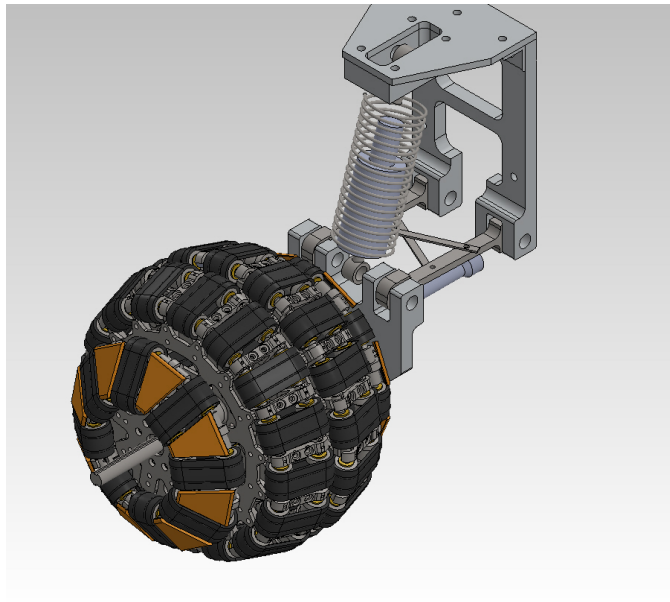


Figure 8.19: Independent wheel suspension concept module.

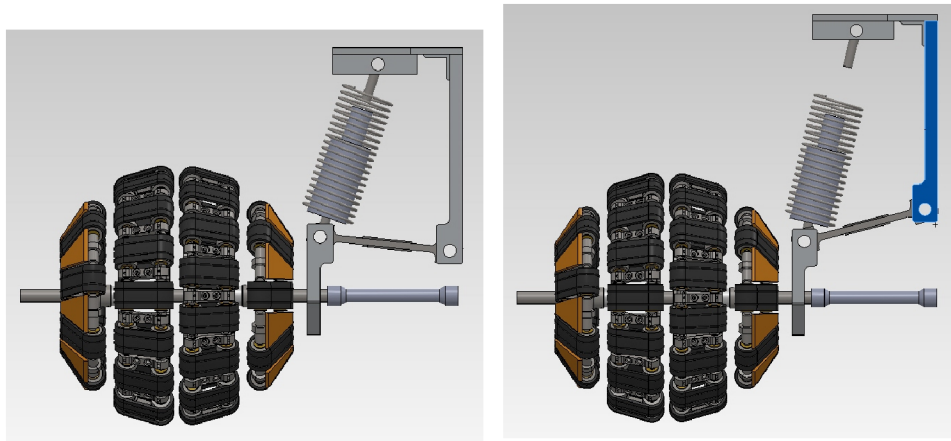


Figure 8.20: Side view of the suspension concept.

of oscillations to the body frame resting on the top plate (Fig. 8.20). The drive shaft that transmits rotary motion to the wheel is the lowest bar in the module. Not shown is the required universal joint at the end of the drive shaft in this design. A U-joint is needed between the drive shaft and the wheel motor, also not shown, housed in the main base. It transmits rotary motion from the motor to the drive shaft while allowing the wheel suspension to move up and down.

The geometry of specific parts was defined for ease of fabrication at the University of Texas facilities. Other factors to consider in a practical application are strength of parts, as well as masses and constitutive properties of the shock absorber components, to optimize resonant frequencies in a system. Nevertheless the overall simple design here can be constructed and tested with relatively few parts (Figs. 8.21-8.22), so it is suitable for initial prototyping.

In future development, other linkage structures besides the MacPherson strut can be tested, such as the double-wishbone suspension concept in modern cars. New

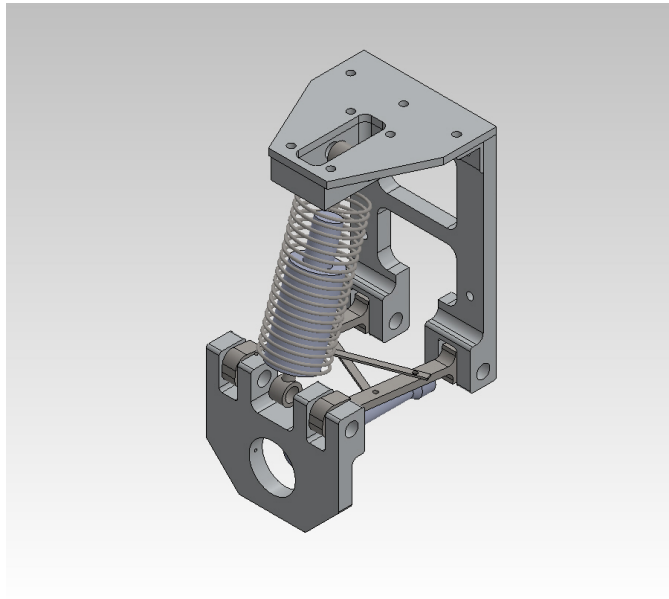


Figure 8.21: CAD of the suspension module, without a wheel.

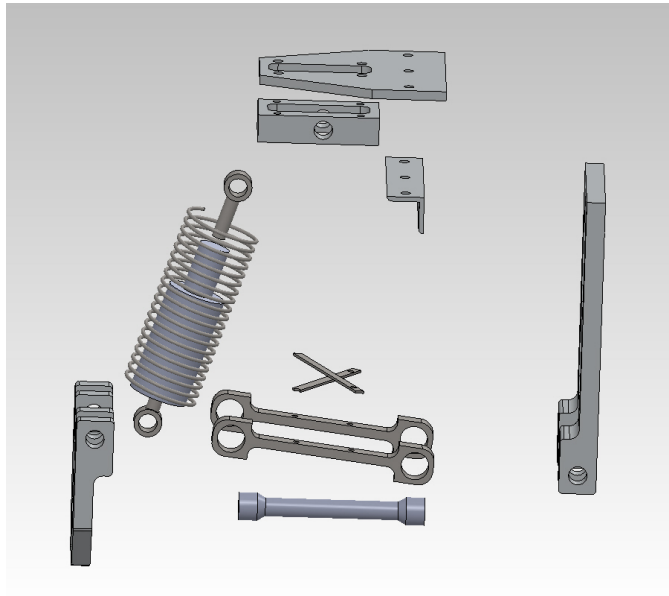


Figure 8.22: Exploded side view of the suspension module, without a wheel.

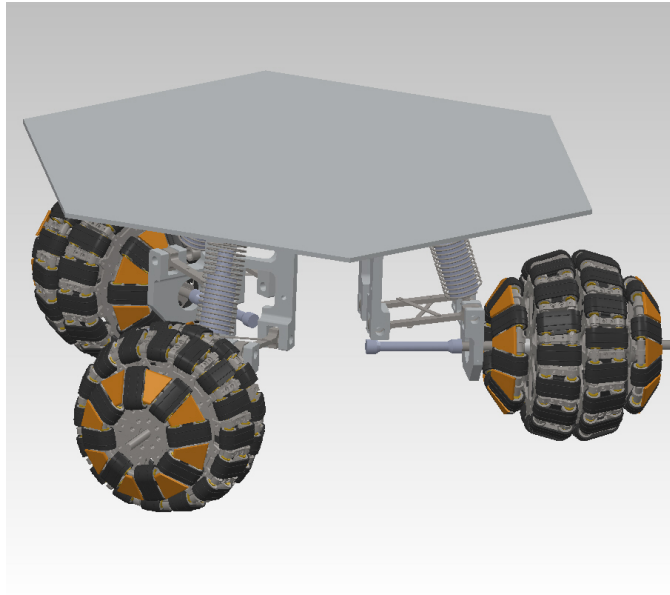


Figure 8.23: Generic robot possible using the wheel and suspension concepts.

active shock absorption technologies may also be tested, such as metallorheological dampers [29]. The purpose of this concept is to give a general overview of the necessary factors to consider when including a suspension into a wheeled robot.

A generic omnidirectional wheeled robot structure using the design concepts presented here is shown in Fig. 8.23. This shows how a suspension could be implemented. The main robot baseplate carries robot motors (not shown), which would have to be placed near the center of this design and protrude below the plate. U-joints transmit rotation to the wheels. The wheels and suspensions are modules that can be independently replaced in the robot.

A robot structure such as in Fig. 8.23 can be used to help characterize rough terrains, before actually building a full rough-terrain robot. Inertial measurement

units similar to the AHRS sensor in Trikey can be attached to the baseplate, and as the robot is dragged along various rough terrains, the ride characteristics can be measured. This work could help in future work on rough-terrain robots, whether human-centered or not.

Appendices

Appendix A

CAD Files and Selected Drawings

Presently the latest 3D models and draftings of the Trikey and Dreamer robots are stored at the University of Texas at Austin Human Centered Robotics Laboratory (HCRL) file share, with backup files on local hard drives in the HCRL and the HCRL network share.

Draftings/drawings are given below for selected parts, beginning with plates used for the electronics and ending with upper body fixtures between Trikey and Dreamer. These parts may be more likely modified or referenced for future projects, as opposed to other parts that are either easy to model or that would be replaced entirely. Additional drawings are stored with the CAD file archives of the HCRL.

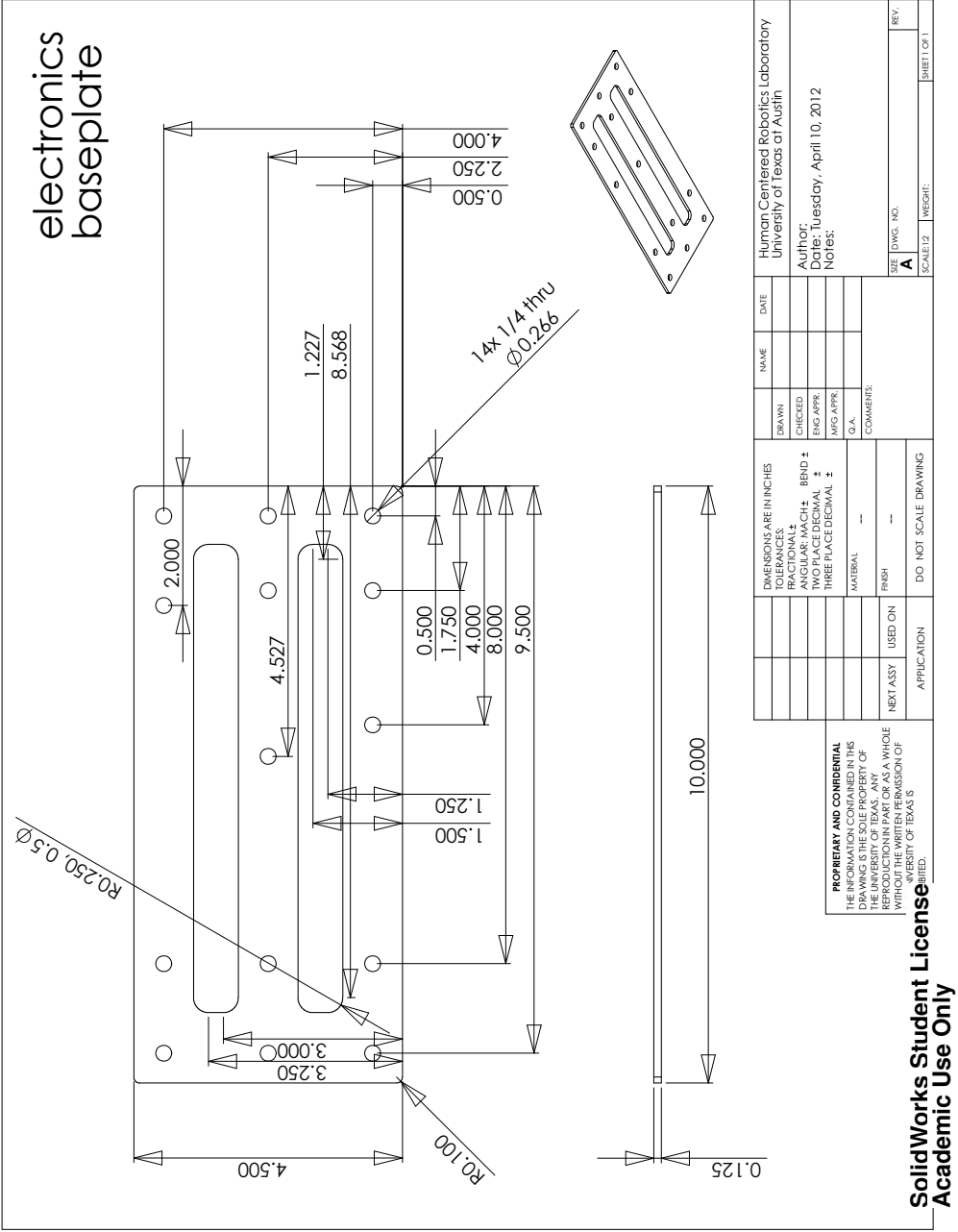


Figure A.1: Electronics baseplate, part C1.

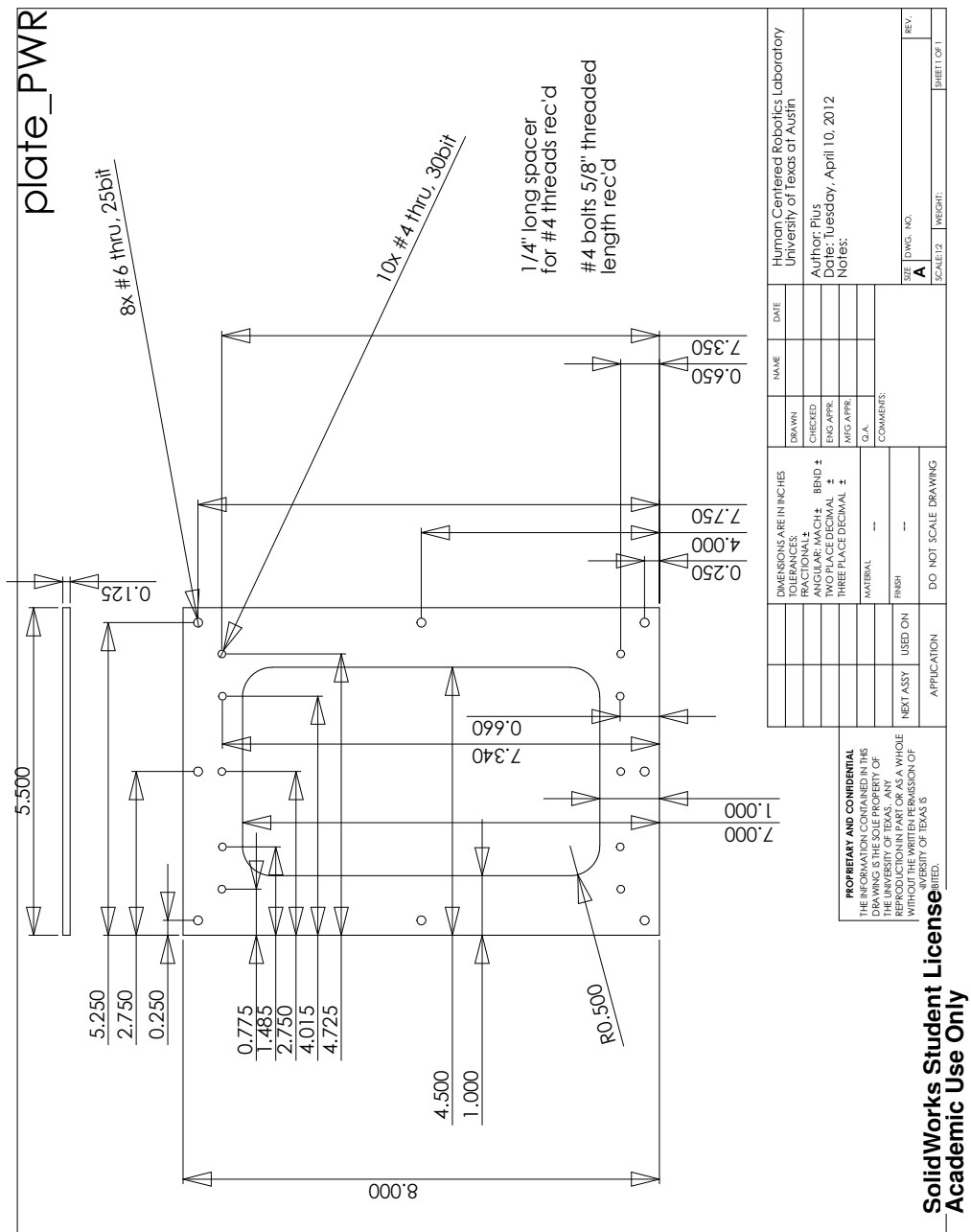


Figure A.3: PWR PCB plate, part C5.

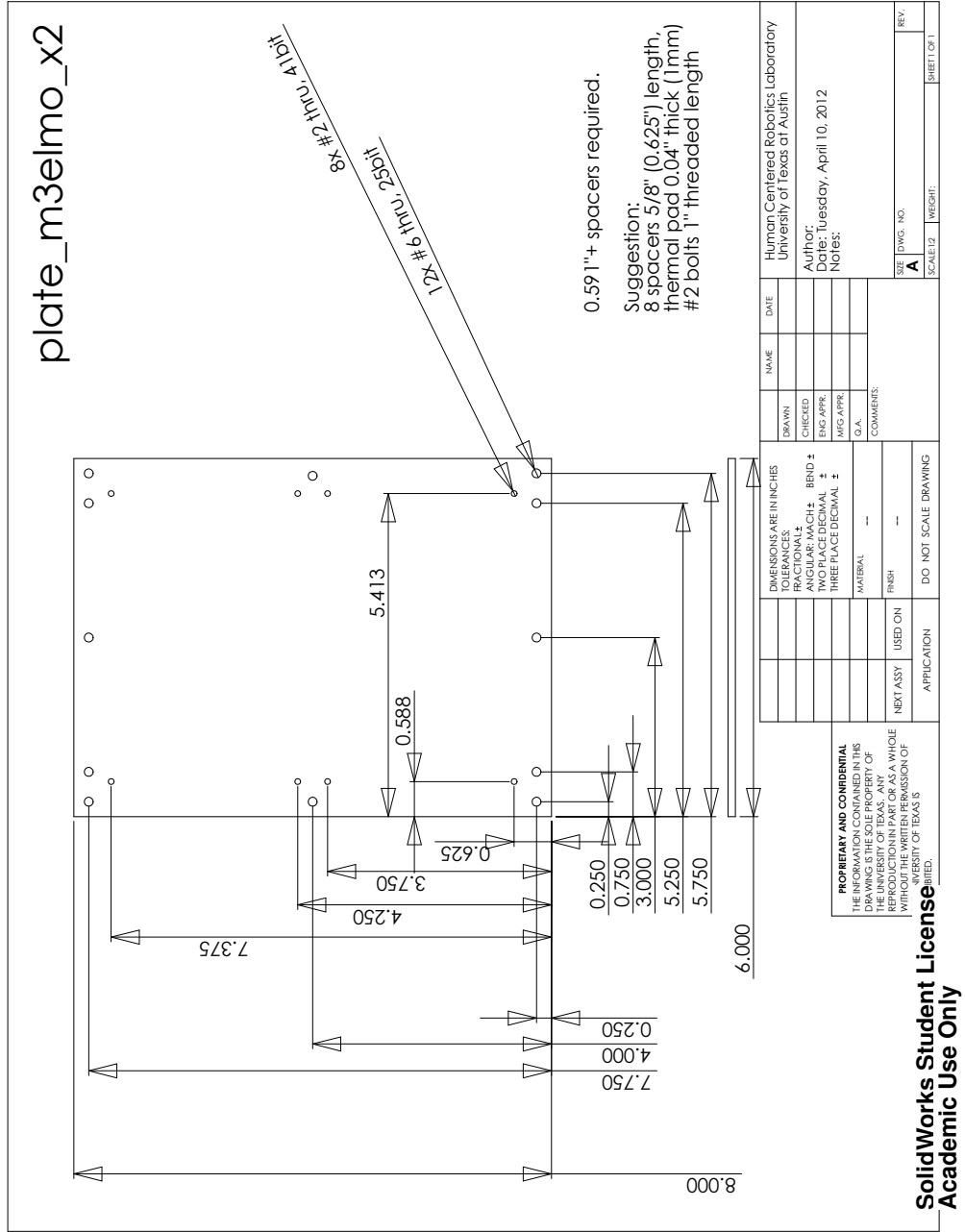


Figure A.4: ELMO PCB plate, part C8.

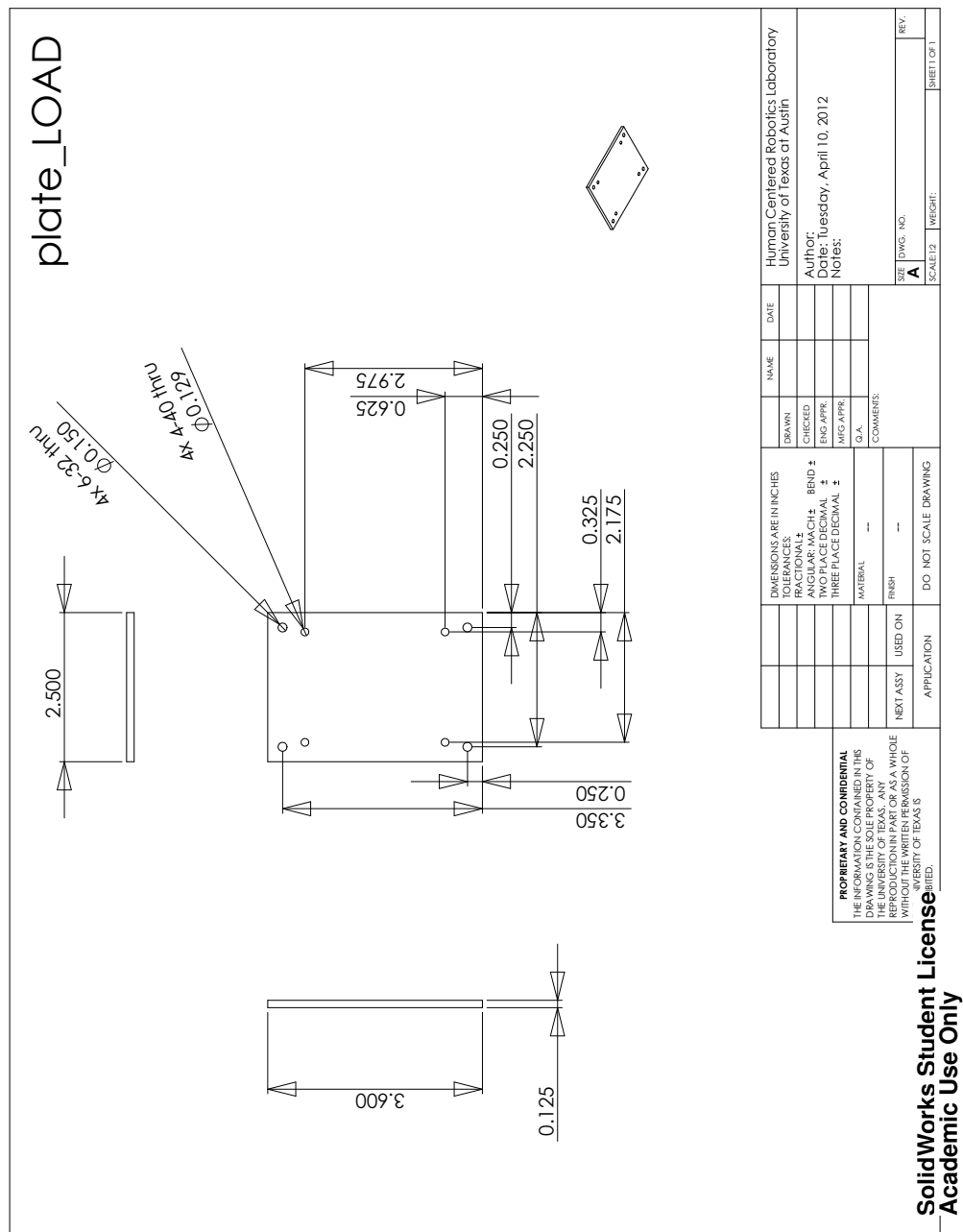


Figure A.5: Load cell PCB plate, part C13.

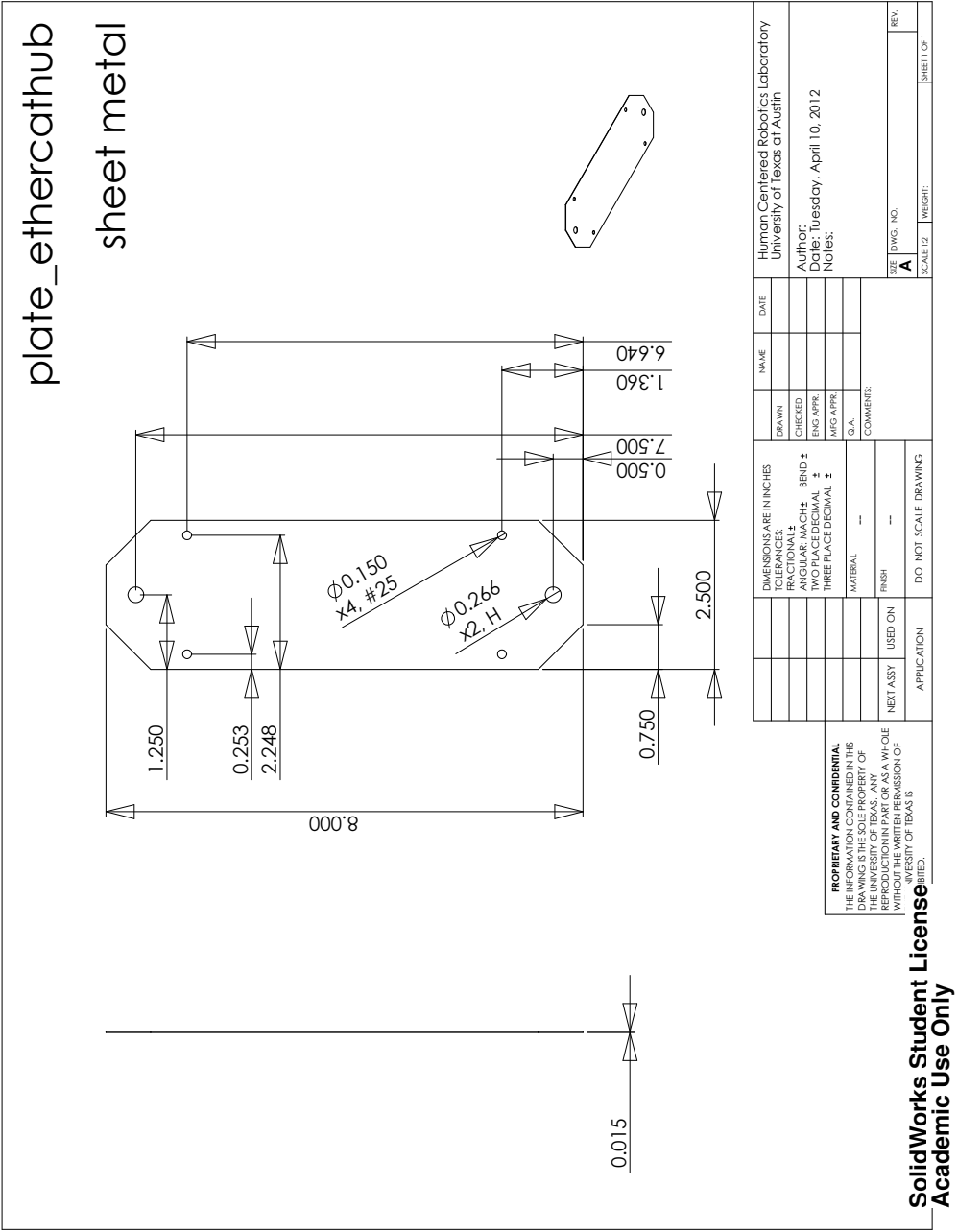


Figure A.6: Ethercat hub plate, part E4.

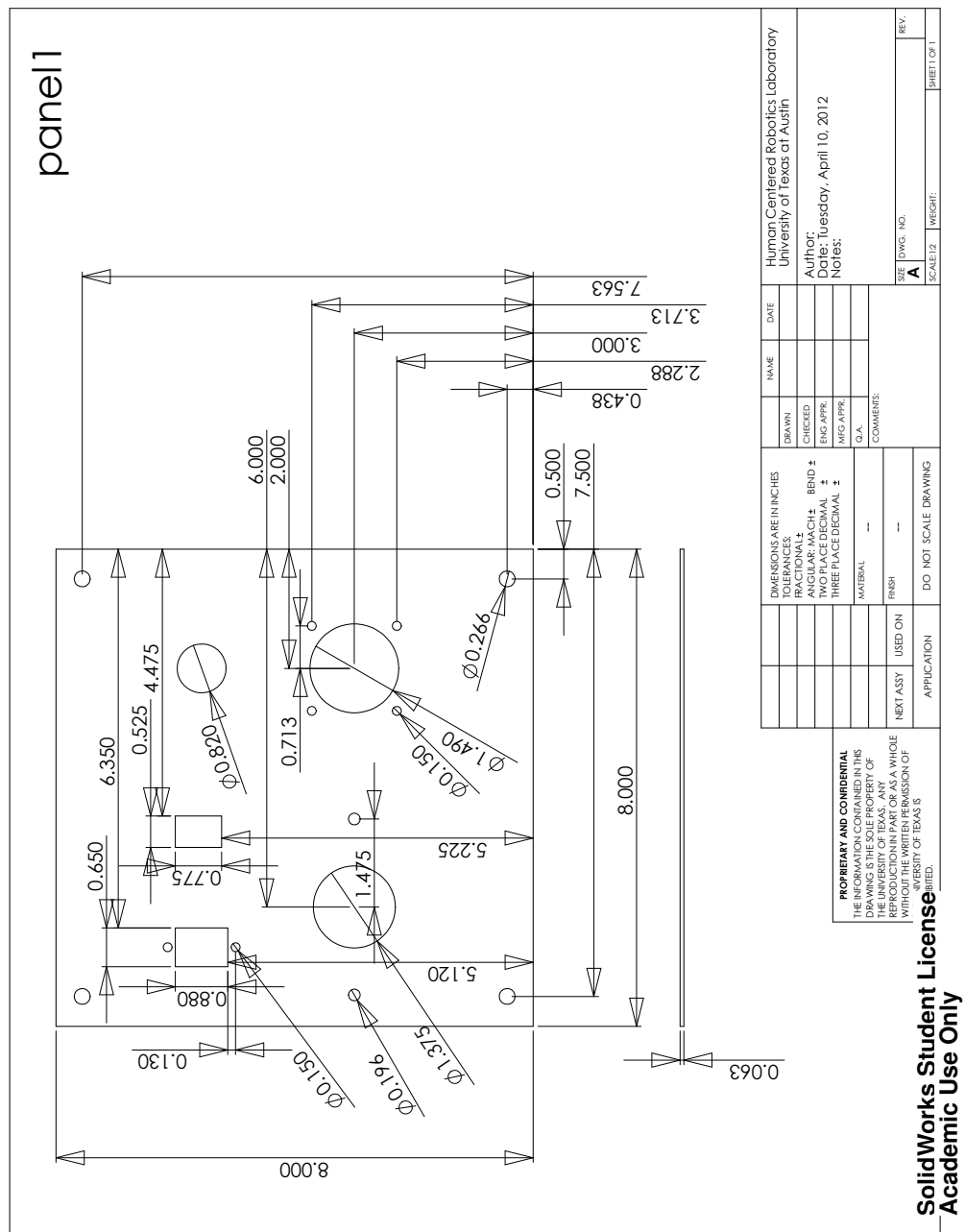


Figure A.7: Back panel, part F6.

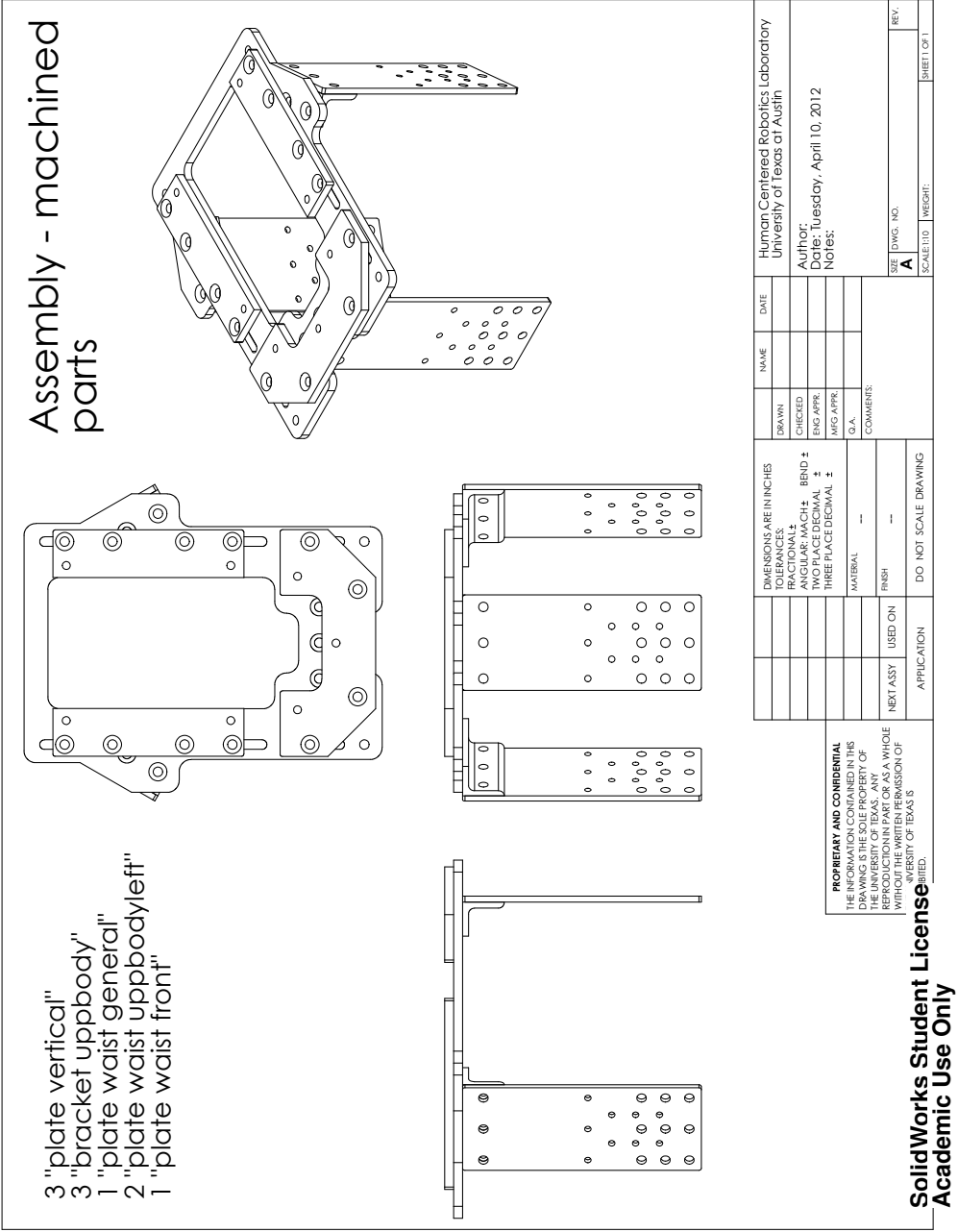
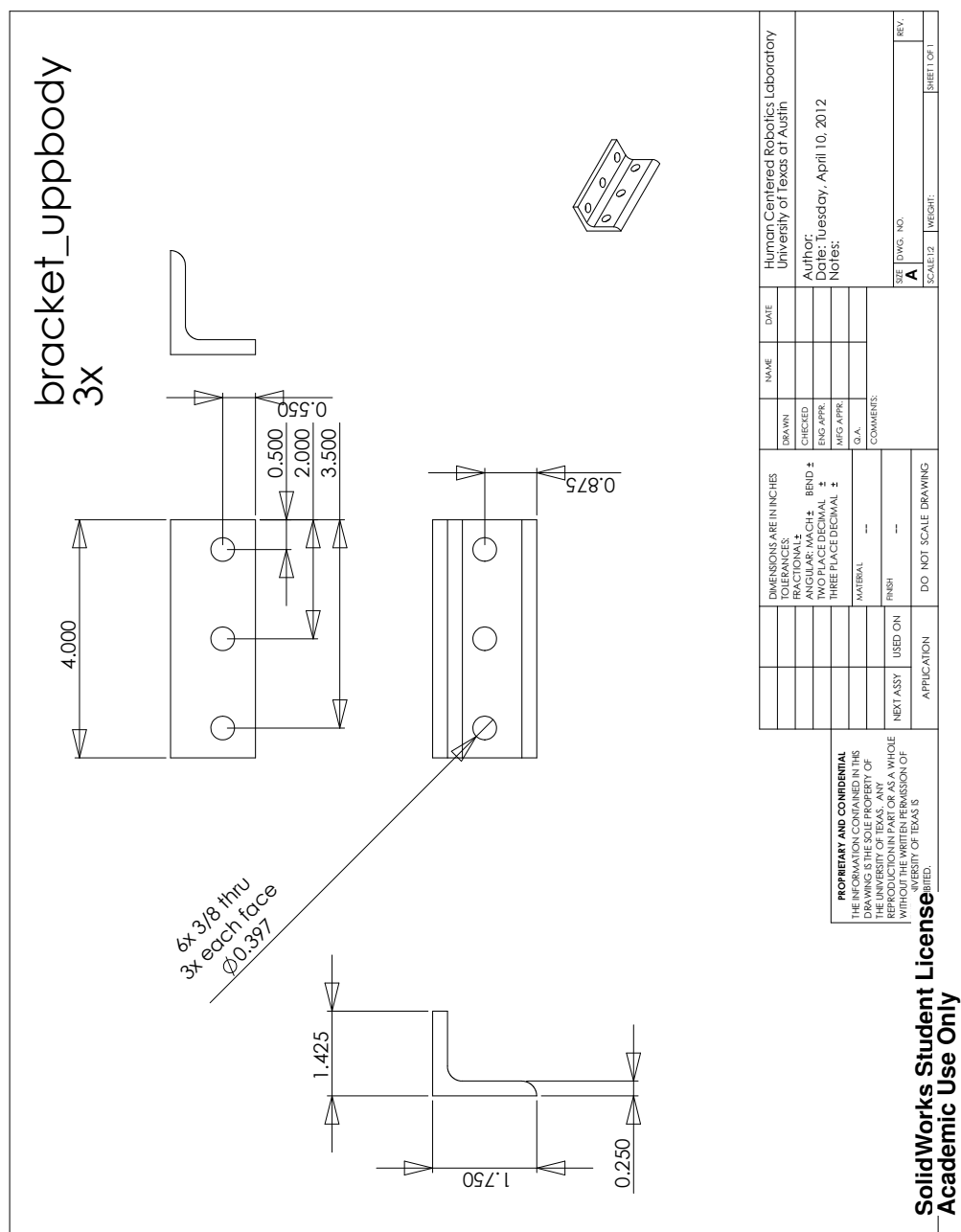


Figure A.8: Assembly of the following Meka upper body attachment fixtures.



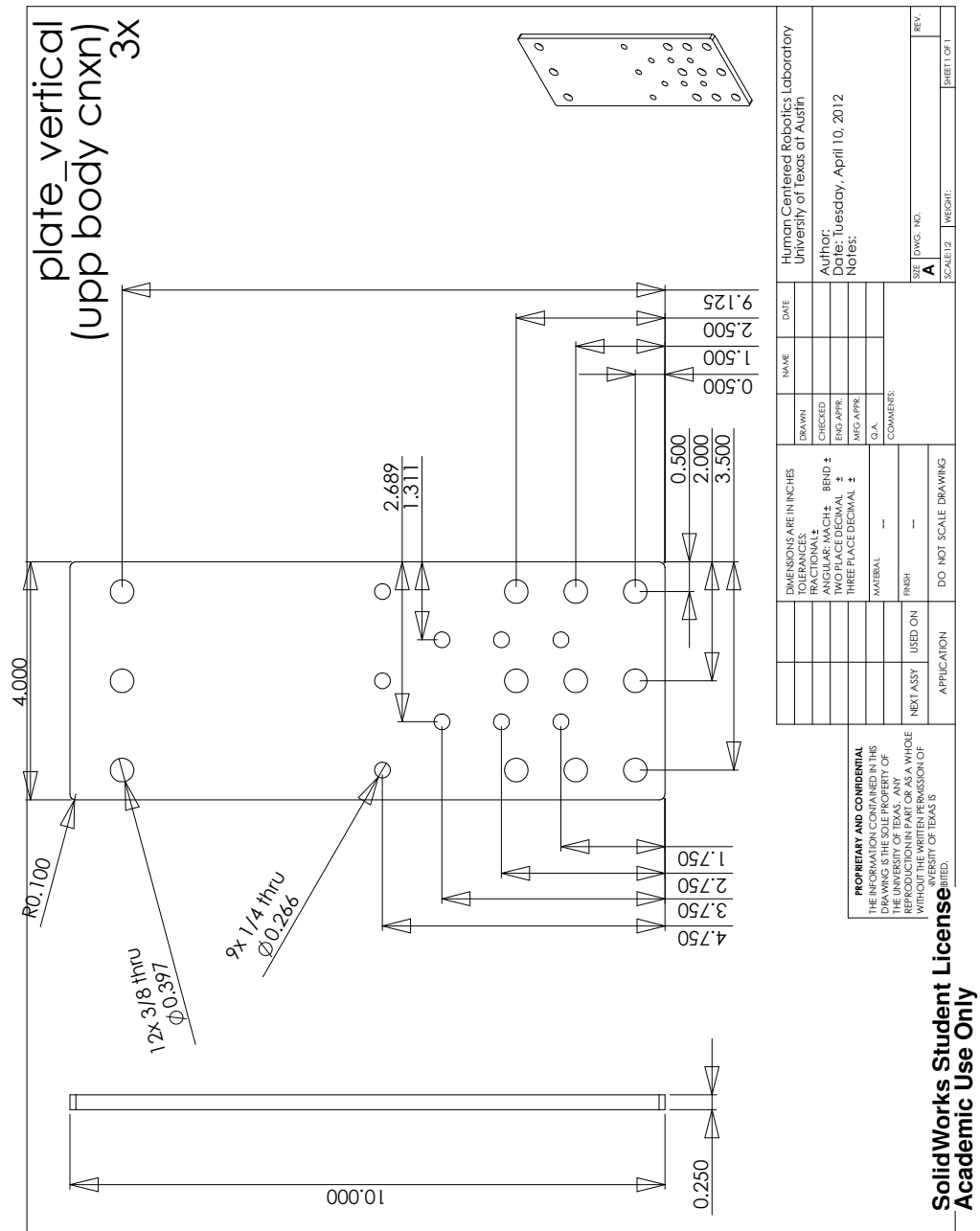


Figure A.10: Upper vertical plate, part B17.

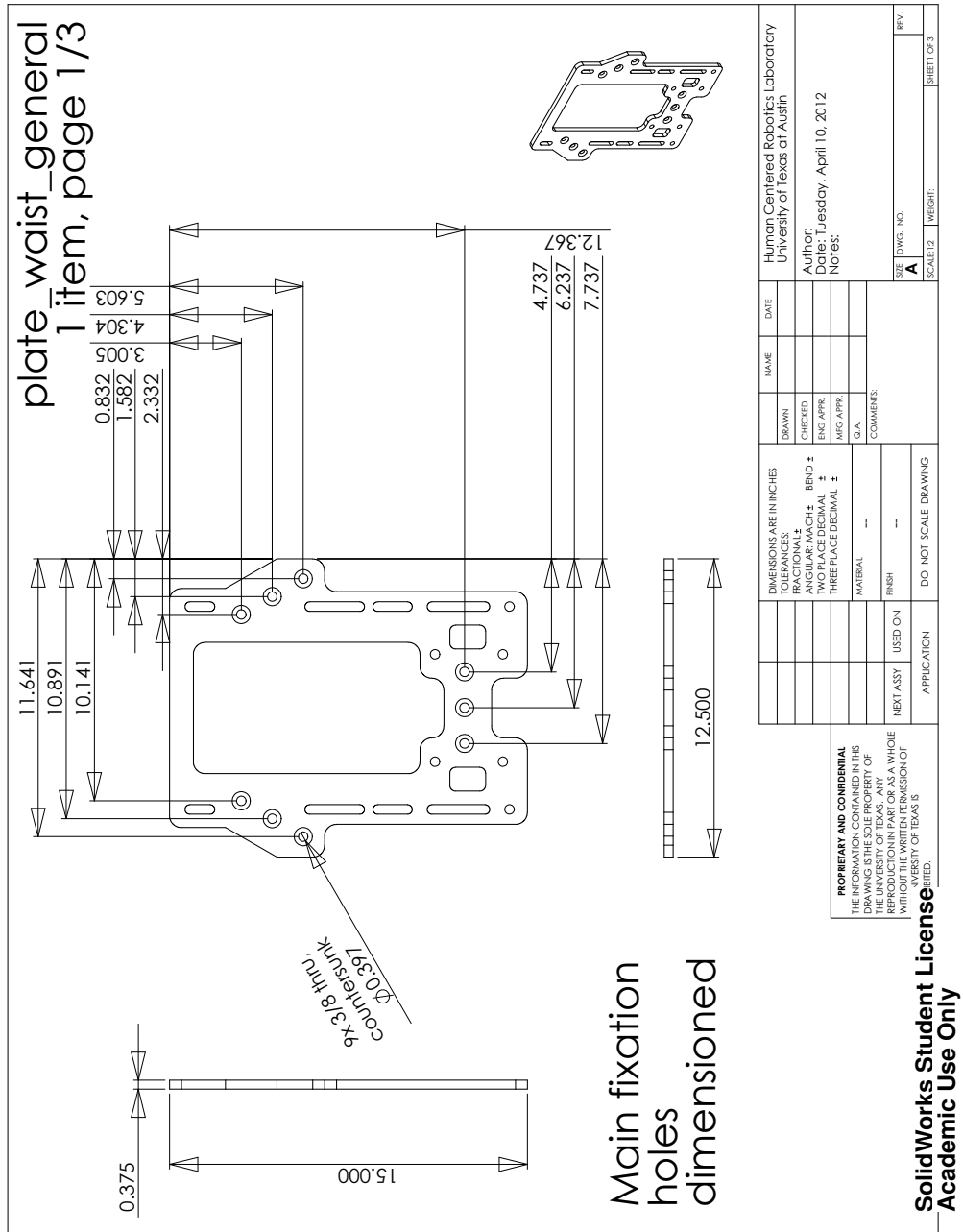


Figure A.11: Main upper body fixation plate, part G1, sheet 1.

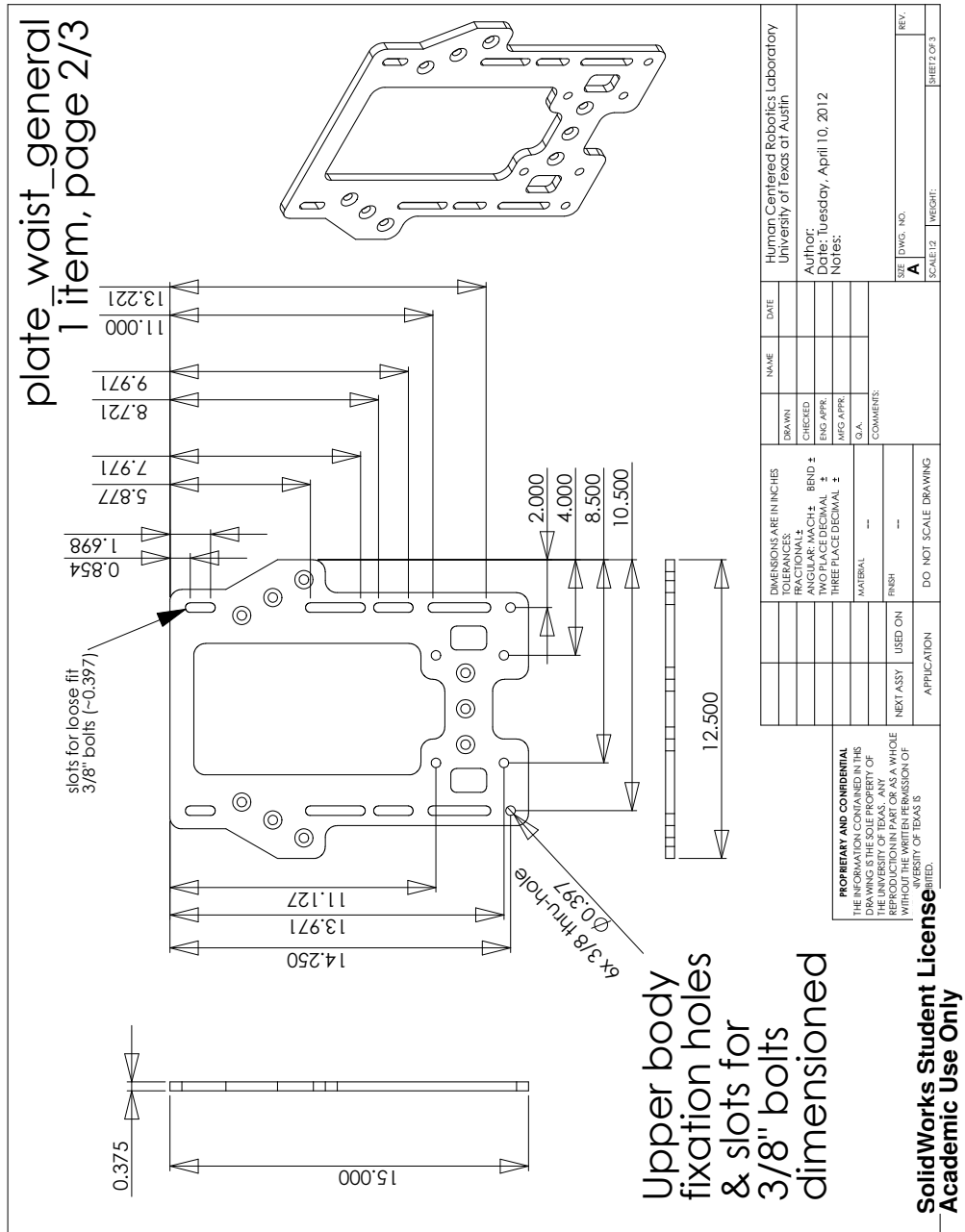
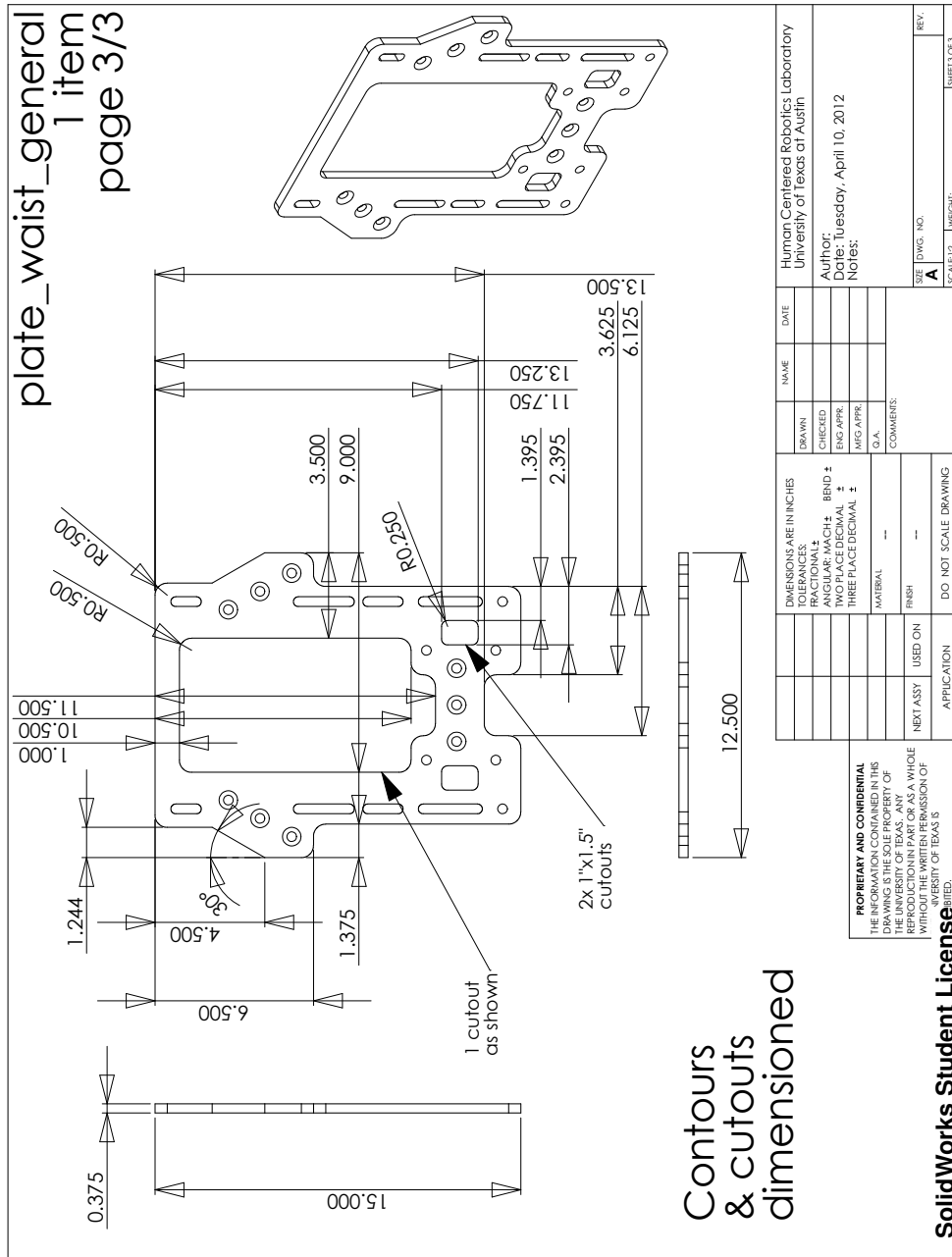
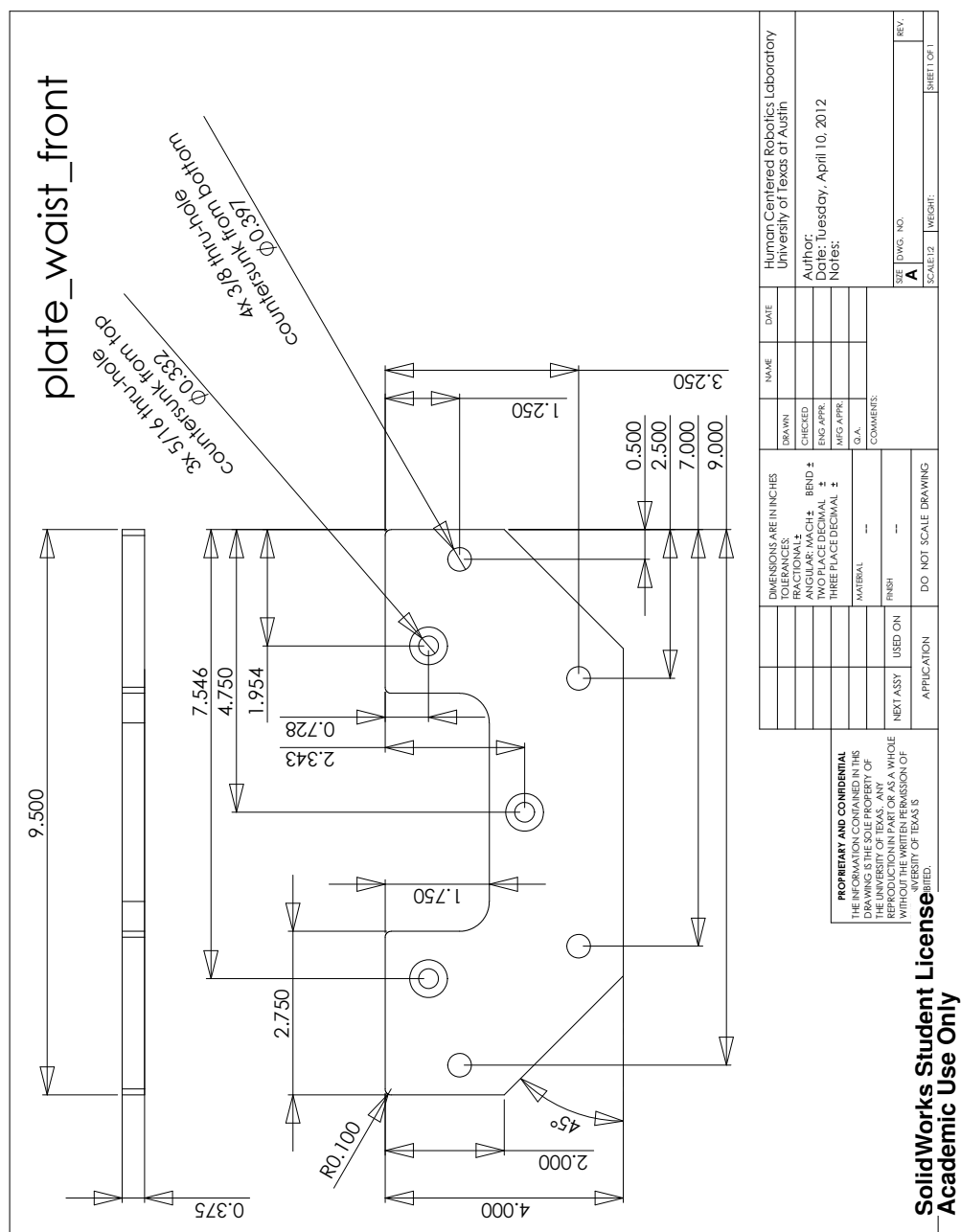


Figure A.12: Main upper body fixation plate, part G1, sheet 2.



197



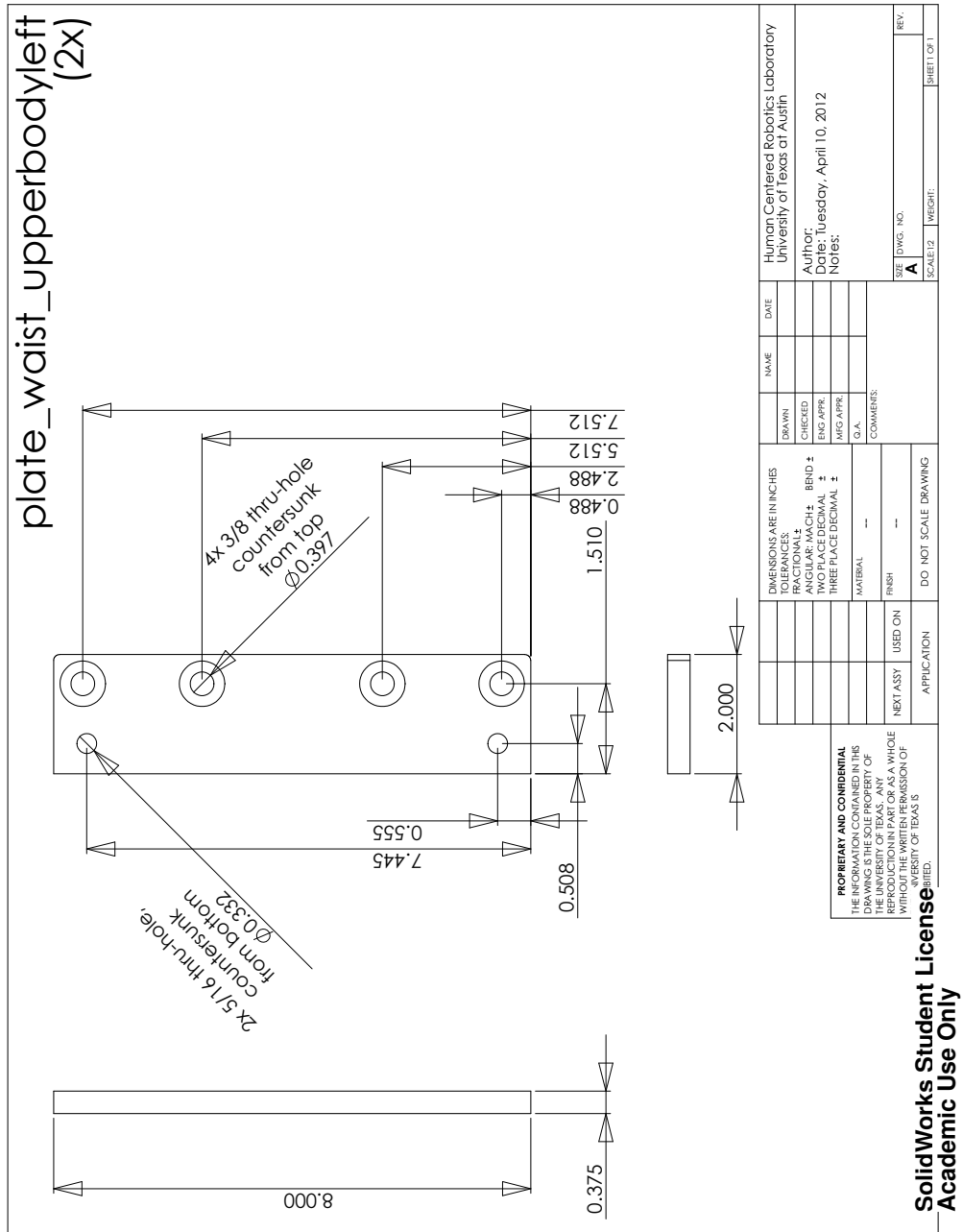


Figure A.15: Left and right upper body fixation plates, parts G3 and G4.

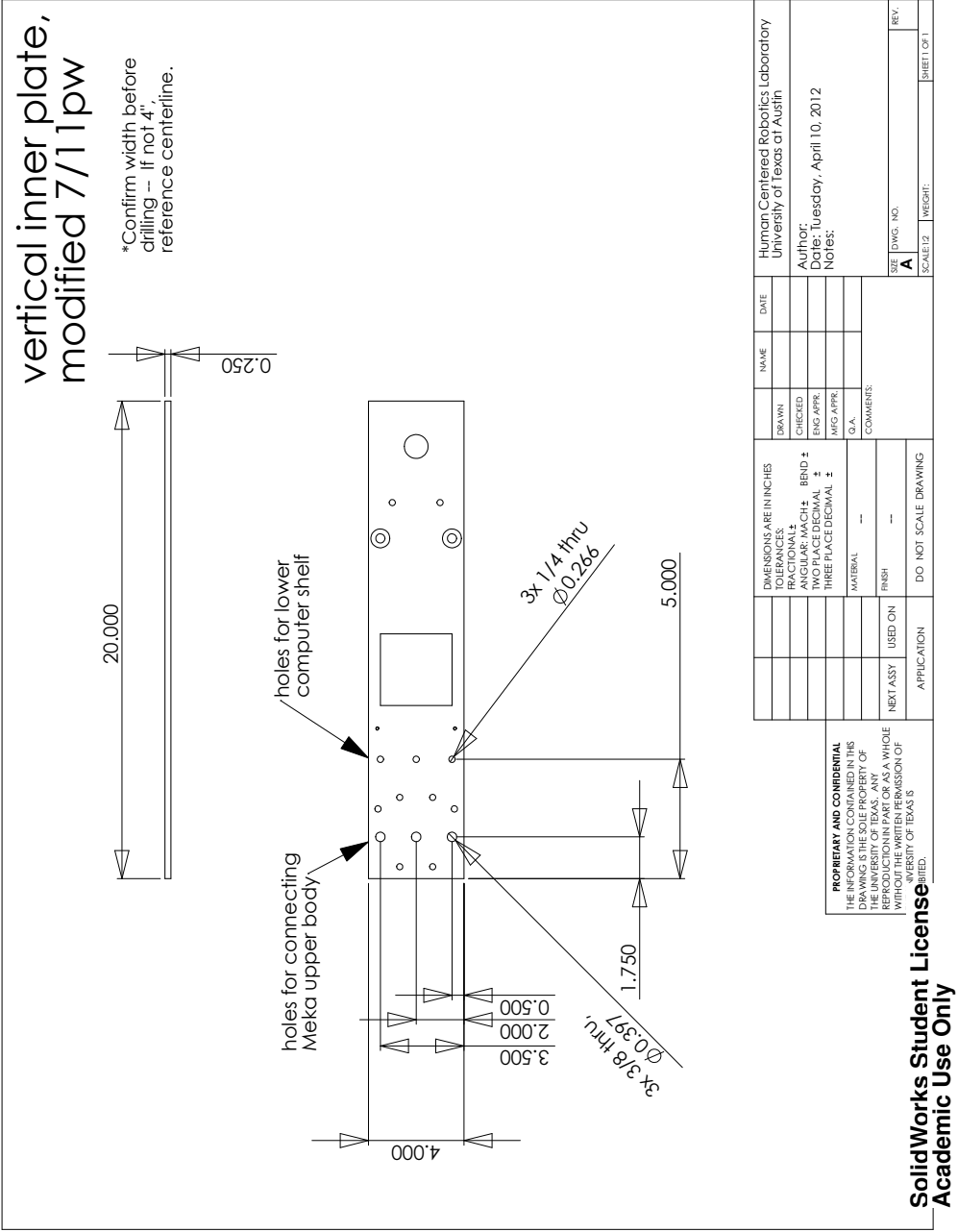


Figure A.16: Motor-wheel module inner vertical plate, part B14

Appendix B

Matlab Code for Kinematic Limit Simulation

```
%% notes
% Pius Wong 2/12
% Model of kinematic limits to prevent tipping over flat terrain...
%   Inputs in "define vars" section--
%   CoM = center of mass coordinate from CAD model
%       SolidWorks gave (y,z,x) positions
%   M = total mass of robot (Trikey + payload)
%   deltaall = angle directions to test
% =====
clear all

% =====
%% define vars
CoM = ...% CoM position
    [
        -0.058112842      0.780890116      0.172030703    % extreme
        -0.021980762      0.724379206      0.117328453    % typical
    ] ;
M = 94.66096009; % mass of robot
deltaall = [0:pi()/100:2*pi()*0.999]';

x = CoM(3);
y = CoM(1);
z = CoM(2);
rw = 0.102 ; % wheel radius
R = 0.288925 ; % leg radius
alpha = deg2rad([0,120,240]); % leg angle offsets

for i=1:3
    w(i,:) = [R*cos(alpha(i)), R*sin(alpha(i))];
end

E12 = w(1,:) - w(2,:);
E23 = w(2,:) - w(3,:);
E31 = w(3,:) - w(1,:);
```



```

c = [x,y];
n12 = cross([0,0,1],[E12,0]);
n12 = n12/norm([E12,0]);
n23 = cross([0,0,1],[E23,0]);
n23 = n23/norm([E23,0]);
n31 = cross([0,0,1],[E31,0]);
n31 = n31/norm([E31,0]);

% =====
%% critical directions
for i=1:3
%   delta(i) = atan2(R*sin(alpha(i))-y, R*cos(alpha(i)- x] + 180 deg
    deltavector = c - w(i,:);
    deltai(i) = atan2(deltavector(2),deltavector(1));
    if deltai(i)<0
        deltai(i) = deltai(i)+2*pi();
    end
end

% =====
%% find safe a's for all deltas
clear alimit

% note: no code was added for considering when delta approaches a critical
% angle; in reality you would want to add this for safety
for i=1:size(deltaall,1);

    delta = deltaall(i,1);
    % find tipping edge Epq
    if (deltai(1) < delta) && (delta < deltai(2))
        Epq = E12;
        npq = n12;
        p = 1; q = 2;
    elseif (deltai(2) < delta && delta <= 2*pi()) || ...
        (0 <= delta && delta < deltai(3) )
        Epq = E23;
        npq = n23;
        p = 2; q = 3;
    elseif ( deltai(3) < delta ) && ( delta < deltai(1) )
        Epq = E31;
        npq = n31;
        p = 3; q = 1;
    else
        error('special angle not coded for yet...')
    end
end

```

```

% find tipping moment arm l
l = dot(npq,[w(p,:),0]-[c,0]);

% find apq limit
apq = 9.81*l/z;

% find safe a limit
alimit(i,1) = apq / (dot([cos(delta),sin(delta),0],-npq) ) ;
li(i,1) = 1;
end

% =====
%% visualization
% positions
wheels = [w;w(1,:)];
normals1 = [0,0; n12(1:2)];
normals2 = [0,0; n23(1:2)];
normals3 = [0,0; n31(1:2)];
for i=1:size(deltaall,1)
    ax2(i,1) = alimit(i,1)*cos(deltaall(i,1));
    ay2(i,1) = alimit(i,1)*sin(deltaall(i,1));
end

figure(1);
hold on
plot(wheels(:,1),wheels(:,2),'-','r', ...
    c(1),c(2),'o','r', ...
    ax2,ay2,'-','r')
%     normals1(:,1),normals1(:,2), '-','r', ...
%     normals2(:,1),normals2(:,2), '-','r', ...
%     normals3(:,1),normals3(:,2), '-','r' ...
axis square equal

% =====
%% angular veloc limit

for i=1:1;

    delta = atan2(-y,-x); % remember first argument is y term
    if delta < 0
        delta = delta + 2*pi();
    end

    % find tipping edge Epq

```

```

    if (deltai(1) < delta) && (delta < deltai(2))
        Epq = E12;
        npq = n12;
        p = 1; q = 2;
    elseif (deltai(2) < delta && delta <= 2*pi()) || ...
        (0 <= delta && delta < deltai(3) )
        Epq = E23;
        npq = n23;
        p = 2; q = 3;
    elseif ( deltai(3) < delta ) && ( delta < deltai(1) )
        Epq = E31;
        npq = n31;
        p = 3; q = 1;
    else
        error('special angle not coded for yet...')
    end

    % find tipping moment arm l
    l = dot(npq,[w(p,:),0]-[c,0]);

    % find apq limit
    apq = 9.81*l/z;

    % find safe a limit
    alimit2 = apq / (dot([cos(delta),sin(delta),0],-npq) ) ;
    omegalimit = sqrt(alimit2/sqrt(x^2+y^2));
end

% =====
%% Display metrics

maxalimit = max(alimit); %maximum acceleration limit
minalimit = min(alimit); %minimum acceleration limit
[maxalimit, minalimit, omegalimit] %angular velocity limit

```

Appendix C

Accessing Whole-Body Compliant Control Code

Different versions of whole-body compliant control (WBC) source code repositories are available in three locations: Sourceforge, github, and Meka Robotics. The Meka Robotics repository is only open to customers of the company. The Stanford University releases are available at:

`http://sourceforge.net/apps/wordpress/stanford-wbc/`

(Fig. C.1)

and

`https://github.com/poftwaresatent/stanford_wbc`

(Fig. C.2)

downloadable through the appropriate links there. The code must run on a Linux kernel and requires several installation steps, detailed in the Stanford_WBC github website. An alternate github repository maintained by the University of Texas at Austin is available at:

`https://github.com/poftwaresatent/utaustin-wbc`

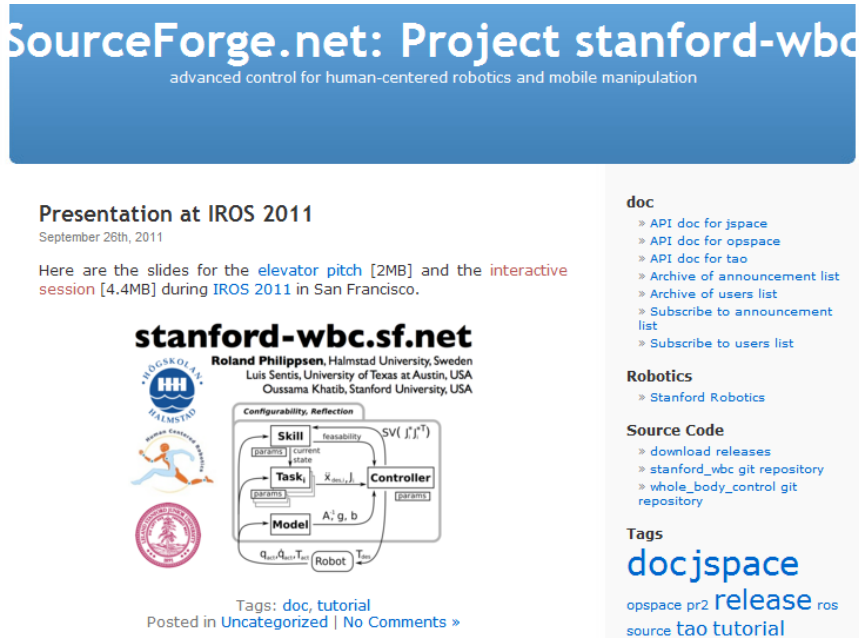


Figure C.1: Sourceforge Stanford-WBC website, April 2012.

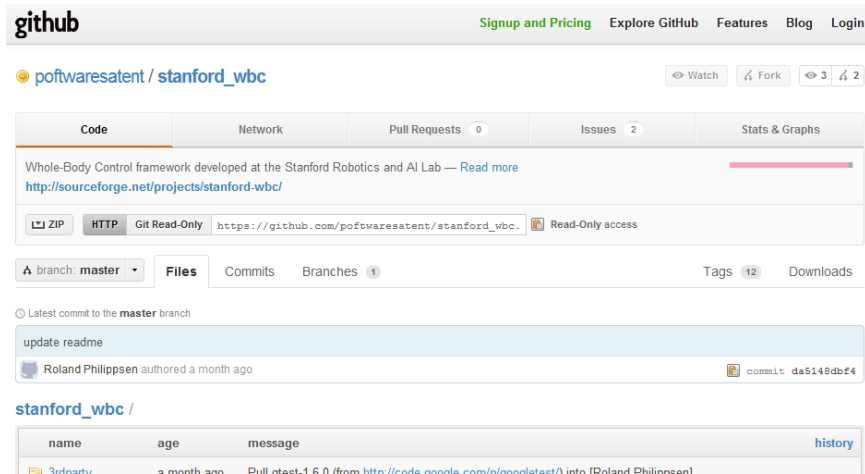


Figure C.2: github Stanford_WBC website, April 2012.

Index

- Abstract, vi
- acceleration limit, 90, 98, 100
- Acknowledgments*, v
- AHRS, 34, 37, 75, 85, 114, 117, 128
- alignment, 126
- American Disabilities Act, 111
- angular velocity limit, 94, 98, 104
- anthropomorphism, 7
- appearance of a robot, 7
- Appendices*, 183
- Appendix
 - Accessing Whole-Body Compliant Control Code*, 205
 - CAD Files and Selected Drawings*, 184
 - Matlab Code for Kinematic Limit Simulation*, 201
- applications, 138
- ARMAR-III, 9
- ASIMO, 132
- assembly, 65
- AZIMUT-3, 8, 9, 132
- back panel fabrication, 63
- backlash, 126
- balance, 117, 128
- battery charger, 23
- Bibliography*, 216
- bill of materials, 46
- BLDC, 26
- brushless DC motor, 22, 26
- brushless DC motor, 114
- calibration, 120
- clutch, 22, 114, 120
- communication, 114
- compliant control, 140
- compliantly controlled robots, 8
- component selection, 58
- controller, 116
- cooling of PCBs, 33, 55
- costs, 44
- coupler, shaft, 63, 64, 140
- Dedication*, iv
- degrees-of-freedom, 111
- Design Analysis*, 72
- Design Evaluation & Method Recommendations*, 132
- Design History*, 20
- disassembly, 65
- DLR-Biped, 132
- Dreamer, 111
- dynamics, 76, 117
- electronics module, 55, 69, 141
- emergency stop, 115, 140, 143
- encoder, 114
- EtherCAT, 55, 115
- exploded views, 55
- eyes, 111
- fabrication, 139
- finite element analysis, 36, 107
- form of a robot, 7
- gearbox, 26, 63, 114
- goals of research, 15

- goals of Trikey, 15
- HCR, 132, 154
- HCRL, 17
- HCRL-BLDCMC, 23
- head, 111
- holonomic, 140
- House of Quality, 153
- Human Centered Robotics Laboratory, 17
- human-centered robotics, 1, 6, 133
- humanoid form, 7, 9
- Implemented Design: Trikey Version* 5, 36
- IMU, 34, 37, 75, 85, 117, 128
- inclined terrain, 74, 84, 128
- inertia, wheel, 78
- Integrated Dreamer Humanoid Robot*, 111
- Introduction*, 1
- Justin robot, 7–9, 132
- keyway laxity, 126
- kinematics, 72
- likeability, 8
- load capacity, 36
- LOLA, 132, 133
- M3 software, 115
- machinability, 139
- machining, 63
- Matlab, 79, 83, 105
- Maxon, 63, 114
- Meka Robotics, 26, 27, 113
- Meka upper body, 113
- metrics of human-centeredness, 133, 154
- MicroStrain, 114
- mobile robots, 9
- modularity, 141
- modules, 44
- motor controllers, 23
- motor-wheel module, 67
- New Design Concepts*, 164
- OEM, 5
- omnidirectional, 9
- omniwheel, 22, 36, 114, 164
- parasolid, 64
- payload, 36
- planetary gearbox, 22, 124
- positioning, variable, 37
- power, 114
- redesign avenues, 133, 142
- redesign concepts, 164
- redesign prioritization, 151
- RTAI, 115
- safety, 6, 110, 140, 142
- SolidWorks, 20, 64, 78, 108
- stability, 96
- suspension, 177
- Test Results*, 120
- timeline, 17, 63
- tolerances, 63
- torque cell, 22, 114, 120
- torque cell calibration, 120
- torque limiter, 22, 63, 114, 120

- torque limiter calibration, 120
- Trikey design evaluation, 139
- Trikey design specifications, 10
- Trikey fabrication, 63
- Trikey summary, 113
- user experience, 129
- Vicor, 55
- Walbot, 8, 9, 132
- WBC, 132
- wheel-motor module, 55
- whole-body compliant control, 8, 116,
128, 132
- worst case analysis, 89, 108

Bibliography

- [1] N. Al-Holou, J. Weaver, T. Lahdhiri, and D.S. Joo. Sliding mode-based fuzzy logic controller for a vehicle suspension system. In *American Control Conference, 1999. Proceedings of the 1999*, volume 6, pages 4188–4192. IEEE, 1999.
- [2] A. Albu-Schaffer, O. Eiberger, M. Grebenstein, S. Haddadin, C. Ott, T. Wimbock, S. Wolf, and G. Hirzinger. Soft robotics. *Robotics & Automation Magazine, IEEE*, 15(3):20–30, 2008.
- [3] T. Asfour, K. Regenstein, P. Azad, J. Schroder, A. Bierbaum, N. Vahrenkamp, and R. Dillmann. Armar-iii: An integrated humanoid platform for sensory-motor control. In *Humanoid Robots, 2006 6th IEEE-RAS International Conference on*, pages 169–175. Ieee, 2006.
- [4] C. Bartneck, T. Kanda, H. Ishiguro, and N. Hagita. Is the uncanny valley an uncanny cliff? In *Robot and Human interactive Communication, 2007. RO-MAN 2007. The 16th IEEE International Symposium on*, pages 368–373. IEEE, 2007.
- [5] G. Berselli, M. Piccinini, G. Palli, and G. Vassura. Engineering design of fluid-filled soft covers for robotic contact interfaces: Guidelines, nonlinear modeling, and experimental validation. *Robotics, IEEE Transactions on*, 27(3):436–449, june 2011.

- [6] R. Bischoff, U. Huggenberger, and E. Prassler. Kuka youbot-a mobile manipulator for research and education. In *Robotics and Automation (ICRA), 2011 IEEE International Conference on*, pages 1–4. IEEE, 2011.
- [7] C. Borst, T. Wimbock, F. Schmidt, M. Fuchs, B. Brunner, F. Zacharias, P.R. Giordano, R. Konietzschke, W. Sepp, S. Fuchs, et al. Rollin’justin-mobile platform with variable base. In *Robotics and Automation, 2009. ICRA’09. IEEE International Conference on*, pages 1597–1598. IEEE, 2009.
- [8] K.S. Byun and J.B. Song. Design and construction of continuous alternate wheels for an omnidirectional mobile robot. *Journal of Robotic Systems*, 20(9):569–579, 2003.
- [9] Kyung-Seok Byun and Jae-Bok Song. *Mobile Robotics, Moving Intelligence*. 2006.
- [10] Charles Louis Xavier Joseph de la Vallée Poussin, 1879. A strong form of the prime number theorem, 19th century.
- [11] T.P. do Nascimento, A.L. da Costa, and C.C. Paim. Axebot robot the mechanical design for an autonomous omnidirectional mobile robot. In *Electronics, Robotics and Automotive Mechanics Conference, 2009. CERMA’09.*, pages 187–192. IEEE, 2009.
- [12] J. Fremy, F. Michaud, and M. Lauria. Pushing a robot along-a natural interface for human-robot interaction. In *Robotics and Automation (ICRA), 2010 IEEE International Conference on*, pages 3440–3445. IEEE, 2010.

- [13] M. Fuchs, C. Borst, P.R. Giordano, A. Baumann, E. Kraemer, J. Langwald, R. Gruber, N. Seitz, G. Plank, K. Kunze, et al. Rollin’justin-design considerations and realization of a mobile platform for a humanoid upper body. In *Robotics and Automation, 2009. ICRA ’09. IEEE International Conference on*, pages 4131–4137. IEEE, 2009.
- [14] E. Garcia, M.A. Jimenez, P.G. De Santos, and M. Armada. The evolution of robotics research. *Robotics & Automation Magazine, IEEE*, 14(1):90–103, 2007.
- [15] Somudro Gupta. Mechatronics of holonomic mobile base for compliant manipulation. Master’s thesis, University of Texas at Austin, Austin, Texas, May 2011.
- [16] G. Ishigami, E. Pineda, J. Overholt, G. Hudas, and K. Iagnemma. Performance analysis and odometry improvement of an omnidirectional mobile robot for outdoor terrain. In *Intelligent Robots and Systems (IROS), 2011 IEEE/RSJ International Conference on*, pages 4091–4096. IEEE, 2011.
- [17] H. Ishihara, Y. Yoshikawa, and M. Asada. Realistic child robot affetto for understanding the caregiver-child attachment relationship that guides the child development. In *Development and Learning (ICDL), 2011 IEEE International Conference on*, volume 2, pages 1–5. IEEE, 2011.
- [18] Dirk Jansen and Holger Büttner. Real-time Ethernet: the EtherCAT solution. *Computing and Control Engineering*, 15(1):16–21, 2004.

- [19] C.C. Kemp, A. Edsinger, and E. Torres-Jara. Challenges for robot manipulation in human environments [grand challenges of robotics]. *Robotics & Automation Magazine, IEEE*, 14(1):20–29, 2007.
- [20] S. Kim, C. Hyun, Y. Cho, and S. Kim. Tracking control of 3-wheels omnidirectional mobile robot using fuzzy azimuth estimator. In *Proceedings of the 10th WSEAS international conference on Robotics, control and manufacturing technology*, pages 47–51. World Scientific and Engineering Academy and Society (WSEAS), 2010.
- [21] C.P. Lam, C.T. Chou, K.H. Chiang, and L.C. Fu. Human-centered robot navigation—towards a harmoniously human–robot coexisting environment. *Robotics, IEEE Transactions on*, (99):1–14, 2011.
- [22] S. Lohmeier, T. Buschmann, and H. Ulbrich. System design and control of anthropomorphic walking robot lola. *Mechatronics, IEEE/ASME Transactions on*, 14(6):658–666, 2009.
- [23] C. Ott, C. Baumgartner, J. Mayr, M. Fuchs, R. Burger, D. Lee, O. Eiberger, A. Albu-Schaffer, M. Grebenstein, and G. Hirzinger. Development of a biped robot with torque controlled joints. In *Humanoid Robots (Humanoids), 2010 10th IEEE-RAS International Conference on*, pages 167–173. IEEE, 2010.
- [24] K.N. Otto and K.L. Wood. *Product Design: Techniques in Reverse Engineering and New Product Development*. 2001.
- [25] R. Philippsen, L. Sentis, and O. Khatib. An open source extensible software

- package to create whole-body compliant skills in personal mobile manipulators. In *Intelligent Robots and Systems (IROS), 2011 IEEE/RSJ International Conference on*, pages 1036–1041. IEEE, 2011.
- [26] Y. Sakagami, R. Watanabe, C. Aoyama, S. Matsunaga, N. Higaki, and K. Fujimura. The intelligent asimo: System overview and integration. In *Intelligent Robots and Systems, 2002. IEEE/RSJ International Conference on*, volume 3, pages 2478–2483. Ieee, 2002.
- [27] P. Sardain and G. Bessonnet. Forces acting on a biped robot. center of pressure-zero moment point. *Systems, Man and Cybernetics, Part A: Systems and Humans, IEEE Transactions on*, 34(5):630–637, 2004.
- [28] L. Sentis, J. Park, and O. Khatib. Modeling and control of multi-contact centers of pressure and internal forces in humanoid robots. In *Intelligent Robots and Systems, 2009. IROS 2009. IEEE/RSJ International Conference on*, pages 453–460. IEEE, 2009.
- [29] A.S. Shafer and M.R. Kermani. Design and validation of a magneto-rheological clutch for practical control applications in human-friendly manipulation. In *Robotics and Automation (ICRA), 2011 IEEE International Conference on*, pages 4266–4271. IEEE, 2011.
- [30] D. Shin, Z.F. Quek, S. Phan, M. Cutkosky, and O. Khatib. Instantaneous stiffness effects on impact forces in human-friendly robots. In *Intelligent Robots and Systems (IROS), 2011 IEEE/RSJ International Conference on*, pages 2998–3003. IEEE, 2011.

- [31] J.B. Song and K.S. Byun. Design and control of a four-wheeled omnidirectional mobile robot with steerable omnidirectional wheels. *Journal of Robotic Systems*, 21(4):193–208, 2004.
- [32] K.T. Song and S.Y. Jiang. Force-cooperative guidance design of an omnidirectional walking assistive robot. In *Mechatronics and Automation (ICMA), 2011 International Conference on*, pages 1258–1263. IEEE, 2011.
- [33] A. Thorstensson and H. Roberthson. Adaptations to changing speed in human locomotion: speed of transition between walking and running. *Acta physiologica scandinavica*, 131(2):211–214, 1987.
- [34] M. Udengard and K. Iagnemma. Design of an omnidirectional mobile robot for rough terrain. In *Robotics and Automation, 2008. ICRA 2008. IEEE International Conference on*, pages 1666–1671. IEEE, 2008.
- [35] US Department of Justice, www.ada.gov. *2010 ADA Standards for Accessible Design*, Sep 2010.
- [36] F. Wilbers, C. Ishi, and H. Ishiguro. A blendshape model for mapping facial motions to an android. In *Intelligent Robots and Systems, 2007. IROS 2007. IEEE/RSJ International Conference on*, pages 542–547. IEEE, 2007.
- [37] T. Wimbock, D. Nenchev, A. Albu-Schaffer, and G. Hirzinger. Experimental study on dynamic reactionless motions with dlr’s humanoid robot justin. In *Intelligent Robots and Systems, 2009. IROS 2009. IEEE/RSJ International Conference on*, pages 5481–5486. IEEE, 2009.

- [38] J.Y. Wong. *Theory of ground vehicles*. Wiley-Interscience, 2001.
- [39] J. Wyatt, W.N. Browne, M.N. Gasson, and K. Warwick. Consumer robotic products. *Robotics & Automation Magazine, IEEE*, 15(1):71–79, 2008.
- [40] M. Zinn, O. Khatib, B. Roth, and J.K. Salisbury. Playing it safe [human-friendly robots]. *Robotics & Automation Magazine, IEEE*, 11(2):12–21, 2004.

Vita

Pius Wong was born outside Chicago, Illinois, as one of six sons to Roman Catholic, Cantonese-Chinese American immigrant parents. While studying at the University of Illinois at Chicago he worked at various service and research positions. In 2005, after receiving a Bachelor of Science in Bioengineering, he joined Smith & Nephew Orthopaedics in Memphis, Tennessee, as a Research Engineer for bone and joint implants and biomechanics. In 2007 he moved to Brussels, Belgium, where he helped start up a new Smith & Nephew research laboratory focused on the human knee. In 2010, after having seen many parts of the world for the very first time, he returned to the US to pursue graduate studies in mechanical engineering at the University of Texas at Austin. There he taught undergraduate differential equations and hands-on mechatronics while conducting research in robotics and design.

Permanent address: 1200 Barton Hills Dr, Apt 327
Austin, Texas 78704

This thesis was typeset with \LaTeX^\dagger by the author.

[†] \LaTeX is a document preparation system developed by Leslie Lamport as a special version of Donald Knuth's \TeX Program.